2017

STRUCTURAL AND FUNCTIONAL ALTERATIONS IN NEOCORTICAL CIRCUITS AFTER MILD TRAUMATIC BRAIN INJURY

Michal Vascak
Virginia Commonwealth University

STRUCTURAL AND FUNCTIONAL ALTERATIONS IN NEOCORTICAL CIRCUITS AFTER MILD TRAUMATIC BRAIN INJURY

A dissertation submitted in partial fulfillment of the requirements for the degree of Doctor of Philosophy at Virginia Commonwealth University.

By

Michal Vascak
B.S. Ramapo College of New Jersey, 2008

Director: John T. Povlishock, Ph.D.
Professor and Chairman
Department of Anatomy and Neurobiology

Virginia Commonwealth University
Richmond, Virginia

April 2017

ACKNOWLEDGEMENTS

To my mentor, Dr. Povlishock, who asked me to ‘find a question’, then told me to ‘take ownership’ and lastly, taught me that science is ‘10% inspiration, 90% perspiration’.

The Povlishock Lab:
- Sue Walker
- Lynn Davis
- Vishal Patel
- Chris Jurgens, PhD
- Yasu Ogino, MD/PhD

and former members:
- Audrey Lafrenaye, PhD
- Anders Hånell, PhD
- Thomas Krahe, PhD
- Jesse Sims

My PhD Committee:
- Tom Reeves, PhD
- Jeff Dupree, PhD
- Ben Churn, PhD
- Clive Baumgarten, PhD
- Kim Jacobs, PhD

Collaboration with Jacobs Lab:
- Xiatao Jin
- Jianli Sun

VCU MD/PhD Program:
- Gordon Archer, MD
- Ross Mikkelson, PhD
- Michael Donnenberg, MD/PhD
- Sandra Sorrell

Dept. of Anatomy and Neurobiology and the Neuroscience Program:
- John Bigbee, PhD
- Rory McQuiston, PhD
- Sharon Toussaint

VCU Microscopy Facility:
- Scott Henderson, PhD
- Francis White

Former Instructors/Mentors:
- Ettore Appella, MD
- Sharlyn Mazur, PhD
- Robert Mentore, PhD
- Arthur Felix, PhD
- Rena Bacon, PhD

Special thanks goes to my family & friends, and especially my lovely wife, Natalie.

I dedicate this Thesis to my parents, Maria (1956–1995) & Milan (1948–2001).

TABLE OF CONTENTS

Page

LIST OF FIGURES

LIST OF ABBREVIATIONS

ABC	avidin-biotin complex
A	amperes
aCSF	artificial cerebrospinal fluid
AIS	axon initial segment
Ai9	Ai9 tdTomato reporter mouse
ANOVA	analysis of variance
ankG	ankyrin-G
AP	action potential
APP	β-amyloid precursor protein
atm	atmospheres
bpm	beats per minute
cFPI	central fluid percussion injury
CNS	central nervous system
Cre	Cre recombinase
d	day
DAB	diaminobenzidine
DAI	diffuse axonal injury
EM	electron microscopy
FSG	fish skin gelatin
GABA	gamma-amino-butyric-acid
GAD67	glutamate decarboxylase 67
GCS	Glasgow coma scale
h	hour
H_2O_2	hydrogen peroxide
HRP	horseradish peroxidase
IAT	impaired axonal transport
IgG	immunoglobulin gamma
IP	intraperitoneal
IQR	inter quartile range
LM	light microscopy
LOC	loss of consciousness
LORR	loss of righting reflex
LSCM	laser scanning confocal microscopy
M	molar
μM	micromolar
mM	millimolar
m	meter
min	minute
μm	micrometer
mm	millimeter
mg	milligram

µg	microgram
mL	milliliter
ms	milliseconds
nA	nanoamperes
NA	numberical aperature
NaV	voltage-gated sodium channel
NGS	normal goat serum
O_2	oxygen
PBS	phosphate buffered saline
p-c-Jun	phosphorylated (Ser63) c–Jun
pA	picoamperes
PSAI	perisomatic axonal injury
PV	parvalbumin
PV-Cre	PV-Cre mouse
PV-Cre;Ai9	F_1 progeny of PV-Cre x Ai9
rpm	respirations per minute
RFP	red fluorescent protein
r2	coefficient of determination
Rr	Pearson's correlation coefficient
s	seconds
SD	standard deviation
SEM	standard error of the mean
SpO2	arterial blood oxygenation
S1	primary somatosensory cortex
S1BF	primary somatosensory cortex barrel field
tdTom	tdTomato
TBI	traumatic brain injury
TBS	tris buffered saline
VGAT	vesicular GABA transporter
V	volts
X2	chi-squared
YFP	yellow fluorescent protein
YFP–H	B6.Cg–Tg(Thy1–YFP–H)2Jrs/J mouse strain

ABSTRACT

STRUCTURAL AND FUNCTIONAL ALTERATIONS IN NEOCORTICAL CIRCUITS AFTER MILD TRAUMATIC BRAIN INJURY

By Michal Vascak, B.S.

A dissertation submitted in partial fulfillment of the requirements for the degree of Doctor of Philosophy at Virginia Commonwealth University.

Virginia Commonwealth University, 2017.

Director: John T. Povlishock, Ph.D.
Professor and Chairman
Department of Anatomy and Neurobiology

National concern over traumatic brain injury (TBI) is growing rapidly. Recent focus is on mild TBI (mTBI), which is the most prevalent injury level in both civilian and military demographics. A preeminent sequelae of mTBI is cognitive network disruption. Advanced neuroimaging of mTBI victims supports this premise, revealing alterations in activation and structure-function of excitatory and inhibitory neuronal systems, which are essential for network processing. However, clinical neuroimaging cannot resolve the cellular and molecular substrates underlying such changes. Therefore, to understand the full scope of mTBI-induced alterations it is necessary to study cortical networks on the microscopic level, where neurons form local networks that are the fundamental computational modules supporting cognition. Recently, in a well-controlled animal model of mTBI, we demonstrated in the excitatory pyramidal neuron system, isolated diffuse axonal injury (DAI), in concert with electrophysiological abnormalities in nearby intact (non-DAI) neurons. These findings were consistent with altered axon initial segment (AIS) intrinsic activity functionally associated with structural plasticity, and/or disturbances in extrinsic systems related to parvalbumin (PV)-expressing interneurons

that form GABAergic synapses along the pyramidal neuron perisomatic/AIS domains. The AIS and perisomatic GABAergic synapses are domains critical for regulating neuronal activity and E-I balance. In this dissertation, we focus on the neocortical excitatory pyramidal neuron/inhibitory PV+ interneuron local network following mTBI. ***Our central hypothesis is that mTBI disrupts neuronal network structure and function causing imbalance of excitatory and inhibitory systems.*** To address this hypothesis we exploited transgenic and cre/lox mouse models of mTBI, employing approaches that couple state-of-the-art bioimaging with electrophysiology to determine the structural-functional alterations of excitatory and inhibitory systems in the neocortex.

CHAPTER ONE

INTRODUCTION

1.1 Definition of Traumatic Brain Injury

Traumatic brain injury (TBI) is a complex and heterogeneous acquired CNS disorder with several neurologic and behavioral consequences. The Demographics and Clinical Assessment Working Group of the International and Interagency Initiative toward Common Data Elements for Research on TBI and Psychological Health propose the following definition:

> *TBI is defined as an alteration in brain function, or other evidence of brain pathology, caused by and external force.*

Alteration of brain function encompasses any period of loss of consciousness (LOC), any loss of memory (antero- or retro-grade amnesia), neurologic deficits (dyspraxia, aphasia, paresis, etc.), and alterations in mental state (confusion, disorientation, slowed thinking, etc.) at the time of injury. Evidence of brain pathology may include visual, radiologic, or laboratory confirmation of damage to the brain (CDC, 2015). Initial clinical assessment after TBI uses the Glasgow Coma Scale (GCS) to index severity based on level of consciousness ranging from mild (13-15), moderate (9-12), to severe (≤8) brain injury (Parikh et al., 2007). Mild TBI (mTBI), popularly known as 'concussion', typically presents as a non-missile, closed-head injury commonly sustained during a motor vehicle collisions, sport-related impact, or blast-wave exposure in the war theater (Borg et al., 2004; Coronado et al., 2015; Hoge et al., 2008). In each case, external forces cause rapid

change in acceleration-deceleration, which evokes subtle CNS dysfunction and/or pathology (Johnson et al., 2013; Povlishock and Katz, 2005). A hallmark of mTBI is that these changes are in the form of diffuse brain alteration that is not detected by conventional x-ray computed tomography (CT) scans or magnetic resonance imaging (MRI) (Bigler and Maxwell, 2012; Mittl et al., 1994; Yuh et al., 2013). Thus, mTBI remains a clinical diagnosis (Sharp and Jenkins, 2015). In contrast, the presence of any intra-parenchymal mass/focal lesions such as hemorrhage and hematoma formation, contusion, and overt cell death/necrosis, which are readily detectable using conventional CT/MRI, is consistent with moderate-to-severe TBI (Povlishock and Katz, 2005). While severe TBI extracts more overt morbidity and can be fatal, mTBI is much more common (Cassidy et al., 2004; Coronado et al., 2011; Corrigan et al., 2010; Langlois et al., 2006; Thurman et al., 1999). Note, for the remainder of this dissertation in both clinical and experimental settings the use of 'TBI' denotes moderate-to-severe TBI. An important distinction implicit when using 'TBI' is the involvement of focal lesions and cell death.

Typically, TBI evokes heterogeneous cellular and vascular perturbation of damage with potential concomitant ionic, neurotransmitter, and metabolic disturbances (Andriessen et al., 2010; Barkhoudarian et al., 2011). These changes are characterized as either primary or secondary post-TBI sequelae (Johnson et al., 2013; Povlishock and Katz, 2005). Primary injury is evoked at the moment of insult. External mechanical forces of TBI can cause direct macroscopic tissue damage such as contusion at the impact site (Andriessen et al., 2010). Alternatively, rapid changes in acceleration-deceleration can cause diffuse microscopic perturbation such as distortion of mechanoporation of neuronal membranes (Povlishock, 1993). Secondary (delayed) injury is initiated at the

moment of insult and progressively develops over time. In this case, pathologic mechanisms such as excitotoxic injury are activated within focal lesions and spread through the surrounding tissue (e.g. pericontusional zone) causing further cell death (Barkhoudarian et al., 2011; Giza and Hovda, 2014; Johnson et al., 2013). Additionally, mechanotransduction can lead to functional and/or microstructural neuronal injury. Functional injury refers to pathophysiological mechanisms including but not limited to ionic shifts (e.g. calcium deregulation), metabolic/energy crisis, or altered neurotransmission (e.g. imbalanced excitation-inhibition) (Barkhoudarian et al., 2011; Guerriero et al., 2015; Povlishock and Katz, 2005). Microstructural injury refers to the acceleration-deceleration induced diffuse brain alteration not detected by routine CT/MRI (Andriessen et al., 2010; Farkas and Povlishock, 2007; Maxwell et al., 1997; Povlishock, 1992). Specifically, a major pathology found across the spectrum of TBI severity is diffuse axonal injury (DAI) (Blumbergs et al., 1995; Povlishock and Stone, 2001; Smith et al., 2013). The large size of the human brain (~1,500 g) constructed of a massive neural nexus makes axons vulnerable to tensile loading and shear forces generated during rapid changes in acceleration-deceleration occurring with TBI (Maxwell et al., 1997; Povlishock, 1993). In a heterogeneous fashion, sites of initial axonal perturbation, leading to local axonal failure, manifest focal swelling that progress over a several hour period until overt disconnection (Christman et al., 1994; Povlishock, 1992; Povlishock and Christman, 1995). Once disconnected, the distal axonal segment undergoes Wallerian degeneration. In this process, the breakdown of the axonal cylinder initiates within hours and potentially progresses for up to several months postinjury (Povlishock and Christman, 1995; Smith et al., 2013). Concomitant with axonal breakdown is the

degeneration of its nerve terminals (presynaptic boutons), commencing within the first week following TBI, eventually leading to widespread loss of inputs at postsynaptic target sites (deafferentation) (Povlishock et al., 1992; Povlishock and Katz, 2005). *Importantly, in both humans and animals, qualitative analysis suggests that the number of degenerating nerve terminals is in far excess than traumatically injured axons, with the assumption that deafferentation of target sites contributes to morbidity* (Andriessen et al., 2010; Erb and Povlishock, 1991; Povlishock, 1992; Povlishock et al., 1992; Povlishock and Christman, 1995; Povlishock and Katz, 2005; Smith et al., 2013). Clinical studies of patients with TBI provide indirect evidence to support this premise using multi-modal anatomical and physiological assessments (Arenivas et al., 2012; Marquez de la Plata et al., 2011; Warner et al., 2010). *Importantly, such diffuse nerve terminal loss also sets the stage for subsequent neuronal reorganization, which may be adaptive – leading to recovery, or maladaptive – resulting in persistent morbidity* (Christman et al., 1997; Patel et al., 2016; Phillips and Reeves, 2001; van der Horn et al., 2016). Lastly, it is important to emphasize that within the described DAI profile heterogeneity exists (Büki and Povlishock, 2006; Povlishock and Stone, 2001; Smith et al., 2013). This consists of multiple initiating pathophysiologic mechanisms that remain to be fully elucidated. Irrespective of the causative mechanisms, it is now clear that DAI and its subsequent impact of neural reorganization have major implications for the structural and functional connectivity of the human brain (Povlishock and Katz, 2005; Wolf and Koch, 2016). *Hence, contemporary view posits TBI morbidity is associated with circuit/network disruption.* Thus, TBI is not marked by a single pathophysiologic event (Andriessen et al., 2010). As will be discussed below, this notion is especially relevant to morbidity

associated with mTBI, which does not involve macroscopic lesions evoked at the moment of insult (McAllister, 1992; Povlishock and Katz, 2005; Smith et al., 2013; Yuh et al., 2013). Rather, mTBI is a progressive and complex disease process that manifests heterogeneously over time (Masel and DeWitt, 2010).

1.2 TBI Epidemiology

TBI constitutes a major global healthcare problem that extracts a devastating personal and societal toll (Langlois et al., 2006). Worldwide, an estimated 10 million people suffer a TBI each year. According to the World Health Organization (WHO), TBI will surpass many diseases as the major cause of death and disability by the year 2020 (Hyder et al., 2007). In the US, the estimated total incidence is 1.7 million and cost is $76.3 billion annually (CDC, 2015; Coronado et al., 2011; Faul et al., 2010). Historically, focus was on severe TBI associated with high-speed motor vehicle collisions (Coronado et al., 2011). In the last decade, the incidence of severe TBI has decreased dramatically because of automotive and transportation regulatory measures (Guerrero et al., 2000; Thurman et al., 1999). Milder forms of TBI elicited by contact sports and blast waves during combat now predominate (Coronado et al., 2015; Hoge et al., 2008; Holm et al., 2005). In fact, the incidence of mTBI is increasing (CDC, 2003). Recent attention has shifted focus on mTBI that represents almost 90% of all TBIs (Cassidy et al., 2004), and extracts significant personal and financial toll in both civilian and military populations (CDC, 2003; Coronado et al., 2015; Hoge et al., 2004). According to the latest WHO estimates, 1-out-of-150 people will suffer a mTBI annually (Holm et al., 2005).

1.3 Definition of Mild TBI

Diagnosis of mTBI remains elusive largely due to the absence of mass/focal or space occupying lesions, which are detected routinely using CT/MRI and typically associated with more severe TBI (Andriessen et al., 2010; Bazarian et al., 2006; Mittl et al., 1994; Povlishock and Katz, 2005; Yuh et al., 2013). Hence, mTBI is frequently termed the 'silent epidemic' because of its relatively subtle nature (Klein, 1981). The current definition of mTBI developed by the mTBI Committee of the Head Injury Interdisciplinary Special Interest Group of the American Congress of Rehabilitation Medicine states that a patient with mTBI is a person who has had a traumatically induced physiological disruption of brain function, as manifested by at least one of the following: 1) any period of LOC; 2) any loss of memory for events immediately before or after the accident; 3) any alteration in mental state at the time of the accident (e.g., feeling dazed, disoriented, or confused); and 4) focal neurological deficit(s) that may or may not be transient; but where the severity of the injury does not exceed LOC of approximately 30 minutes or less, after 30 minutes, an initial GCS of 13–15, and posttraumatic amnesia not greater than 24 hours (Kay et al., 1993).

However, even with the mild subgroup of TBI this broad clinical definition includes a wide range of severity (Alexander, 1995; Parikh et al., 2007). For example, a mTBI patient with LOC of 30 min presenting with a GCS of 13 may demonstrate profound confusion (e.g. not be oriented to time, place, and person) and may not have spontaneous eye opening responses. According to this same definition, a mTBI patient can also present without LOC, having a GCS of 15, but remain dazed/confused and demonstrate substantial cognitive impairment. Within this clinical definition of mTBI

there is also disparate pathology. Specifically, mTBI can be categorized and uncomplicated or complicated, corresponding to CT/MRI negative and positive lesions, respectively. As mentioned previously, CT/MRI positive results indicative of mass lesions are typically associated with more severe TBI (Andriessen et al., 2010; Povlishock and Katz, 2005). This is an important distinction because it involves two separate pathologies that correspond to mutually exclusive morbidities (Lange et al., 2009; McGinn and Povlishock, 2016; Nortje and Menon, 2004; Povlishock and Katz, 2005). Uncomplicated mTBI is associated with diffuse functional and/or microscopic structural injury causing 'diffuse' morbidity such as cognitive impairment (Iverson, 2005; McAllister, 1992). Conversely, complicated mTBI is associated with mixed diffuse functional/microstructural changes and macroscopic focal lesions (Andriessen et al., 2010). In this case, CT/MRI positive lesions may be associated with more severe co-morbidities like seizure (Alexander, 1995; Gentry et al., 1988; Iverson et al., 2000; Stiell et al., 2001). On the other hand, the presence of focal lesions does not always portend the clinical sequelae (Kasahara et al., 2010), suggesting that a subtler pathophysiology below limit-of-detection of conventional CT/MRI is responsible for morbidity. While the clinical definition of mTBI encompasses a relatively heterogeneous subpopulation of patients, the most common form of mTBI seen in sports usually involves minimal-or-no LOC period, GCS of 14/15, and when obtained, conventional CT/MRI scans are negative (Alexander, 1995; Borg et al., 2004; Cassidy et al., 2004; Coronado et al., 2015; Scheid et al., 2006). While this form of mTBI is subtler, the consequences are not mild. Recent findings in patients with mTBI linking acute cognitive network dysfunction with potential life-long morbidity have captured the attention of media and raised public

concern (Mannix et al., 2016). Hence, the term mTBI is misleading in many ways, referring to a sub-spectrum of severity and marked heterogeneity (Sharp and Jenkins, 2015).

1.4 Morbidity Associated with mTBI

Clinically, mTBI is associated with several neurological and behavioral sequelae that may either resolve or persist indefinitely (Alexander, 1995; Dean et al., 2015; Iverson, 2005; McAllister, 1992; Sterr et al., 2006). The constellation of signs and symptoms composing 'post-concussive syndrome' are observed across the spectrum of TBI severity. An objective tool that demonstrates common patient complaints following mTBI is the Rivermead Post-Concussion Questionnaire (King et al., 1995). The three major components are: 1) somatic e.g. headache, dizziness, visual disturbance; 2) behavioral e.g. sleep disturbance, irritability, depression; and 3) cognitive e.g. poor (working) memory, attention/concentration deficits, slow processing speed.

Although mTBI has important consequences in several aspects of the brain function, cognitive impairments are common sequelae and perhaps extract the most substantial personal, financial, and societal tolls (CDC, 2003; Cicerone, 1996; Sterr et al., 2006). The biomechanics of mTBI have been linked to particular injury profiles that are associated with stereotyped neurological abnormalities (McAllister, 1992). Cognitive impairments are likely due to alterations in the structural and functional connectivity of cortical (neocortical and hippocampal) circuits/networks (Fagerholm et al., 2015; Sharp et al., 2014; Wolf and Koch, 2016). Clinical studies have shown that white matter (WM) tract DAI affecting areas such as the corpus callosum have been associated with cognitive

impairments like poor attention and slow processing speed (Kinnunen et al., 2011; Sharp and Ham, 2011).

Moreover, the natural history of disease and recovery following mTBI is highly variable (Alexander, 1995). For example, there may be transient somatic symptoms that present acutely postinjury but resolve overtime, followed by a delayed manifestation of long-lasting cognitive impairment. The consequences of long-lasting impairments may be severely debilitating, wherein patients may have difficulty with even simple cognitive tasks, months to years after mTBI (Blyth and Bazarian, 2010; Dean et al., 2015; Sterr et al., 2006; Vanderploeg et al., 2005). On the other hand, patients with neuroimaging evidence of WM tract DAI may be asymptomatic and have no other ascribed clinical sequelae (Dodd et al., 2014; Tremblay et al., 2014). Conversely, clinically diagnosed mTBI marked by significant cognitive impairment can also occur without evidence of WM tract DAI (Ilvesmäki et al., 2014). Together, these findings reflect the complex nature of DAI and highlight the issue of undetected pathophysiology. While, the specific substrates of mTBI-induced morbidity remain to be fully elucidated, both pathologic (structural) and physiological (functional) abnormalities are likely involved (Antonakakis et al., 2016; Bouix et al., 2013; Dimitriadis et al., 2015; Ling et al., 2013; Mayer et al., 2011; Sponheim et al., 2011; Thatcher, 2006; Thatcher et al., 1997; Wolf and Koch, 2016; ZOURIDAKIS et al., 2012). The fact that cognitive impairment is a major consequence after mTBI supports this premise. Specifically, cognitive networks rely on both neocortical structural and functional connectivity to support high-order information processing (Bassett and Sporns, 2017; Bullmore and Sporns, 2009). Accordingly, structural and functional changes like DAI and imbalance excitation/inhibition,

respectively, have been associated with cognitive network disruption after mTBI (Bashir et al., 2012; Luo et al., 2013; Palacios et al., 2017; Tremblay et al., 2011, 2015).

1.5 Neocortical Networks: Neural and Neuronal

1.5.1 Large-Scale Neocortical Networks and Macro-Circuits

Based on the above, it is now becoming clear that neocortical network disruption influenced by both structural and functional change impacts upon the cognitive morbidity associated with mTBI. In this context, it is well know that the network architecture of the cerebral cortex supports cognition (Bullmore and Sporns, 2009). In humans, the neocortical gray matter (GM) comprises ~76% of brain volume (Kandel, ER; Schwartz, JH; Jessell, 2000). Cognition is the product of synergistic information processing by these structurally-functionally connected neocortical networks (Bullmore and Sporns, 2009). Large-scale *neural* networks (Figure 1.1) are composed of distributed areas of neocortical GM (nodes) connected by WM tracts (lines). Nodes are anatomically distinct, functionally homogenous areas of neocortical GM that process and encode information (Mountcastle, 1979). Sets of inter- or intra-hemispheric nodes connected via WM tracts like the corpus callosum and subcortical WM (SCWM) tracts form large-scale distributed neocortical networks (Hagmann et al., 2008). Locally encoded information within a node is relayed to different neocortical areas via WM tracts (Bassett and Sporns, 2017). Specialized nodes that either connect local clustered networks and/or multiple remote networks form higher-order multi-modal networks (van den Heuvel and Sporns, 2011). These specialized nodes, called hubs, are highly interconnected, receiving converging information from one network and sending diverging information to other networks

(Bullmore and Sporns, 2009; van den Heuvel and Sporns, 2013). In this way, large-scale neocortical network small-world topology enables complex integrated information processing that supports cognition (Bassett and Bullmore, 2006; Bressler and Menon, 2010). Embedded within large-scale neocortical networks are macro-circuits, which are a set of nodes connected in series forming a closed path (Bullmore and Sporns, 2009). In a neocortical macro-circuit, information is sent and received by the same node. Thus, cognition reflects integrated information processing by these higher-order multi-modal networks, where nodes encode signals that are relayed via WM tracts. While higher-order processing is a function of large-scale multi-modal networks, the communication between nodes is dependent on coherent activity (Fries, 2015; Scheeringa et al., 2011). Specifically, within nodes, information processing and encoding relies on balanced interplay between local excitatory and inhibitory systems within the neocortical GM (Aron, 2007; Fries, 2009; Haider et al., 2006; Raichle, 2010). The fine details of local information processing by small-scale excitatory-inhibitory systems reveals the structural unpinning's of large-scale network function (Douglas and Martin, 2007; Fries, 2009; Haider and McCormick, 2009).

1.5.2 Small-Scale Neocortical Networks and Microcircuits

While varying widely in surface area, the thickness and architecture of the neocortex is fairly conserved across mammals (DeFelipe et al., 2003). Compared to surface area, the thickness of neocortex varies relatively little between brains of different species/sizes. For example, the mass of human neocortex (~1,500 g) is ~3000 times greater than mouse neocortex (~0.5 g). Laid flat, human neocortex would be approximately the size of a

large pizza, whereas the mouse neocortex would be about the size of a nickel. In contrast, the neocortical thickness varies more within humans (approximately 2–4.5 mm) than the average (~2.5 mm) does compared to mice (approximately 0.6–1.2 mm). In terms of structure, the neocortex is a cellular sheet composed of long-distance projection pyramidal neurons (glutamatergic/excitatory) and local projection interneurons (GABAergic/inhibitory) deployed in horizontal layers, intersected by vertical (radial) columns (Horton and Adams, 2005). Neocortical columns are in the range of several hundred microns in diameter and their microarchitecture is stereotyped, demonstrating canonical microcircuitry in several different brain regions and across mammals (DeFelipe et al., 2003; Douglas and Martin, 2004). Similar to nodes, these microcircuits are embedded within small-scale (local) *neuronal* networks. Within these columns small-scale networks are composed of feedforward and feedback recurrent microcircuits between excitatory and inhibitory neurons (Douglas et al., 1995; Haider et al., 2006; Isaacson and Scanziani, 2011; Raichle, 2010; Somogyi et al., 1998). Hence, neocortical column information processing reflects a neuronal symphony thought to represent a fundamental computational unit (Fries, 2009; Horton and Adams, 2005; Mountcastle, 1979). While excitatory pyramidal neurons encode and relay information via WM tracts, inhibitory interneurons orchestrate this process within neocortical GM (Haider et al., 2006; Haider and McCormick, 2009; Hasenstaub et al., 2005; Shu et al., 2003). Specifically, inhibitory interneurons entrain ensembles of excitatory pyramidal neurons to fire synchronously (Buzsaki, 2004; Buzsáki and Wang, 2012a, 2012b; Kepecs and Fishell, 2014; Markram et al., 2004). GABAergic-mediated inhibition also controls the lateral spread of synchronized activity (Chagnac-Amitai and Connors, 1989).

Accordingly, large clusters of homotypic neocortical columns are the building blocks of nodes within large-scale distribute neocortical networks (Petersen and Sporns, 2015). Cognition is an emergent property of higher-order integrated information processing across structurally-functionally connected nodes comprising large-scale neocortical networks (Sporns, 2014; Tononi et al., 2016; Tononi and Koch, 2008). During cognitive loading, neocortical nodes demonstrate fast rhythmic electrical activity, known as gamma oscillation, which indicates recurrent synaptic neurotransmission consistent with local neocortical information processing (Bartos et al., 2007; Buzsáki and Draguhn, 2004; Buzsáki and Wang, 2012b; Raichle, 2010; Sohal et al., 2009). Large-scale neocortical networks become functionally connected when the frequency of multiple nodal gamma oscillations become in-phase, known as phase-locking or binding (Varela et al., 2001). This state of 'resonance' depends on balanced excitation-inhibition within local/small-scale neocortical networks, which in turn is regulated by GABAergic interneurons (Buzsáki, 2006). Taken together, these properties of small-scale excitatory-inhibitory networks during local information processing within neocortical GM demonstrates the role of activity at the neuronal level in large-scale networks that support higher-order function. Additionally, this puts forth the more abstract concept of scale-free network topology.

1.5.3 Scale-Free and Small-World Network Topology

Networks can be modeled using dots (nodes) connected by lines (WM tracts) (Bullmore and Sporns, 2009). In mathematics, these structures are called graphs and the study of their interconnectivity is known as graph theory. Using graph theory Watts and Strogatz

discovered the phenomena of ‘small-world’ network properties observed across spatial scales and various real-world examples such as social groups, electrical power grids, and the worldwide web (Watts and Strogatz, 1998). Specifically, networks tend to be organized in highly interconnected clusters of nodes with short path lengths and sparse long paths connecting remote areas (Bassett and Bullmore, 2006). Specifically, in large-scale neocortical networks, short paths involve intra-hemispheric interactions between nearby nodes (local clustered networks), and long paths refer to inter-hemispheric interactions between remote nodes and/or networks via WM tracts like the corpus callosum. Further, in small-scale neocortical networks, short paths relate to recurrent/intracolumnar microcircuitry and long paths refer to transcolumnar lateral axonal projections (Bullmore and Sporns, 2009). Networks with small-world network properties are highly efficient in terms of the cost associated with connecting nodes (Bassett and Bullmore, 2006). In the evolution of the brain, this architecture represents a trade-off by minimizing wiring while retaining structural-functional complexity required for information integration supporting cognition (Raichle, 2010; Van Essen, 1997). In brains, the scale-free nature of these structures is reflected by the conservation of small-world topology from neuronal (small-scale) to neural (large-scale) networks, i.e. interactions within nodes and between groups of nodes. Another important feature of small-world networks are specialized nodes that are highly interconnected and link remote networks across the brain. During higher-order information processing, large amounts of information converge on hubs, which in turn send large amount of diverging information (Bullmore and Sporns, 2009; Petersen and Sporns, 2015; van den Heuvel and Sporns, 2011, 2013). In small-scale networks, hubs are represented by highly

interconnected neurons, particularly inhibitory interneurons (Bonifazi et al., 2009). Using graph theory, these scale-free networks can be modeled based on experimental (e.g. electrophysiological) or clinical (e.g. fMRI) data (Buzsáki and Wang, 2012a; Caeyenberghs et al., 2012; Logothetis et al., 2001; Traub et al., 1996; Whittington et al., 2000). This further illustrates how studying small-scale neuronal networks can be used to gain insight into higher-order information processing by large-scale networks.

1.5.4 Examples of Human Brain Networks

In humans, complex frontoparietal large-scale neural networks support some of the higher-order cognitive processes like sustained attention and working memory. The classic model of working memory consists of interactions between executive and storage components (Reynolds et al., 2009). Executive functions include monitoring and updating information processing by the inferior frontal cortex and dorsolateral prefrontal cortex (DLPFC). The inferior parietal cortex acts as a storage buffer, which holds information 'online' for manipulation by the executive components. This network also involves the premotor area, which is associated with sub-vocal rehearsal of phonological information and storage of verbal information (Collette and Van der Linden, 2002).

Although the cognitive process of sustained attention requires activation of frontoparietal systems, lapses in attention can also be monitored by measuring neocortical activity within the default mode network (Buckner et al., 2008; Fox et al., 2005; Weissman et al., 2006). When not concentrating, e.g. day dreaming, the default mode network (DMN) is active, whereas during cognitive processing that requires sustain attention, the DMN is deactivated (Raichle et al., 2001). The DMN consists of a set of

neocortical areas that show highly correlated activity and high metabolic demand at rest. Dense WM tracts connect the midline components of the DMN, which consist of the ventromedial prefrontal cortex, posterior cingulate cortex, and ventral precuneus. Recently, it was found that 'resting-state' networks such as the DMN not only reveal underlying structural connectivity, but also are anti-correlated with complementary functional connectivity of attention networks during cognitive loading (Raichle et al., 2001; Schölvinck et al., 2010).

1.6 Structural and Functional Disruption of Circuits/Networks

A simple circuit is constructed by two conducting elements that are structurally and functionally connected. Structural connections (synapses) enable activity of one conducting element (presynaptic neuron) to influence the activity of a downstream conducting element (postsynaptic neuron) via signal transmission. As the signal travels along the circuit, it is processed; hence, rendering functional connectivity. More complex circuits with both excitatory and inhibitory components can either relay or terminate signals. Without inhibition, simple circuit temporal-dynamics would limit computational power and lead to runaway excitation. Hence, complex circuit function depends on *balanced excitation and inhibition* (Haider et al., 2006).

A circuit can be damaged/disconnected via structural and/or functional disruption (Figure 1.2). For example, structural disruption (e.g. presynaptic neuron DAI) can disconnect a circuit (loss of input/deafferentation) causing downstream functional disruption (e.g. postsynaptic neuron activity changes) and lead to imbalance excitation-inhibition. The initial circuit disruption may potentially evolve, resulting in further

functional disruption and changes in excitation-inhibition. Alternatively, the circuit may adapt and modify structural and/or functional connectivity to regain signal transmission and restore information processing. As discussed above circuits are embedded in both large- and small-scale neocortical networks. In an analogous fashion, these networks may re-organize in response to structural and/or functional disruption (van der Horn et al., 2016). Furthermore, since integrated information processing occurs across special scales, initial microcircuit disruption leading to imbalanced excitation-inhibition of small-scale networks may disrupt the coherence/binding between nodes of large-scale networks (Siegel et al., 2012; Stam, 2014; Varela et al., 2001; Zhang and Raichle, 2010). Analogously, if the acoustics of homeostatic network function reflects state of harmony, then cognitive impairment following mTBI is consistent with network dissonance, where excitation-inhibition are out-of-tune. Thus, a paragon of human brain network dysfunction is mTBI-induced disintegration of neocortical information processing.

1.7 Importance of Balanced Excitation and Inhibition in Neocortex

1.7.1 Development and Neuroplasticity

Essential to the proper functioning of neocortical circuits is balanced neocortical excitation and inhibition. This is first evident during human development, where a delicate balance between excitatory and inhibitory plasticity mechanisms is required for proper maturation (Murphy et al., 2005). The ‘critical period’ during early postnatal development is marked by peak sensitivity to sensory experience concomitant with maximal neuroplasticity. After the critical period, there is a reduction of neuroplasticity. However, experimental studies of adult brains have found ways to restore neuroplasticity

levels similar to early postnatal development, and suggest intracortical inhibition may be an important mechanism (Spolidoro et al., 2009). Specifically, it is thought that changes to both excitatory and inhibitory neurotransmitter receptor expression enable the reactivation of neuroplasticity (He et al., 2006). Shifts in excitation and inhibition were observed in response to sustained sensory stimulation wherein mechanisms of adaptation involved depression of inhibitory synapses (Heiss et al., 2008). Similarly, direct intracortical microstimulation induction of neocortical reorganization involves differential spatiotemporal expression of excitatory/glutamatergic and inhibitory/GABAergic systems (Benali et al., 2008). The spatio-temporal variance of excitation-inhibition seen in homeostatic development and experimentally induced neuroplasticity has been recapitulated in the context of TBI.

1.7.2 mTBI Disrupts Neocortical Balance of Excitation and Inhibition

Based on the scale-free small-world properties of neocortical networks described above, cognitive impairment invariably reflects altered information processing (Stam, 2014; Zhang and Raichle, 2010). The balance of excitatory-inhibitory systems is essential for integrated information processing by neocortical networks (Buzsáki and Wang, 2012b; Fries, 2015; Lisman and Jensen, 2013). A potential consequence of mTBI-induced, widespread circuit/network disruption is unbalanced neocortical excitation and inhibition (Cohen et al., 2007; Paterno et al., 2016). Studies suggest mTBI induces these two opposite process (Guerriero et al., 2015). Glutamatergic overload causing NMDA-mediated excitotoxicity following more severe TBI is well documented, and it is posited that similar events occur with mTBI (Andriessen et al., 2010; Giza and Hovda, 2014;

Guerriero et al., 2015). While limited, more recent studies also implicate GABAergic disruption in cognitive impairment after mTBI (Sponheim et al., 2011; Tremblay et al., 2011, 2015). Clinical studies measuring neocortical metabolic and electrophysiological change reveal a wide range of intrinsic (local) neocortical (small-scale) network dysfunction involving abnormal spontaneous, rhythmic, and excitatory-inhibitory activity, thereby supporting this premise (Bashir et al., 2012; De Beaumont et al., 2012; Huang et al., 2016b; Luo et al., 2013; Mayer et al., 2011; Palacios et al., 2017; Sponheim et al., 2011; Tremblay et al., 2011). Specifically, neural oscillations, serving as an in vivo proxy of excitatory-inhibitory balance (Atallah and Scanziani, 2009; Fries, 2009; Isaacson and Scanziani, 2011) reflect local neocortical changes linked to cognitive network impairment after mTBI (Logothetis et al., 2001; Palacios et al., 2017; Pevzner et al., 2016; Schölvinck et al., 2010; Sponheim et al., 2011). Hence, structural disruption in the form of DAI and/or functional disruption such as abnormal electrophysiological status may result in overall circuit/network abnormalities.

1.8 mTBI Induces Structural & Functional Disconnection of Neocortical Networks

1.8.1 Historical Perspective: Postmortem Examination and 'WM Vulnerability to DAI'

'One can spend an entire lifetime correcting a flawed paper published in a reputable journal and still loose the battle if people like the basic idea'
-Victor Hamburger

For over 30 years, DAI research across the spectrum of TBI has centered on WM tracts. The etymology of the term 'diffuse axonal injury' traces back to early clinical studies of patients with severe and/or fatal TBI (Adams, 1982; Strich, 1956). Importantly, the vast majority of these patients were between 60–90 years of age (Blumbergs et al., 1995). Clinical evaluation of these patients with prolonged LOC or coma revealed profound

neurological morbidity in the absence of overt focal brain lesions (Adams et al., 1982a, 1982b, 1989; Graham et al., 1983). Postmortem gross examination of these patients' brains also showed limited focal change other than isolated petechial hemorrhage, frequently observed within the corpus callosum and dorsolateral quadrant of the superior cerebellar peduncle (Adams, 1982; Adams et al., 1982b, 1989, 1991; STRICH, 1961). Histopathology revealed theses scattered petechial hemorrhages were associated with axonal swellings. A key observation was that these axonal swellings were scattered around intact fibers. Later studies using routine immunohistochemistry (IHC) provided insight into their pathogenesis, finding that amyloid precursor protein (APP), which undergoes fast anterograde transport, accumulates in axonal swellings indicative of impaired axonal transport (Gentleman et al., 1993; Sherriff et al., 1994b). A later study established a standardized method of systematically quantifying burden of injury employing APP immunoreactivity to evaluate 31 fatally injured pedestrians (Ryan et al., 1994). Specifically, a sector scoring method was used that a superimposed grid over WM regions, excluding neocortical GM. Historically, DAI has been widely reported in severe TBI cases owning to the more lethal nature. Postmortem studies of mTBI have been much more limited (Bigler and Snyder, 1995; Blumbergs et al., 1994). Blumbergs and colleagues (1995) were the first (and only) to compare the topography of DAI defined by APP using the sector scoring method described above (Blumbergs et al., 1995). Specifically, six mTBI (GCS 14,15) cases (years of age: average = 79, range = 69–89; LOC 1–40 min; survival 4 h – 28 d) were compared with six severe (fatal; GCS 3,4) TBI cases (years of age 8–69; LOC/survival 2 h – 8 d). While, mTBI cases died of causes unrelated to mTBI, some had focal lesions i.e. 'complicated mTBI'. Using the

standardized scoring method of the DAI burden, they found mTBI elicited 4–88 and severe 76–107 APP+ sectors.

Collectively, based on these limited studies, these investigators concluded that WM DAI is a major component of TBI neuropathology and is proportional to injury severity. The observation of frequent involvement of the corpus callosum and fornices gave support to the premise of WM tracts' selective vulnerability to the forces of TBI. Further, because (m)TBI is associated with cognitive impairment and memory deficits, the finding of WM tract DAI was also suggested as the underlying cause of morbidity.

In humans it is estimated that axonal density in WM tracts can be over two-orders of magnitude greater than neocortical GM (Carlo and Stevens, 2013; Walhovd et al., 2014; Zhang and Sejnowski, 2000). No study has taken this into account. Illustrating this point is an early study that reported APP+ swellings were most commonly observed in the splenium of the corpus callosum, but was also found in central GM and very occasionally in the cortex in patients that sustained TBI after falling (Abou-Hamden et al., 1997). The investigators report that their results were consistent with previous findings suggesting WM tract vulnerability, especially the splenium of the corpus callosum. However, the splenium has the highest axonal density of any WM tract (Walhovd et al., 2014). Because this known property of the corpus callosum was not accounted for, the investigator's interpretation that the splenium is particularly vulnerable to the forces of TBI was invalid. Therefore, the notion of WM tract vulnerability to DAI in mTBI is not based on empirical evidence, rather than theoretical presumption based on limited and confounded data that has come to be accepted as dogma.

1.8.2 Evidence for Structural Disconnection: Diffusion Tensor Imaging

Conventional MRI generates brain images using an electromagnetic field to align hydrogen atom nuclei (protons), and measuring relaxation following perturbation by a radio frequency pulse (Hagmann et al., 2006). Diffusion tensor MRI (DTI) extends this principle by employing variable electromagnetic field strengths to detect the diffusion of water within a structure, such as WM, where the random motion of water is constricted by the parallel arrangement of axonal fibers. This asymmetrical or 'anisotropic' diffusion can be measured using DTI, and affords the investigation of WM structural integrity and connectivity at particular anatomical locations. In DTI, water molecular diffusion data is fitted to a 'tensor' model, and then quantitatively analyzed yielding a measurement of fractional anisotropy (FA), where 0 denotes equal diffusion in all directions and 1 denotes diffusion along a single direction only (Le Bihan and Johansen-Berg, 2012). Other quantitative measurements used to described DTI findings reflect mean diffusivity (MD) and total diffusivity of water (apparent diffusion coefficient; ADC). Furthermore, by analyzing the directional components of DTI data, the mapping of major WM tracts can be achieved, affording a means to evaluate connectivity between two anatomical regions of interests in a process called tractography (Jones, 2008). Overall, the high axonal density and homogenous structure of WM tracts allows for non-invasive assessment for DAI via DTI. This technology combined with renewed interest in mTBI helped reinforce the concept that the WM remains as the region-of-interest for clinical investigation (Shenton et al., 2012).

To date, the reported anatomical distribution of DTI abnormalities has remained remarkably consistent with postmortem findings across the spectrum of TBI severity

(Hellyer et al., 2012; Sharp and Ham, 2011). Further in agreement with postmortem findings these DTI studies also indicate that the burden of WM damage increases with injury severity (Bigler and Bazarian, 2010; Kraus et al., 2007). As discussed above, current thought suggests mTBI causes cognitive dysfunction by disconnecting neocortical networks via WM tract DAI (Sharp et al., 2014). To date, several investigations of TBI patients ranging from mild to severe have associated cognitive deficits to WM abnormalities detected by DTI both in acute and chronic phases of injury (Dodd et al., 2014; Gardner et al., 2012; Shenton et al., 2012). Further, the neuroanatomical location of DTI abnormalities along key WM pathways have been linked to specific cognitive functions. For example, chronic memory deficits after TBI have been correlated with loss of structural integrity of the fornix, a WM tract connected to the hippocampi, in patients with varied severity (Kinnunen et al., 2011) and mTBI alone (Sugiyama et al., 2009). Such a relationship was also seen in the acute setting, where impaired executive function after mTBI was linked to DAI within the DLPFC (Lipton et al., 2009). These investigations are important because they link specific impairments to evidence of pathologic changes in regions known to support the respective functions. Acutely, this may reflect the clinical manifestation of initial posttraumatic pathologic changes. Conversely, the long-lasting deficits shed light on either enduring deleterious processes or a consequence of maladaptive response. For example, DTI analysis in the chronic stage post-mTBI has yielded evidence of progressive axonal pathology that correlates with cognitive impairments (Lipton et al., 2008). Specifically, retrospectively analyzed mTBI patients that were otherwise asymptomatic, with no significant clinical sequelae ascribed after initial evaluation, presented several months to years post-trauma with

symptoms including difficulty with attention, concentration, memory, and job performance. In these patients, DTI revealed evidence of WM damage most likely reflecting Wallerian degeneration of the distal disconnected axonal shaft. Overall, these DTI studies contributed to advancing knowledge about mTBI structural pathobiology underlying morbidity via promoting the concept of network disruption. Together, these reports support the premise that DAI is involved in the initial pathogenesis associated posttraumatic dysfunction, and also address downstream mechanisms involved in more chronic stages.

Although well ingrained in the literature, these DTI studies have not been without controversy, especially in the case of mTBI (Dodd et al., 2014; Ilvesmäki et al., 2014; Zhang et al., 2010). In fact, after almost 10 years of DTI studies their related findings remain inconsistent (Shenton et al., 2012). While considerable debate has focused on studies showing disparate results such as increased vs. decreased FA after mTBI, a major inconsistency that has been routinely overlooked is the substantial body of literature reporting negative DTI findings and/or lack of significant correlations between DTI abnormalities and morbidity. Even in moderate TBI (average GCS = 8), Huisman and colleagues only reported significant differences of ADC in the splenium, which has the highest axonal density, and not the internal capsule (Huisman et al., 2004). Several groups reported clinically diagnosed mTBI marked by substantial cognitive impairment without significant WM involvement (Ilvesmäki et al., 2014; Mac Donald et al., 2011; Wäljas et al., 2014; Zhang et al., 2010). For example, a study of U.S. military personal that were clinically diagnosed with mTBI following blast-related trauma demonstrated DTI abnormalities consistent with DAI only in a fraction of the patient cohort (Mac

Donald et al., 2011). This suggests an undetected structural-functional pathophysiology within neocortical GM, where local (intrinsic) network processing relies on balanced excitatory-inhibitory neural activity. Supporting this possibility, some DTI (measuring diffusion kurtosis) investigations show evidence for axonal perturbation within neocortex itself (Bouix et al., 2013; Ling et al., 2013; Newcombe et al., 2011). While DTI is insensitive to axonal changes in neocortical GM due to the structural complexity, a recent clinical study has demonstrated mTBI-induced alterations consistent with neocortical gliosis (Ling et al., 2013). Such pathology indirectly suggests the presence of neocortical DAI, which has been demonstrated in human post-mortem brains, as well as animal models of mTBI. Specifically, these diffusion kurtosis abnormalities after human mTBI are entirely consistent with previous work from our lab and others showing neocortical DAI associated microglial activation (Bigler, 2004; Bigler and Maxwell, 2012; Kelley et al., 2007; Lafrenaye et al., 2012, 2014; Pilz, 1983; Singleton et al., 2002; Ziebell et al., 2012).

In mTBI, even if there is evidence of WM tract DAI, albeit relatively less than more severe TBI, the interplay between the variable injury profile and dynamic response of neocortical structure-function results in wider and more divergent outcomes. For example, two mTBI patients may have an initial GCS of 15, yet only one fully recovers while the other experiences a delayed manifestation of debilitating cognitive symptoms. In this respect, acute observations using DTI of WM tracts are limited in that they do not reflect upon the subsequent traumatically induced neocortical responses involving local excitatory-inhibitory network interactions and recurrent circuitry. These local/intrinsic neocortical mechanisms and associated structural-functional reorganization may lead to

either recovery or chronic neurologic impairment. From this stand point, local neocortical mechanisms overshadow the contribution of initial WM tract DAI in long-term changes that lead to either recovery of persistent morbidity.

Recent advances in neuroimaging have reaffirmed DAI as a signature lesion in TBI and major contributor to morbidity (Shenton et al., 2012). However, many of these studies involved heterogeneous TBI populations and the interpretations of findings in moderate-to-severe TBI were applied to mTBI (Sharp and Ham, 2011). These missteps in clinical DTI studies have reinforced the notion of WM tract vulnerability to DAI after TBI, even when mild. While across the spectrum of TBI severity WM involvement cannot be dismissed (Kinnunen et al., 2011; Mayer et al., 2010), this presumption remains controversial in mTBI (Dodd et al., 2014; Ilvesmäki et al., 2014; Zhang et al., 2010). While DTI studies have been helpful in characterizing some of the structural aspects of neocortical network disruption following mTBI, they are limited in that correlations with functional deficits do not equate causation. Hence, in order to develop a more comprehensive understanding (m)TBI, functionally approaches must be employed and ultimately coupled to structural findings.

1.8.3 Evidence for Functional Disconnection: fMRI, EEG, TMS

Functional MRI (fMRI) using blood oxygen level dependent (BOLD) contrast is based on the principle of differential magnetic susceptibility of deoxy- versus oxy-hemoglobin (Logothetis et al., 2001). The BOLD signal reflects local changes in hemodynamics, including alterations in flow and blood volume, as a consequence neurotransmitter driven synaptic activity i.e. neural signaling (Buckner et al., 2013; Lauritzen, 2001; Logothetis

et al., 2001; Tagamets and Horwitz, 2001). In addition to mapping neocortical activation, fMRI can be used as a means of studying the connectivity of neural networks by tracking spatial and temporal dynamics of BOLD responses (Fox et al., 2005; Kasahara et al., 2010; Mayer et al., 2011). In a typical study, fMRI data is acquired before and after a cognitive task, and superimposed on anatomical data retrieved using conventional MRI, in order to determine which areas of the neocortex are activated during executive of the given task (Friston et al., 1997). Functional connectivity between neocortical regions can be determined via psychophysiological interaction analysis, which yields spatio-temporal information of neocortical activation during task performance (Kasahara et al., 2010). The majority of fMRI studies have focused on the neocortical response to cognitive tasks or stimuli. However, it has been discovered during 'resting-state' the neocortex is active, manifesting as spontaneous fluctuations in BOLD signal (Raichle et al., 2001). Resting-state fMRI uses the BOLD signal to assess spontaneous neural activity, which reveals intrinsic functional architecture of the neocortex, such as the DMN (Fox et al., 2005; Logothetis et al., 2001). In the context of (m)TBI, both cognitive task and resting-state fMRI studies reveal change in neocortex activation and network structure (Han et al., 2014; Palacios et al., 2017; Sponheim et al., 2011). Even though fMRI measures activity within neocortical GM (Lauritzen and Gold, 2003), the interpretation of any observed changes have been made through the same lens at DTI studies focused on WM tract DAI (Marquez de la Plata et al., 2011; Mayer et al., 2011; Messé et al., 2013; Sponheim et al., 2011).

Another clinical tool used to measure neocortical function is electroencephalography (EEG), which evaluates the patterns of neural activity via

recording extracellular voltage changes with time (Amyot et al., 2015). Similar to fMRI, modern EEG techniques can evaluate neocortical networks by assessing spatial and temporal dynamics of coordinated neocortical activity (Pevzner et al., 2016). As mentioned above, excitatory-inhibitory network processing involves synchronized neural activity reflected as oscillations in EEG recordings (Buzsáki et al., 2012). The functional connectivity of neocortical networks is determined by measuring time-frequency based phase synchronization between specific neocortical areas. EEG has been coupled with both DTI and fMRI to demonstrate the structural-functional disruption of large-scale neocortical networks after mTBI (Amyot et al., 2015; Arenivas et al., 2012; Sponheim et al., 2011). As with the interpretation of fMRI, EEG data has also been only viewed through the lens of WM tract DAI, especially when coupled with DTI (Sponheim et al., 2011). EEG can also be coupled with transcranial magnetic stimulation (TMS). Such an approach provides neurophysiologic measures of excitation-inhibition and can also be used to evaluate neuroplasticity (Bashir et al., 2012; Tremblay et al., 2015).

In cognitive testing involving the motor systems, transcallosal inhibition is an important step in coordinated activity. The motor network is relatively simple and well understood, consisting of the primary motor cortex (M1), supplementary motor area, cerebellum, and frontoparietal cortices (Hanakawa et al., 2003; Lotze et al., 1999). An early fMRI study used to assess the integrity of the motor network during a finger-thumb opposition task demonstrated compromised activation of several nodes, with only M1 indicating normal physiology (Kasahara et al., 2010). Even more crucial, an overall compromise of network connection occurred, affecting both inter- and intra-hemispheric interactions. Disrupted interhemispheric connectivity may reflect damage to the corpus

callosum. However, the loss of both positive and negative interactions between nodes ipsi- and contra-lateral nodes suggests alternative mechanisms.

Specifically, interhemispheric inhibitor interactions are an important function in controlling M1 output (Bashir et al., 2012; De Beaumont et al., 2012; Hammond-Tooke et al., 2010). Loss of these interactions may reflect compromised structural integrity of transcallosal fibers. Alternative, these changes in inhibitory interactions may reflect disruption of local GABAergic systems in the absence of WM tract damage. The structural and/or functional aberrations of the motor network may manifest clinically as delayed planning during a task, which is a common sequelae of mTBI. In addition to showing alteration of activity within discrete areas of neocortex (nodes), evidence for widespread network dysfunction (interaction between nodes) was also found, implying functional reorganization (Kasahara et al., 2010). Supporting this premise, evidence of *increased* activation in neocortical regions that were not involved in neocortical processing in control subjects, suggested compensatory neocortical responses to support performance during the task. In other words, the outcome of the study indicated that an adaptive functional response occurred after TBI.

Alteration of neocortical physiology may occur independent of abnormal DTI findings within WM tracts (Ilvesmäki et al., 2014; Wäljas et al., 2014; Zhang et al., 2010). In line with fMRI findings in the motor network, studies employing EEG/TMS also showed changes in neocortical excitation-inhibition, mechanisms of plasticity, functional connectivity, and overall neocortical activation via coupling to motor-evoked potential (MEP) measurements (Bashir et al., 2012; De Beaumont et al., 2012; Tremblay et al., 2015). Intracortical inhibition and plasticity were evaluated by performing a

method that involved stimulating the M1 and measuring MEPs in the contralateral hand muscles. Specifically, after mTBI increased intracortical facilitation and decreased intracortical inhibition was observed (Bashir et al., 2012). This agreed with the observed inverse of plasticity mechanisms indexed by MEP facilitation instead of suppression demonstrated by control subjects. Together, these observations indicate altered TMS induced neocortical excitation-inhibition and neocortical plasticity. At this time, EEG topographical maps indicated less intense, albeit more widespread activation of M1 in response to a single pulse of TMS compared to controls. This finding was complemented by the observation of a massive increase in activation in response to a pulse following a period of continuous TMS, whereas activation decreased in controls. Functional connectivity appeared to be compromised based on reduced correlation between temporal EEG signals recorded at M1 and ipsilateral parietal upon TMS of M1, wherein abnormal EEG temporal correlation suggests altered functional connectivity. This is a particularly interesting find considering neuroimaging studies were negative, which suggest that the substrate for altered functional connectivity may be physiologic (functional) rather than structural (connectivity) as discussed above. Interestingly, at follow-up 6 weeks after injury, all measures normalized, which coincided with patient improvement (Bashir et al., 2012). In summary, abnormal balance of excitation and inhibition in the absence of structural aberrations upon DTI suggests there may be a neurophysiologic substrate for (long-lasting) deficits induced by mTBI. These findings suggest at more subtle neural perturbations that do not involve overt disconnection as in the case of DAI. An alternative explanation may be structural-functional alterations in excitatory of inhibitory neuronal systems of intrinsic neocortical networks (Zhang and Raichle, 2010).

Investigating perturbation of excitation-inhibition balance is important in understanding mTBI-induced pathology versus neurobiological responses, which may either be protective (adaptive) or harmful (maladaptive plasticity) (Povlishock and Katz, 2005).

Clinical reports that have linked neocortical areas with abnormal neurophysiology to WM tract DAI also show evidence of local neocortical excitatory-inhibitory network disruption. EEG coupled with DTI was used to show clinical evidence for WM tract DAI with attendant deafferentation. Specifically, blast injured soldiers that sustained mTBI showed decreased EEG phase synchrony between contralateral areas in the frontal cortex (Sponheim et al., 2011). This finding suggests decreased interhemispheric coordination of neocortical activity, which was correlated with compromised structural integrity of WM tracts of the frontal lobe and anterior corpus callosum (Sponheim et al., 2011). Interestingly, EEG recordings also showed significant changes in gamma oscillations, suggesting disrupting excitatory-inhibitory balance of intrinsic/local networks within neocortical GM. In another investigation which used fMRI, patients with TBI consistent with DAI showed decreased interhemispheric functional connectivity between the hippocampus and anterior cingulate cortex, which was correlated with delayed recall of verbal information (Marquez de la Plata et al., 2011). Together, these studies illustrate how DAI can disrupts cognitive networks via disconnecting WM tracts, but also introduces the potential for local changes in neocortical GM involving structural-functional alterations of excitatory and inhibitory neuronal systems.

Overall, these clinical tools used to assess neocortical network function measure *intrinsic* neocortical activity. The fMRI BOLD signal indirectly measures neural activity in discrete regions or nodes of neocortex . Specifically, the BOLD signal reflects synaptic

activity. By coupling fMRI with EEG, researchers found that the BOLD signal correlated with local field potentials (LFP), which in turn reflects intracortical processing of inputs (afferents) (Logothetis et al., 2001). EEG signals reflect excitatory synaptic activity (Buzsáki et al., 2012). The vast majority of excitatory synapses in the neocortex are from local projections in recurrent circuits (Douglas et al., 1995; Douglas and Martin, 2004, 2007). Specifically, on a microscopic subcellular level, this intracortical input processing is associated with subthreshold integrative processing of synapses along somato-dendritic domains of excitatory pyramidal neurons. Hence, LFP are the weighted average of synchronous somato-dendritic components of inputs signals of neural populations (Buzsáki et al., 2012). Since the majority of synapses within the neocortex are from local recurrent excitatory afferents, LFP oscillations reflect *local* neuronal activity. Further, BOLD signals are correlated with LFP synchronous activity at the gamma range frequency (Lauritzen, 2001; Logothetis et al., 2001; Mazzoni et al., 2010). As discussed above inhibitory interneuron networks coordinate gamma oscillations of neuronal assemblies of excitatory pyramidal neurons (Buzsáki and Draguhn, 2004). Therefore, the BOLD signal reflects the metabolic demand of such intrinsic coordinated excitatory-inhibitory interaction within intrinsic neocortical networks. The purpose of recurrent networks is to increase the gain of the relatively weak and sparse inputs from WM tracts (Douglas and Martin, 2007). Accordingly, alterations in WM connectivity can be influence intrinsic neocortical signal, reflected in either BOLD fMRI or EEG signals. However, information processing relies on balanced excitation and inhibition with neocortical networks (Atallah and Scanziani, 2009; Haider et al., 2006; Isaacson and Scanziani, 2011; Raichle, 2010). As mentioned, the majority of synapses within the

neocortex are recurrent excitatory synapses whose activity is coordinated by inhibitory interneurons (Markram et al., 2004). Since LFP reflects local activity, by extension this means the BOLD fMRI signal is largely independent of WM input. Rather, the BOLD signal reflects local metabolic activity of synchronized neural ensembles firing at the gamma range (Buzsáki et al., 2012; Logothetis et al., 2001).

Of special consideration is the use of 'inhibition' in the clinical setting. Inhibition has a clear definition in neuroscience. While ubiquitously used in the clinical setting, whether describing fMRI, EEG, psychometric testing, and/or motor responses, seldom is the neural basis of inhibition considered. It may not be surprising that GABAergic neurotransmission are in fact the neural basis for 'inhibition' of cognitive processes (Aron, 2007). While several clinical functional studies of mTBI have reported changes in 'inhibition', the neuronal constituents have not been considered. Specifically, the coordinated activity of neocortical-integrated information processing across networks is also reflected in LFP (Donner and Siegel, 2011; Siegel et al., 2012; Varela et al., 2001). This coordinated activity underlies the (fast) oscillations in the gamma range frequency seen during EEG recordings and the spontaneous fluctuations of the BOLD signal during resting state fMRI (Schölvinck et al., 2010). A crucial feature of this activity is that it is synchronized and the mechanism by which this occurs is mediated by GABAergic interneurons. Specifically, the synchrony is in the gamma frequency range, which is regulated by fast-spiking parvalbumin (PV) interneurons that target the perisomatic domain of pyramidal neurons (Bartos et al., 2007; Buzsaki, 2004; Cardin et al., 2009; Galarreta and Hestrin, 2001; Sohal et al., 2009). The origin of the gamma oscillations generated by neural ensembles scales back the intrinsic membrane properties of fast-

spiking inhibitory interneurons (Buzsáki, 2006). In the same vein, discussion of the neuronal unpinning's is absent in EEG studies that determine functional connectivity between nodes via coordination of neocortical activity by measuring time-frequency based phase synchronization (Han et al., 2014; Sponheim et al., 2011). Here, GABAergic neurotransmission mediated by PV+ interneurons is also at work, involved in both synchronizing and phase-locking homotypic neuronal assemblies at distributed across regions of neocortex (Buzsáki et al., 2007; Kim et al., 2016; Varela et al., 2001). It is thought that alignment of distributed nodes rhythmic activity (phase-locking) underlies structural-functional linkage of large-scale networks. Notwithstanding the de facto involvement of intrinsic neocortical circuits and networks, the vantage point of functional studies to date regards changes following mTBI exclusively as downstream consequences of WM tract DAI.

1.8.4 Clinical Summary

Progress in neuroimaging has afforded several critical insights toward understanding the full spectrum of mTBI structural-functional sequelae. Converging evidence now suggests that more subtle structural and functional disconnection of neocortical networks underlies cognitive impairment seen after mTBI. Although mTBI pathophysiology remains unclear, it is now recognized that microscopic DAI contributes to mTBI morbidity (Smith et al., 2013). It has been assumed that this DAI elicits neocortical network disconnection primarily via the WM tracts' vulnerability for deformation (Sharp et al., 2014). As noted, this belief stemmed primarily from human post-mortem examination and was later reinforced by DTI of patients with TBI, which both revealed DAI signatures in the

SCWM, corpus callosum, and other deep WM tracts (Blumbergs et al., 1994; Sharp and Ham, 2011). While across the spectrum of TBI severity WM involvement cannot be dismissed (Kinnunen et al., 2011; Mayer et al., 2010), this presumption remains controversial in mTBI (Dodd et al., 2014; Ilvesmäki et al., 2014). Several groups reported clinically diagnosed mTBI marked by substantial cognitive impairment without significant WM involvement. This suggests an undetected structural-functional pathophysiology within neocortical GM, where local (intrinsic) network processing relies on balanced excitatory-inhibitory neural activity (Haider et al., 2006). Supporting this possibility, studies measuring neocortical metabolic (fMRI) and electrophysiological (EEG) change, revealed a wide range of intrinsic neocortical network dysfunction involving abnormal spontaneous, rhythmic, and excitatory-inhibitory activity (Bashir et al., 2012; Huang et al., 2009a; Luo et al., 2013; Palacios et al., 2017; Sponheim et al., 2011; Tremblay et al., 2015; Zhang et al., 2012). Additionally, recent DTI studies of neocortical GM have detected reactive changes suggesting that mTBI disrupts local structural connectivity (Bouix et al., 2013; Ling et al., 2013; Newcombe et al., 2011). Collectively, these clinical findings strongly implicate that mTBI disrupts structural and functional connectivity in local neocortical networks formed by excitatory (glutamatergic) pyramidal neurons and inhibitory (GABAergic) interneurons (Guerriero et al., 2015). Since fMRI cannot resolve excitatory vs. inhibitory neuronal activity and DTI is insensitive to GM axonal changes (Hagmann et al., 2006; Logothetis, 2008), to understand the full scope of mTBI-induced alterations it is necessary to study neocortical networks on the microscopic level, where neurons form local networks that are the fundamental computational modules (DeFelipe et al., 2003; Mountcastle, 1979).

Although clinical studies provide crucial information regarding the clinical sequelae of TBI, in order to move forward, animal models must be investigated to determine the underlying neuropathophysiological substrates of traumatically induced neocortical dysfunction.

1.9 Experimental TBI Studies

Human studies are limited in scope when probing for neuropathophysiological sequelae after TBI. Although these issues are extremely difficult to rigorously assess in humans, our lab and others critically evaluated (m)TBI-induced circuit/network disruption. Experimental TBI investigations enable the integrated analysis of structural, functional, and behavioral endpoints. The utility and validity of rodent models in studying human-relevant TBI is well documented (Lifshitz et al., 2016). In the absence of any abnormalities after routine MRI, a significant correlation was found between DTI metrics and density of APP immunoreactive axonal swellings was found (Spain et al., 2010). Similarly, ex vivo DTI findings mapped to regions of axonal debris visualized using silver staining (Hylin et al., 2013). Further, human mTBI behavioral alterations can be reproduced experimentally, including neurological suppression (i.e. LOC measuring via loss of righting reflex; LORR), motor (e.g. balance) deficits, as well as impaired learning and memory (Grimm et al., 2015; Hylin et al., 2013). These behavioral findings were consistent with evidence of trauma-induced change at the cellular level. Specifically, immunohistochemical (IHC) labeling of various biomarkers indicated inflammation in the absence of cell death (Hylin et al., 2013; Spain et al., 2010). Alterations in resting-state fMRI of anesthetized rats were directly correlated with learning and memory

deficits and recovery postinjury (Heffernan et al., 2013). Hence, these studies highlight that rodents are good models of accessing structural and functional changes that are relevant to human mTBI (Lifshitz et al., 2016; Shultz et al., 2016).

1.9.1 Experimentally Induced DAI and Anterograde Sequelae

Historically, various injury paradigms have been used to generate brain damage in both large gyrencephalic (pigs) and small lissencephalic (mice/rats) animal models. WM tract DAI has been studied in pigs exposed to non-impact inertial brain trauma. Interestingly, this large gyrencephalic animal model of mTBI, rapid changes in acceleration-deceleration also generated DAI within neocortical GM. Specifically, pyramidal neuron perisomatic axonal injury (PSAI) was observed and associated with gliosis (Ross et al., 1994). In the rodent mild midline central fluid percussion injury (cFPI) model, our lab and others demonstrated consistent and reproducible DAI generation in both WM tracts and neocortical GM (Baker et al., 2002; Hånell et al., 2015b; Lifshitz et al., 2016; McGinn et al., 2009; Reeves et al., 1995; Ziebell et al., 2012). Similarly, in these rodent models of mTBI, neocortical DAI was also associated with gliosis similar to pig studies and also diffusion kurtosis imaging in human mTBI (Kelley et al., 2007; Ling et al., 2013; Ross et al., 1994).

Although the experimental evidence is limited, and direct clinical evidence is lacking, the underlying assumption is that DAI resulting in more divergent disconnection via widespread nerve terminal deafferentation underlies morbidity across the spectrum of TBI severity (Povlishock and Katz, 2005). In an important study, the course of nerve terminal loss and recovery was assessed following moderate FPI in a cat (Erb and

Povlishock, 1991). Specifically, the investigation capitalized on the dense GABAergic perisomatic innervation of neurons populating the dorsal lateral vestibular nucleus (DLVN), which allowed for IHC visualization of GABAergic puncta at both LM and EM levels. Within 1 week postinjury, scattered axonal damage was seen throughout the DLVN, with some neurons demonstrating loss of perisomatic GABA-immunoreactive puncta, while other somata appeared unchanged. Importantly, ultrastructural analysis demonstrated degenerating GABAergic terminals, which correlated with loss of immunoreactive puncta upon light microscopy. This loss was followed by the period of recovery occurring 2 – 12 months postinjury, in which light and electron microscopy findings also directly correlated. Interestingly, nascent GABAergic terminals re-innervation occurred at previously deafferentated perisomatic sites, suggesting traumatically induced DAI followed by terminal loss may set the stage for adaptive neuroplastic mechanisms.

Considering the arborization of axonal terminals occurs near synaptic sites, DAI may have more profound remote consequences (Povlishock et al., 1992). Specifically, the divergent effect of disconnecting the distal axonal arbor may explain certain aspects of initial morbidity and recovery seen in human mTBI (Povlishock and Katz, 2005). Further, imbalanced excitation-inhibition may exacerbate the burden of DAI with attendant deafferentation leading to more severe morbidity. It is well documented that more severe TBI induces widespread neuronal depolarization leading to excitotoxicity (Barkhoudarian et al., 2011; Guerriero et al., 2015). Coupled with DAI, trauma evoked neuroexcitatory injury appears to result in a maladaptive response upon deafferentation-induced synaptic plasticity (Phillips and Reeves, 2001). Such a combined effect of DAI

and unbalanced excitation has major implications in the initial pathogenesis underlying morbidity and subsequent reorganization and/or repair after human brain trauma. Together, these studies suggest the fate of neural reorganization varies with injury severity (Erb and Povlishock, 1991; Patel et al., 2016; Phillips et al., 1994). Mild-to-moderate TBI induced nerve terminal loss, followed by recovery of homotypic synaptic inputs at initially deafferentated sites, may lead to adaptive neuroplasticity and recovery (Erb and Povlishock, 1991; Patel et al., 2016). In contrast, reactive neuroplasticity after more severe TBI yielding a disparate profile of nascent/heterotypic synaptic inputs may lead to maladaptive structural reorganization causing progressive circuit/network dysfunction (Phillips and Reeves, 2001).

1.9.2 mTBI-Induced Excitatory-Inhibitory Disruption of Hippocampal Circuits/Networks

To date, TBI-induced disruption of circuit/network balance of excitation-inhibition has focused on the hippocampus. Postmortem examinations of TBI patients often reveal damage to the hippocampus prompting experimental investigation of this region (Cohen et al., 2007; Graham et al., 1995). Interestingly, in rodent models of TBI shifts in the balance of excitation and inhibition were attributed to loss of GABAergic neurons and their respective synapses on glutamatergic neurons, and in some cases correlated with cognitive deficits (Lowenstein et al., 1992; Reeves et al., 1997; Toth et al., 1997; Witgen et al., 2005). Experimentally, the hippocampus and dentate gyrus (DG) of rodent brains provide a feasible means of studying circuit behavior due to the well-characterized and stereotyped connectivity (Cohen et al., 2007). Information flows into the circuit via the perforant path of the enterohinal cortex, which synapses with dendrites of granule cells

populating the DG The input-output activity of granule cells is tightly regulated by hilar interneurons via feed-back mechanisms that modulate the DG, effectively rendering it as a filter mechanism for aberrant/excessive input. Information from the DG then is relayed to CA3, which amplifies the signal before sending it to CA1, where the signal is transduces and relayed back to the neocortex (Hollrigel et al., 1996; Phillips and Reeves, 2001; Witgen et al., 2005).

As discussed previously, trauma-induced widespread neuronal depolarization leading to excitotoxic pathobiology has been demonstrated extensively in both clinical and experimental settings (Barkhoudarian et al., 2011; Cantu et al., 2015). Pathological neuroexcitatory processes involve N-methyl-D-aspartate (NMDA) receptors, which have a key role in hippocampal long-term potentiation (LTP), hence may interfere with learning and memory functions (Reeves et al., 1995). Using in vivo recordings of field excitatory postsynaptic potential (fEPSP) in anesthetized rats whose brains were subjected to moderate FPI, Reeves and associates demonstrated persistent hippocampal LTP deficits, contrasted by transient neuronal excitability changes. Specifically, LTP of the Schaffer collateral system (CA3→CA1) was compromised postinjury and did not recover within 15 days. In contrast, population spikes reflecting pyramidal neuron discharging was elevated at 2 days postinjury but subsequently returned to baseline within 15 days. Together, these results suggest differential impairment of extrinsic (synaptic) and intrinsic (neuronal excitability) mechanisms.

A similar dichotomy between neuronal excitability and synaptic efficacy was also observed in a later study that addressed the effects of TBI on recurrent inhibition in the hippocampus and dentate gyrus (Hunt et al., 2011). Strength of recurrent inhibition was

determined by measuring evoked responses to orthodromic paired-pulse stimulation in a similar animal preparation as above. Agreeing with increased pyramidal excitability within the Schaffer collateral system, recurrent inhibition was deceased at 2 days post injury. In contrast, recurrent inhibition of granular cells in the dentate gyrus was increased at 2 and 15 days postinjury. Interestingly, this correlated with increases in GABA-immunoreactivity within the DG. Moreover, low stimulus (below threshold for population spikes) of Schaffer collaterals evoked fEPSPs with increased paired-pulse facilitation in CA1 at 2 days, perhaps explaining the increased excitability observed in the previous experiment. Collectively, these two experiments shed light on the effect of TBI on recurrent inhibitory pathways, creating a more complete picture of the events that disturb the balance of excitation (excitotoxicity) and inhibition. Furthermore, it demonstrates that inhibitory systems can either undergo primary damage at the time of injury, or respond with compensatory changes to counterbalance neuroexcitation, which would prevent further damage and restore balance of excitation and inhibition.

Interestingly, a study employing a similar model, in vitro slice recordings revealed decreased feed-forward inhibition of granule cell discharge (Toth et al., 1997). Specifically, 7 days after injury, fEPSP recordings of perforant path-evoked granule cell responses revealed a prominent decrease in feed-forward $GABA_A$ receptor mediated inhibition of granule cell discharges. Loss of feed-forward inhibition correlated with decreased frequency of miniature inhibitory postsynaptic currents (mIPSC) measured by whole-cell patch clamp. However, there were no changes in the amplitude and kinetic properties of $GABA_A$ receptor mediated synaptic events, indicating loss of presynaptic input. Consistent with electrophysiological data, IHC labeling showed decreased

immunoreactivity of GABAergic interneuron subsets known to play a central role in perforant path feed-forward inhibition of granule cells. Additionally, silver stain indicated that these interneurons were damaged instantaneously post-trauma. Further, abnormal excitation and inhibition demonstrated by these studies has been correlated with hippocampal-dependent cognitive impairment. Collectively, experimental TBI investigations of hippocampal circuit/network disruption add credence to the premise that TBI not only evokes electrophysiological disequilibrium via neuroexcitatory mechanisms, but also through regional variable alterations of inhibitory neuromodulation.

The precise functional consequences of network reorganization during long-term recovery remain poorly understood. Nonetheless, the studies described above show the role of not only excitatory but also inhibitory mechanisms causing electrophysiological abnormalities. Critically, experimental TBI studies of hippocampal circuit/network disruption show primary injury to subsets of GABAergic interneurons. In addition to electrophysiological changes associated with GABAergic loss, studies have also shown inhibitory interneurons are involved in subsequent neuroplasticity with the hippocampus/dentate gyrus. Specifically, a counterbalanced profile consisting of increase of excitatory drive to inhibitory neurons that provided decreased GABAergic inputs to some of the respective glutamatergic neurons was observed postinjury (Hunt et al., 2011). Although the functional consequences of this example of network remodeling after TBI remain unknown, such rewiring may either reflect a compensatory/maladaptive response or contribute to network destabilization via unbalanced excitation and inhibition in the posttraumatic dentate gyrus.

In summary, these experimental TBI studies demonstrate shifts in the balance of excitation and inhibition involving primary GABAergic interneuron injury and loss respective synapses on postsynaptic glutamatergic neuron. While highlighting the important role of inhibition in TBI-induced circuit/network disruption, it is crucial to emphasize that most of these studies were focused on mechanisms of post-traumatic epileptogenesis, which is not associated with mTBI morbidity (Alexander, 1995; Hunt et al., 2013; Pitkänen and McIntosh, 2006). Specifically, these studies use moderate-to-severe animals models of TBI that induced cell death, which is also inconsistent with mTBI pathobiology (Greer et al., 2011; Kelley et al., 2006; Singleton et al., 2002). Therefore, the effect of mTBI on neocortical circuits/networks remains poorly understood. However, recent advances by our lab have shed new light on both structural and functional mechanisms of circuit/network disruption.

1.9.3 Local Neocortical Network Disruption after mTBI in Transgenic Mice

Our lab has begun to critically evaluate the potential for mTBI-induced neocortical change using a well-controlled mouse model of mTBI. Specifically, following experimental mTBI using transgenic mice, we observed primary neocortical damage involving scattered DAI within a subset of layer 5 pyramidal neurons expressing a yellow variant of green fluorescent protein (YFP) labeling the soma as well as their dendrites and axons (Greer et al., 2011). A unique advantage in this approach is the ability to identify intact and traumatically injured axons by via routine fluorescent microscopy. Exploiting cytosolic fluorescent protein expression we conducted structural and functional assessments within neocortical GM of both DAI and non-DAI (intact) populations in a

discrete subset (Thy1-expressing) of long-distance projecting excitatory pyramidal neurons (Greer et al., 2012, 2013). Capitalizing on restricted neuronal labeling with YFP including the total axonal length, readily traceable within the neocortical gray, allowed the unequivocal identification of mTBI-induced DAI vs. non-DAI/intact populations in both fixed tissue sections and live slices.

We reported that the retrograde consequences of DAI do not involve cell death (Singleton et al., 2002) by showing retrograde activation of c-Jun via phosphorylation (p-c-Jun), a nuclear transcription factor associated with cell survival and axonal regeneration (Greer et al., 2011; Raivich et al., 2004; Wang et al., 2013). Additional, we reported that DAI within this pyramidal neuron subset primarily occurred near the soma of origin (Greer et al., 2013). Specifically, mTBI induces DAI primarily within the axon initial segment (AIS) of the YFP+ layer 5 pyramidal neurons (Greer et al., 2013). Thus, perisomatic axonal injury (PSAI) is significantly associated with retrograde p-c-Jun nuclear expression. Additionally, in a former publication we showed that APP did not colocalize with YFP axons in either the SCWM or corpus callosum (Hånell et al., 2015b). We also found that this same PSAI was unresponsive to therapeutic targeting that proved neuroprotective within the underlying SCWM and corpus callosum. Importantly, these findings suggested DAI within neocortical GM vs. the underlying WM tracts involved different pathophysiological mechanisms. Taken together, these findings also strongly support the premise that virtually all YFP+ pyramidal neuron DAI occurs within the neocortical gray. Based on this premise, YFP+ pyramidal neurons undergoing DAI can be reliably identified by examining their axonal segment spanning neocortical layers 5/6 to the SCWM interface.

Further exploiting this model allowed for precise electrophysiological analysis, and thereby structure-function relationships of neurons altered by TBI. Using *ex vivo* slice preparations of injured cortex, whole-cell patch-clamp was used to measure various neurophysiologic parameters. In concert with neocortical DAI we also observed widespread electrophysiological abnormalities among intact pyramidal neurons associated with local network hyperexcitability post-mTBI (Greer et al., 2012; Hånell et al., 2015a; Sun and Jacobs, 2016). Specifically, intact pyramidal neurons were readily identified by following YFP+ axons from their soma of origin to the SCWM interface (Greer et al., 2012). For both populations of neurons, there was an initial trend toward hypoexcitability, followed by a persistent decreased excitability for the DAI population, yet a trend toward hyperexcitability of the intact neurons. Interestingly, 2 day postinjury intrinsic bursting activity is lost within the intact population, yet the slope of frequency of action potential discharge versus injected current is increase, suggesting an overall state of hyperexcitability. Perhaps even more biologically significant was our parallel observation that the non-DAI (intact) YFP+ neuronal population showed altered electrophysiological properties without any evidence of overt structural damage. Over time, these same intact YFP+ pyramidal neurons became hyperexcitable, entirely consistent with some form of mTBI-induced circuit disruption within local neocortical networks. At present, the neurobiological basis for this hyperexcitability in this intact neuronal population remains unknown. While several different mechanisms can alter neuronal excitability, our observations are most consistent with structural-functional changes within the axon initial segment (AIS), the site of action potential (AP) generation (Kole et al., 2008; Popovic et al., 2011). While we found increased excitatory

neurotransmission contributes to network dysfunction, our data also implicated GABAergic interneuron involvement. Since GABAergic interneurons regulate neocortical network activity (Isaacson and Scanziani 2011), these findings strongly implicated inhibitory interneuron disruption (Lazarus et al., 2015; Yizhar et al., 2011; Zhou et al., 2009).

These observations have major implications in both the initiating pathobiology and subsequent reorganization associated with brain injury. The fact that the DAI neurons did not die, instead falling into a hypoexcitable state has important long-term implications as it has been demonstrated previously that injured neurons undergo atrophy but may also generate axonal sprouts. Such a neuroplastic response in the neocortex, a convoluted neural web, would likely form inappropriate synapses that make shift the balance of excitation-inhibitions and/or cause general neural circuit failure (Hånell et al., 2015a). In terms of the pathophysiological sequelae of head injury, the loss of bursting activity within the intact population, suggests a novel and more subtle form of axonal injury (function disruption). A recent report, shows pharmacological inhibition of voltage-gated sodium channels within the first node of Ranvier inhibits bursting activity in layer 5 pyramidal neurons (Kole, 2011). Also, it has been shown that axon stretch can induce sodium channel dysfunction and altered expression at injury thresholds below those producing axon swelling (Yuen et al., 2009). Hence, an example of TBI evoked 'functional disruption' may be in the form of sodium channel alteration at the AIS. Lastly, the observation that the mTBI initial caused a decreased excitability in both the intact population and axotomized neurons implies local activity, ion, or neurotransmitter concentrations drive the underlying currents (Greer et al., 2012). Moreover, as it appears

that the intact neurons gradually recover from an initial hypoexcitable state, by 2 days postinjury they have progressed to a hyperexcitable state. Whether this is a compensatory response remains to be determined, as well as resolving adaptive from maladaptive alterations in neuronal excitability. Because neocortical pyramidal neuron AIS function is strongly regulated by perisomatic GABAergic synaptic transmission from PV+ interneurons, concomitant involvement of these inhibitory inputs could potentially induce changes in AIS structure-function after mTBI (Buffington and Rasband, 2011). Collectively, these observations have profound implications in overall neocortical network disruption with concomitant shifts in excitation and inhibition, and the structural and functional substrates underlying processes that contribute to morbidity following mTBI.

Although other investigations of excitatory-inhibitory imbalance have shown neocortical GABAergic interneuron changes, these were in the context of cell death using models of blunt-force trauma or more severe TBI involving mass lesions/contusion to model epileptogenesis, which is not an outcome of clinical or experimental mTBI (Cantu et al., 2015; Carron et al., 2016; Hsieh et al., 2016; Kobori and Dash, 2006). Further, while cell death was for many years viewed as the primary contributor to morbidity after TBI, it is now recognized that mTBI pathophysiology conditions ensue without neuronal loss (Andriessen et al., 2010; Farkas and Povlishock, 2007). Thus, it remains unknown if loss of GABAergic interneuron control over neocortical networks excitatory-inhibitory balance via DAI after mTBI.

1.10 Potential Cellular and Neurophysiologic Substrates of Neocortical Disruption

Converging evidence provided by our lab and others underscores that TBI involves both excitatory and inhibitory systems. This could occur through multiple mechanisms involving perturbation of *intact* pyramidal neuron AIS and/or PV+ interneuron axons. Information processing occurs in anatomically distinct neocortical gray regions (nodes) via balanced interplay between excitatory-inhibitory systems. Collectively, these clinical findings strongly implicate that mTBI disrupts structural and functional connectivity in local neocortical networks formed by excitatory (glutamatergic) pyramidal neurons and inhibitory (GABAergic) interneurons.

1.10.1 The Axon Initial Segment

At the neuronal level, the dynamics between extrinsic/synaptic and intrinsic AIS properties underlie neuronal coding, whereby analog signal inputs are propagated via digital output (Gerstner et al., 1997; Gütig and Sompolinsky, 2009; Shadlen and Newsome, 1994). The AIS is a conserved structure with a highly developed sub-axolemmal cytoskeleton integrated with a unique extracellular matrix via cell adhesion molecules (Hedstrom et al., 2007; Ogawa and Rasband, 2008; Rasband, 2011). Specifically, the AIS is a critical subdomain regulating neuronal excitability by integrating synaptic (excitatory and inhibitory) input to determine whether to fire an action potential AP, thereby acting as a gatekeeper of neuronal output (Kole and Stuart, 2012). The high density of voltage-gated sodium channels (NaV) at the distal AIS sets the threshold for action potential generation (Kole et al., 2008; Van Wart et al., 2007). Ankyrin-G (ankG) is the structural protein regulating neuron excitability via clustering voltage-gated sodium channels (NaV) (Hedstrom et al., 2008). Ankyrin-G (ankG), a

widely used AIS marker, is the master structural organizer that clusters ion channels via linkage to the sub-axolemmal cytoskeleton (Grubb and Burrone, 2010b). In pyramidal neurons, NaV1.6 density at the distal AIS sets the threshold for action potential initiation (Kole et al., 2008). AIS gatekeeping of neuronal excitability, which is modulated by activity-dependent structural plasticity, highlights its crucial role in network function.

Several reports demonstrate how changes in presynaptic input/activity can induce AIS structural and functional plasticity. Importantly, presynaptic input fine-tunes excitability via AIS structural plasticity (Grubb and Burrone, 2010a; Gutzmann et al., 2014; Kuba et al., 2010). Specifically, Kuba and associates (2010) showed that cochlear deprivation, which decreased presynaptic excitatory input, results in postsynaptic AIS elongation correlated with increased neuronal excitability. Further, Gutzmann and colleagues (2010) demonstrated AIS length dynamics in the visual cortex during the critical period in visual development could be altered by ocular deprivation. This homeostatic fine-tuning of AIS structure has been associated with neuronal information processing (Grubb et al., 2011; Kuba, 2012). The AIS ion channel distribution differs across neuronal subtypes (Lorincz and Nusser, 2008), and even within a neuronal subtype substantial variability exists in position and length (Bender and Trussell, 2012). Recent reports from other labs showing that in rodent neocortex, AIS length from the distal end appears to be more dynamic than its position with respect to the soma of origin . Also, layer 5 pyramidal neurons, which are subdivided into layer 5a and 5b and populated by multiple subtypes characterized by different morphological and electrophysiological properties (Chagnac-Amitai et al., 1990; Hattox and Nelson, 2007; Le Bé et al., 2007).

1.10.2 GABAergic Interneurons

Processed information is transmitted by excitatory (glutamatergic) pyramidal neurons, representing 80% of neocortical neurons, via long-distance projections that comprise white matter tracts connecting intra- & inter-hemispheric nodes (Somogyi et al., 1998). In order to be functionally useful, information processed at the neuronal level needs to be integrated across networks (Kepecs and Fishell, 2014; Mesulam, 1990). However, excitatory networks are intrinsically unstable and have extremely time-limited dynamics, therefore require modulation via inhibitory inputs from locally projecting GABAergic interneurons (Kepecs and Fishell, 2014; McBain and Fisahn, 2001). While excitatory pyramidal neurons comprise 80% of neocortical neurons, their activity is controlled by the remaining 20% of inhibitory interneurons (Markram et al., 2004).

The largest neocortical GABAergic interneuron subclass (40–50% of all interneurons) is genetically/molecularly characterized by PV expression and physiologically via their fast-spiking action potentials (Rudy et al., 2011). PV+ interneurons are a well-characterized subtype that control integration of excitatory activity in individual pyramidal neurons and within neuronal networks. In the neocortex, the balance of excitation-inhibition is regulated by PV+ interneurons that are highly interconnected with local pyramidal neurons (Hu et al., 2014). Although they represent ~10% of neocortical neurons, PV+ interneurons are the dominant source of inhibition in the neocortex. A critical feature of the interplay between synaptic transmission and intrinsic neuronal excitability is perisomatic inhibitory input, which strongly regulates pyramidal neuron AIS output (Freund and Katona, 2007). This proximity of PV+ terminals to the AIS allows for strong inhibitory control over AIS output. PV+

interneurons have powerful inhibitory control between excitatory drive and action potential firing rate in pyramidal neurons due to the proximity of their GABAergic synapses to the AIS. By controlling the gain of pyramidal neuron firing dynamics, PV+ interneurons fine-tune excitatory-inhibitory balance, sharpening neocortical responses and increasing computational power (McBain and Fisahn, 2001). Further, PV+ interneurons are highly interconnected and orchestrate neocortical network information processing by entraining large groups of pyramidal neurons to fire synchronously (Bartos et al., 2007; Salkoff et al., 2015). Specifically, the expansive axonal arbors of PV+ interneurons highlight their role in balancing neocortical excitation-inhibition to synchronizing neuronal ensembles, which play major roles in plasticity and behavior (Kepecs and Fishell, 2014). The extensive axonal arbor of a single PV+ interneuron can innervate up to a thousand neighboring postsynaptic neurons (Howard et al., 2005; Packer and Yuste, 2011). In turn, PV+ interneurons receive converging inputs from excitatory pyramidal neurons (Buhl et al., 1997; Tamás et al., 2000) and other PV+ interneurons (Pfeffer et al., 2013), forming highly interconnected local neocortical networks that underlie gamma oscillations seen during cognitive loading (Howard, 2003). Operationally, the strong and selective connectivity between PV–PV interneurons leads to disynaptic disinhibition forming powerful local neocortical networks (Kuhlman et al., 2013). Since PV+ interneurons sample heavily from local pyramidal neuron ensembles that they coordinate, PV+ interneuron activity reflects a summary of local neocortical activity (Scholl et al., 2015). Hence, PV+ interneuron firing is a ‘pulse’ of local excitatory-inhibitory network activity (Trachtenberg, 2015). Multi-nodal rhythmic activity is thought to underlie cognition (Donner and Siegel, 2011; Hipp et al., 2012;

Siegel et al., 2012; Varela et al., 2001). PV+ interneuron activity increases and facilitates during neocortical information processing (Cardin et al., 2009; Sohal et al., 2009). Both clinical and experiment mTBI studies have shown changes in these local neocortical firing patterns, which reflect changes in excitatory-inhibitory balance and information processing/encoding (Engel et al., 2001; Fries, 2009; Paterno et al., 2016; Scheeringa et al., 2011; Sponheim et al., 2011).

1.11 Chapter Summary

Considering the preponderance of pyramidal neurons and the vital role of their respective AIS for information processing, as well as the instrumental role of PV+ interneurons, it is not surprising that disruption of these systems has been suggested in mTBI, as well as several other neurological disorders (Buffington and Rasband, 2011; Gogolla et al., 2009; Hinman et al., 2013; Imbrosci and Mittmann, 2011; Kaphzan et al., 2011; Lewis, 2013; Yizhar et al., 2011; Zhou et al., 2009). In the subsequent chapters we address these issues using a clinically relevant mouse model of mTBI that evokes both WM tract and neocortical DAI without mass lesions and/or contusion. Using multifaceted approaches, we measured the dynamic structural-functional properties of the pyramidal neuron AIS and PV+ interneuron axons, representing crucial components of the major neocortical excitatory and inhibitory systems, respectively.

In Chapter 2, we describe our study that continued to exploit the YFP-H mouse line to examine to assess for AIS plasticity of intact layer 5 pyramidal neurons as a potential postsynaptic response to neocortical circuit disruption after mTBI. In this study we operational defined the synaptic interconnectivity between inhibitory PV+

interneurons (presynaptic) and excitatory pyramidal neurons (postsynaptic) as a neocortical microcircuit. Specifically, we assessed for monosynaptic circuit disruption via loss of PV+ interneuron inputs, a major source of GABAergic inhibition, along the perisomatic domain of intact layer 5 pyramidal neurons at 2 d post-mTBI. Pyramidal neuron AIS output (intrinsic activity) mediated by PV+ interneuron input (extrinsic/synaptic activity) sets the perisomatic domain as an interface for excitation and inhibition, respectively.

Additionally, in Chapter 3, we built upon this strategy by employing cre/lox mice to specifically label the total population of neocortical PV+ interneurons with tdTomato, a red fluorescent protein variant, enabling us to probe for mTBI-induced local (small-scale) neocortical inhibitory network disruption via GABAergic interneuron DAI. In this study we operational defined the PV–PV interneuron interconnectivity as a small-scale neocortical network. The affect of mTBI forces on PV+ interneuron axons was evaluated using traditional methods coupled with novel approaches. Specifically, we assessed PV+ interneuron axon morphology and also retrograde signaling in the somas of origin from 3 h to 1 d post-mTBI to determine if this local inhibitory network was structural disconnection. Since PV+ interneurons strongly and selectively inhibit one another, by adding glutamatergic blockers we pharmacologically isolated GABAergic neurotransmission, affording a means to probe for functional disconnection with this small-scale neocortical network.

In Chapter 4 we discuss how our experimental observations of structural and functional changes provide direct evidence for disruption of excitatory-inhibitory balance in local neocortical circuits/networks. Lastly, we discuss the implications of our

experimental findings in operationally defined microcircuit and small-scale neocortical networks for mechanisms of structural-functional disruption that underlying cognitive impairment after mTBI.

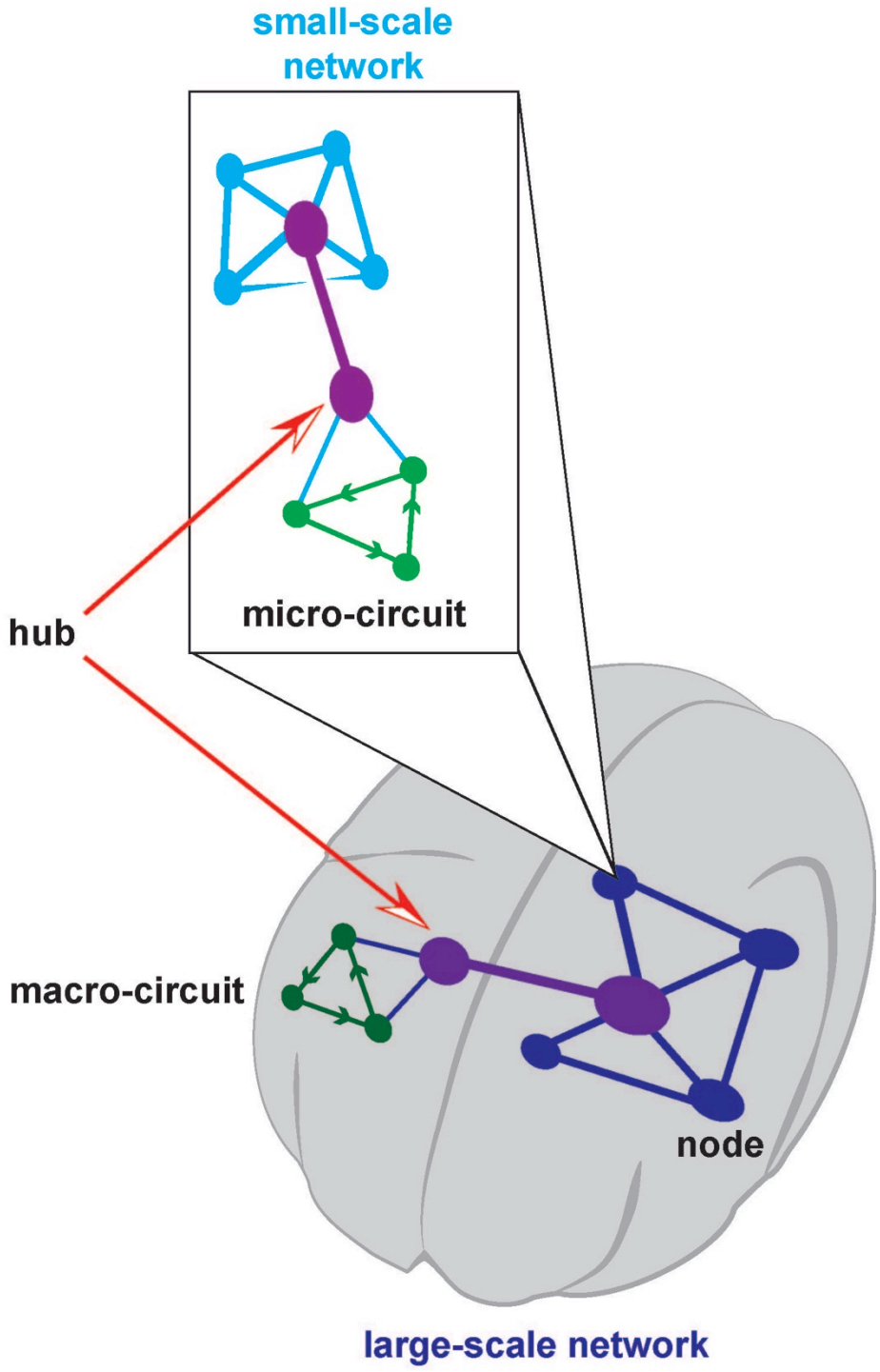

Figure 1.1. Scale-free, small-world neocortical networks.

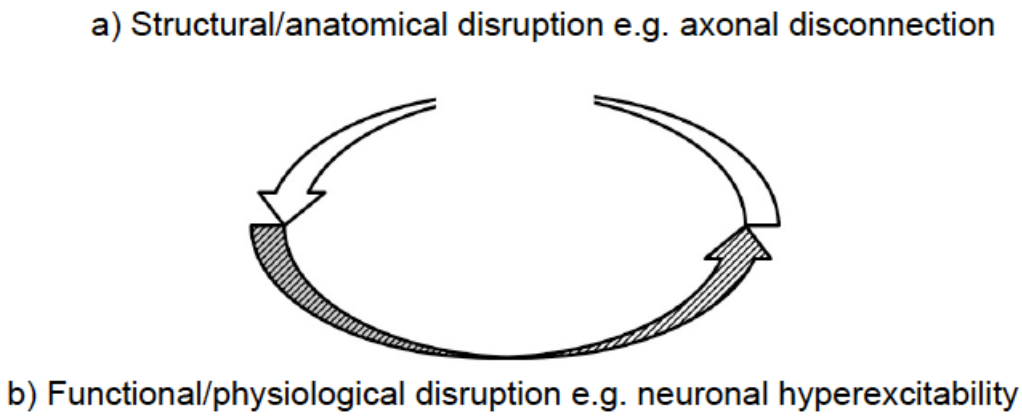

Figure 1.2. Structural and Function Circuit Disruption.

CHAPTER TWO

Intact Pyramidal Neuron Axonal Initial Segment Structural and Functional Plasticity Occurs in Concert with Diffuse Disconnection of Neocortical Circuits after Mild Traumatic Brain Injury

Michal Vascak, Jianli Sun, Matthew Baer, Kimberle M. Jacobs, John T. Povlishock

ABSTRACT

The axon initial segment (AIS) is the site of action potential (AP) initiation and a crucial regulator of neural activity. Homeostatic fine-tuning of AIS structure has been associated with neuronal information processing. In sensory circuits, altered presynaptic input induces AIS plasticity that modifies neuronal excitability. Ankyrin-G (ankG) is the structural protein regulating neuron excitability via clustering voltage-gated sodium channels (NaV). In pyramidal neurons, NaV1.6 density at the distal AIS sets the threshold for AP initiation. Recently, in mTBI-mice we demonstrated substantial electrophysiological changes in non-axotomized/structurally intact neocortical pyramidal neurons, consistent with AIS-specific alterations, and mTBI related circuit disruption. Since altered neural activity modifies AIS architecture and neuronal excitability, the current study sought to determine if mTBI induces AIS structural and/or functional plasticity within a specific, well-defined subset of intact pyramidal neurons. Thy1-YFP

mice exposed to either sham or mTBI were perfused 2-days postinjury. Antibodies to ankG and NaV1.6 were used to fluorescently label the AIS. Confocal microscopy was employed to identify YFP+ intact pyramidal neurons in layer 5 of S1 barrel field, whose axons were continuous from the soma of origin to the subcortical white matter. Immunofluorescent profiles of ankG and NaV1.6 were then superimposed on YFP+ axonal traces to determine the proximal (start) and distal (end) positions from which length was computed. We found that while mTBI had no effect on ankG start position, the end position and length were decreased significantly. AIS shortening from the distal end corresponded to the peak NaV1.6 immunofluorescent signal, consistent with the site of AP initiation. However, NaV1.6 position or length did not change after mTBI. In concert with these AIS studies we quantitatively assessed GABAergic input along the perisomatic domain of intact layer 5 pyramidal neurons post-mTBI and found a significant decrease in GAD67+/PV+ bouton density. To probe for functional AIS plasticity we measured intrinsic properties using patch-clamp recordings in these same intact YFP+ pyramidal neurons, which revealed AP acceleration is attenuated post-mTBI. Collectively, these findings speak to a complex pattern of neocortical circuit disruption after mTBI involving changes in both intrinsic AIS structural-functional properties and extrinsic GABAergic perisomatic input.

INTRODUCTION

Traumatic brain injury (TBI) constitutes a major global healthcare problem that extracts a devastating personal and societal toll (Langlois et al., 2006). Historically, TBI research focused on severe head injuries associated with high-speed motor vehicle incidents. In

the last decade, the incidence of severe TBI decreased dramatically (Coronado et al., 2011; Thurman et al., 1999), with milder forms of TBI elicited by contact sports and blast waves during combat now predominating (Cassidy et al., 2004; Hoge et al., 2008; Holm et al., 2005). Mild TBI (mTBI) is frequently termed the 'silent epidemic' because of its relatively subtle nature typically occurring without any evidence of macroscopic brain damage such as contusion or hematoma formation (CDC, 2003; Povlishock and Katz, 2005). However, recent findings in patients with mTBI linking acute cognitive network dysfunction with potential life-long morbidity have captured the attention of media and raised public concern (Mannix et al., 2016). Despite the focus of current research shifting to mTBI, its cellular and physiological substrates remain controversial (Andriessen et al., 2010; Dodd et al., 2014). Using advanced structural neuroimaging of patients with mixed severity TBI multiple groups have demonstrated that diffuse axonal injury (DAI) occurs within various subcortical white matter (SCWM) tracts and callosal domains (Bazarian et al., 2007; Kinnunen et al., 2011; Mayer et al., 2010; Salmond et al., 2006). These findings led to the inference that white matter DAI causes cortical network dysfunction that underlies acute and/or chronic cognitive impairment (Sharp et al., 2014). However, other groups using the same imaging tools have not confirmed this finding in well-controlled studies of patients with mTBI and clinically significant cognitive dysfunction (Ilvesmäki et al., 2014; Mac Donald et al., 2011; Wäljas et al., 2014; Zhang et al., 2010). In fact, some reports suggest the potential for primary neocortical gray involvement (Bouix et al., 2013; Huang et al., 2016; Ling et al., 2013; Newcombe et al., 2011; Palacios et al., 2017; Tremblay et al., 2011), wherein local information processing relies on balanced excitatory and inhibitory unitary neuronal activity to support function of large-scale

distributed neurocognitive networks (Aron, 2007; Bullmore and Sporns, 2009; Haider et al., 2006; Haider and McCormick, 2009; Raichle, 2010). Several multi-modal studies using functional MRI and electrophysiological approaches have reported local neocortical network dysfunction following mTBI, supporting this premise (Bashir et al., 2012; Mayer et al., 2011; Sponheim et al., 2011; Tremblay et al., 2014).

Although these issues are extremely difficult to rigorously assess in humans, our lab critically evaluated the potential for mTBI-induced neocortical change in a well-controlled animal model. Specifically, following experimental mTBI using transgenic mice, we observed primary neocortical damage involving scattered DAI within a subset of layer 5 pyramidal neurons expressing a yellow variant of green fluorescent protein (YFP) labeling the soma as well as their dendrites and axons (Greer et al., 2011). Perhaps even more biologically significant was our parallel observation that the non-DAI (intact) YFP+ neuronal population showed altered electrophysiological properties without any evidence of overt structural damage (Greer et al., 2012; Hånell et al., 2015a; Sun and Jacobs, 2016). Over time, these same intact YFP+ pyramidal neurons became hyperexcitable, entirely consistent with some form of mTBI-induced circuit disruption within local neocortical networks (Wolf and Koch, 2016a; Zhang and Raichle, 2010). At present, the neurobiological basis for this hyperexcitability in this intact neuronal population remains unknown. While several different mechanisms can alter neuronal excitability, our observations are most consistent with structural-functional changes within the axon initial segment (AIS), the site of action potential (AP) generation (Kole et al., 2008; Popovic et al., 2011). The AIS is a critical subdomain regulating neuronal excitability by integrating synaptic input to determine whether to fire an AP, thereby

acting as a gatekeeper of neuronal output (Kole and Stuart, 2012). Specifically, the high density of voltage-gated sodium channels (NaV) at the distal AIS sets the threshold for AP generation (Hu et al., 2009; Kole et al., 2008; Van Wart et al., 2007). Ankyrin-G (ankG), a widely used AIS marker, is the master structural organizer that clusters ion channels via linkage to the subaxolemmal cytoskeleton (Grubb and Burrone, 2010b; Kole and Stuart, 2012). Importantly, presynaptic input fine-tunes excitability via AIS structural plasticity (Grubb et al., 2011; Kuba et al., 2010). Because neocortical pyramidal neuron AIS function is strongly regulated by perisomatic GABAergic synaptic transmission from parvalbumin (PV)-expressing interneurons (Cobb et al., 1995; DeFelipe and Fariñas, 1992; Freund and Katona, 2007; Hu et al., 2014; Somogyi et al., 1998; Wefelmeyer et al., 2015), concomitant involvement of these inhibitory inputs could potentially induce changes in AIS structure-function after mTBI (Buffington and Rasband, 2011).

To address these AIS-related issues, the current report builds upon our previous studies that utilized YFP-expressing transgenic mice in a well-characterized model of mTBI to examine the potential for changes in layer 5 pyramidal neuron AIS and its associated perisomatic domain, both of which are critical for regulating neuronal excitability. Specifically, to assess AIS structural plasticity, immunohistochemical approaches targeting ankG and NaV1.6 distribution were quantitatively assessed in the early stage post-mTBI using confocal microscopy. These assessments of AIS structural plasticity in non-DAI/intact layer 5 pyramidal neurons were also accompanied by parallel morphological studies examining perisomatic GABAergic presynaptic bouton density. Lastly, these imaging studies were interfaced with patch-clamp electrophysiology and computational modeling of layer 5 pyramidal neurons to establish a functional match

with the AIS structural plasticity posited above. Using these multifaceted approaches, we show for the first time that mTBI evokes structural plasticity at the distal AIS, occurring independent of detectable changes in sodium channel distribution, in a specific subset of neocortical neurons with intact axons. These same events within intact neurons were also recognized to occur in concert with PV+ GABAergic terminal loss at their perisomatic domain. Lastly, the observed intrinsic/postsynaptic (AIS) and extrinsic/presynaptic (perisomatic) structural plasticity within intact neurons were also accompanied by a reduction in AP acceleration, likely reflecting a change in sodium channel density. Collectively, these findings reshape our understanding of mTBI and have major implications as we continue to better understand the brain's response to milder injury in terms of the functionality of its intrinsic networks within neocortex.

METHODS AND MATERIALS

Animal maintenance and experimental protocols were approved by the Virginia Commonwealth University Institutional Animal Care and Use Committee and complied with principles in the National Research Council *Guide for the Care and Use of Laboratory Animals: 8th Edition*.

Breeding and genotyping of YFP-H transgenic mice

The Thy1-YFP-H line [B6Cg-TgN(Thy1-YFP-H)2Jrs, stock number 003782] was obtained from Jackson Laboratories (Bar Harbor, ME) and maintained as heterozygotes upon a C57BL/6J background. Inheritance of the fluorescent transgene was determined from an ear punch taken at weaning (~21 d). The tissue from the ear punch was mounted on a glass slide and examined using a FITC filter on an Olympus DP71 digital camera

(Olympus, Center Valley, PA) where YFP expression could easily be identified in mice that inherited the transgene. YFP expression in these mice is under the control of the neuronal specific Thy1 promoter, resulting in YFP expression within the neocortex that is primarily restricted to layer 5 pyramidal neurons (Feng et al., 2000).

Experimental Design

This study used a total of 18 young adult (age: 6–10 weeks; weight: 20–24 g) male mice randomly assigned to either sham-injury (control) or mTBI (experimental) groups. Based on our previous work showing mTBI consistently generates DAI within primary somatosensory barrel fields (S1BF), we assessed layer 5 intact YFP+ pyramidal neurons for AIS structural-functional changes at 2 d postinjury within this well-characterized region of neocortical gray matter. For confocal microscopy studies, a total of 11 mice (age 8–10 weeks) were surgically prepared for sham-injury (n = 5) or mTBI (n = 6) and perfused for immunohistochemical labeling of tissue sections. To identify the AIS we fluorescently labeled ankG, the master scaffolding protein that is widely used as a surrogate marker for AIS position and length (Grubb and Burrone, 2010b; Kole and Stuart, 2012). Additionally, we targeted NaV1.6, which sets the threshold for AP generation (Kole et al., 2008), to structurally assess the membrane channels underpinning AIS function/output. In addition to intrinsic/postsynaptic AIS structural plasticity within intact YFP+ pyramidal neurons, we assessed their perisomatic domain for extrinsic/presynaptic changes in GABAergic bouton density. To probe for any AIS functional plasticity correlated with potential structural changes we recorded intrinsic electrophysiological data from intact YFP+ pyramidal neurons in layer 5 of S1BF within *ex vivo* slice preparations from a total of 7 mice (age 6–8 weeks) at 2 d following sham-

injury (n = 3) or mTBI (n = 4). Lastly, we determined the functional consequences of any potential AIS structural changes using a realistic computational model of a layer 5 pyramidal neuron based on experimentally derived properties (Hallermann et al., 2012).

Surgical Preparation and central Fluid Percussion Injury

To model mTBI we used midline central fluid percussion injury (cFPI) first described by Dixon et al., (1987) using rats, which our lab modified for mice as described previously (Greer et al., 2011). Briefly, anesthetized mice were surgically prepared for cFPI induction by installing a hub surrounding a craniectomy centered on the superior sagittal suture, midway between bregma and lambda. Intraoperative rectal temperature was maintained at 37 ± 0.2°C using a thermostatically controlled heating pad (Harvard Apparatus). Additionally, heart rate (BPM), respiratory rate (RPM), and arterial blood oxygenation (SpO_2) were monitored using a thigh-clamp pulse oximeter sensor (MouseOx; STARR Life Sciences) to ensure maintenance of physiological homeostasis. After a post-operative recovery (~1.5 h), mice were re-anesthetized and then connected to the fluid percussion apparatus (Custom Design & Fabrication, Virginia Commonwealth University) forming a closed mechanical system. Releasing the pendulum, striking the piston in the fluid-filled cylinder generated a mild pressure wave (~12 ms) that was delivered onto the intact dura. This action simulates human brain inertial loading during trauma-induced rapid acceleration-deceleration causing a mild diffuse brain injury (Dixon et al., 1987). The peak amplitude (mean ± SEM) of the pressure wave (1.6 ± 0.03 atmospheres) was measured by a transducer and displayed on an oscilloscope (Tektronix TDS 210). For sham-injury, an identical procedure was used with the exception of the pendulum's release. Mice were disconnected from the apparatus immediately after injury

and visually monitored while removing the hub, suturing the incision, and checking reflexes. None of the mice showed signs of seizure or apnea. Severity of injury (peak amplitude) and duration of loss of righting reflex (LORR), a rodent behavioral surrogate of loss of consciousness (LOC), were recorded for each animal (Grimm et al., 2015). We determined the degree of mTBI by comparing LORR duration with shams (Morehead et al., 1994). After recovering from LORR, animals were transferred to a warmed cage to maintain normothermia and monitored before returned to the vivarium. Physiology data and LORR were statistically analyzed using unpaired *t*-tests.

Perfusion and Tissue Processing

Mice received a lethal dose of sodium pentobarbital (1.6 mg/g IP) 2 d postinjury. After loss of pain reflexes mice were transcardially perfused, first with heparinized (10 units/ml) saline for 1 min then 4% paraformaldehyde in Millonig's buffer pH 7.4 for 20 min. Brains were dissected and then sectioned coronally at 60 μm using a vibratome (Leica VT1000S). Sections directly below the craniectomy (bregma level −0.6 to −2.4 mm) were collected in 24-well plates filled with Millonig's buffer pH 7.4. To quantitatively assess for intrinsic AIS and extrinsic/synaptic perisomatic structural plasticity, for each animal, we labeled ankG, NaV1.6, and GAD67/PV in sections taken from a randomly selected and two adjacent wells, respectively, containing caudal S1BF (bregma level –1.5 to –2.0). This was done because of the consistency with which cFPI generates DAI within this well characterized area of neocortex, which was also the rational for choosing this region-of-interest (ROI) in our previously published electrophysiological studies (Greer et al., 2012; Hånell et al., 2015a; Sun and Jacobs, 2016).

Immunohistochemistry

Free-floating sections were rinsed with PBS. Heat-induced epitope retrieval was performed by incubating sections in 10 mM sodium citrate buffer pH 8.5 for 10 min in an 80 °C water bath (Jiao et al., 1999). After cooling to room temperature sections were rinsed with PBS then incubated for 1 h at room temperature with 10% normal goat serum, 2% fish skin gelatin, and 0.5% Triton X-100 in PBS. To mask any potential endogenous mouse immunoglobulin, the blocking buffer was supplemented with Mouse-on-Mouse reagent (MOM; Vector Laboratories, MKB-2213). Then, sections were rinsed with 1% normal goat serum, 1% fish skin gelatin, and 0.5% Triton X-100 in PBS (working buffer). Primary antibody solutions were prepared by dilution with working buffer and the sections were incubated overnight at 4 °C with agitation. Specifically, we used monoclonal antibodies against ankG (1:500; mouse IgG2a, clone N106/36; NeuroMab), NaV1.6 (1:200; mouse IgG1, clone K87A/10; NeuroMab), PV (1:2000; mouse IgG1; Swant, PV235), and GAD67 (1:1000; mouse IgG2a, clone 1G10.2; Millipore, MAB5406). For qualitative double-labeled overview images, we used a polyclonal antibody against NaV1.6 (1:200; Alomone). The following day, sections were rinsed with working buffer and incubated with isotype-specific goat-derived secondary antibodies conjugated to Alexa Fluor 568 for quantitative analyses and a combination of Alexa Fluor 568 and 633 for qualitative colocalization (1:500: ThermoFisher Scientific) for 2 h at room temperature. After final rinses using working buffer then PBS, sections were mounted on glass slides and cover-slipped using non-hardening Vectashield with DAPI (Vector Laboratories, H-1200) to prevent shrinkage and preserve morphology of tissue.

The AIS quantitative analysis on the YFP+ background used separate single-labeled sections opposed to double-labeled single sections in an effort to match the fluorescent quantum yield and stoichiometry via monoclonal primary antibodies to immunolabel ankG and NaV1.6, which were both visualized using Alexa Fluor 568 (Lichtman and Conchello, 2005). In the same vein, mouse immunoglobulin isotype-specific secondary antibodies were used in all studies, which also optimized the signal-to-noise ratio (Manning et al., 2012). Parallel control studies were conducted to ensure both primary and secondary antibody fidelity (Lorincz and Nusser, 2008b). In all cases, primary antibody omission abolished immunoreactivity. Secondary antibody specificity evaluated via cross-reactivity showed no signal between all possible primary × secondary host and/or isotype combinations.

Confocal Microscopy

Image acquisition was performed using a laser-scanning confocal microscope (LSM 710, Carl Zeiss). Since sham vs. mTBI groups could be readily differentiated based on YFP+ profiles, we used DAPI visualized under epifluorescence to center the stage over the ROI. In this way, the investigator was blinded from the experimental/dependent variable channel, thus adhering to stereological principles including random sampling. Using a 10× objective (low-power) the field-of-view (FOV) was centered over the S1BF region along the dorsolateral edge of the hippocampus. We used continuous laser scanning to guide rotation of the FOV until it was orthogonal to the underlying subcortical white matter. Images were acquired with optimal Nyquist sampling using Plan-Apochromat 10×/0.45 NA (XY = 0.41 μm/pixel; Z = 5.8 μm), 20×/0.8 NA (XY = 0.152 μm/pixel; Z = 0.94 μm), 40×/1.4 (XY = 0.094 μm/pixel; Z = 0.52 μm), and 63×/1.2 NA (XY = 0.088

μm/pixel) oil immersion objective lenses. All multichannel images were acquired using sequential scanning at the lowest possible laser power to avoid crosstalk (488 Argon, 561 DPSS, and 633 HeNe). All images for quantitative analysis were acquired using identical laser settings per channel across samples. Gain and offset were adjusted for optimal signal range. The pinhole was set to 1.0 ± 0.2 Airy units to maintain identical optical slice thickness in multichannel z-stack images.

Intact YFP+ Pyramidal Neuron Sampling

Within the 10× overview images we measured ever YFP+ pyramidal neuron that met our inclusion criteria. Specifically, intact neurons were defined by YFP+ axons that were continuous from the soma of origin to the SCWM interface. YFP+ that were transected during tissue processing were excluded in both sham and mTBI samples. Since AIS structure and composition vary highly even within a particular neuronal subtype, we set *a priori* conditions to control for any potential confounds. Layer 5 is subdivided into layer 5a and 5b, which are populated by multiple subtypes of pyramidal neurons with different morphological and physiological properties, as well as projections to different anatomical regions of the brain. Therefore, we excluded samples with axons emerging from basal dendrites. Overall, the Wilcoxon test showed sample sizes between sham and mTBI groups were similar for both ankG (Sham: $n = 53$ AIS from 5 mice; mTBI: $n = 54$ AIS from 6 mice; $X^2 = 0.079$, $p = 0.7782$) and NaV1.6 (Sham: $n = 54$ AIS from 5 mice; mTBI: $n = 43$ AIS from 6 mice; $X^2 = 3.36$, $p = 0.0666$) analyses of AIS structure as well as for perisomatic GABAergic bouton density Sham: $n = 48$ somas from 5 mice; mTBI: $n = 50$ somas from 5 mice; $X^2 = 0.1$, $p = 0.7518$). To control for potential confounding of neurons based on neocortical depth, we also measured the distance of each AIS from the

SCWM junction. Specifically, we measured from the axo-somatic vertex to where YFP+ profiles entered SCWM, indicated by the sharp change in trajectory. Statistical analyses tested for covariance of distance from SCWM with AIS measurements.

Quantification of AIS

To capture ankG and NaV1.6 fluorescent profiles along YFP+ intact pyramidal neurons, a 40× objective at 3× zoom (760 pixels × 760 pixels) in z-stacks (mean 4.5 μm, range 2.7—5.3 μm). Because of the diffuse nature of YFP+ pathology following mTBI, these constrained images allowed tracing the YFP+ axon through and past the AIS region in a blinded fashion. Further, we set a limit of 10 optical slices to minimize error caused by tilted AIS orientation in the z-plane. AIS measurements were performed using a previously described method (Evans et al., 2013; Grubb and Burrone, 2010a). Specifically, z-stacks were collapsed into a single maximum intensity projections that were imported into MATLAB software (MathWorks) for analyses using custom-written functions (Matthew Grubb and Thomas Watkins, King's College London, UK; freely available at www.mathworks.com/matlabcentral/fileexchange/28181-ais-quantification). While visualizing only the YFP channel, an axonal profile was traced starting at the edge of the soma, continuing distally along the axon, through and past the region of the AIS. Immunofluorescent profiles of ankG/NaV1.6 were then superimposed on traces of YFP+ axons. At each pixel along this profile, fluorescent intensity values were averaged over a 3×3 pixel square centered on the pixel of interest. Averaged profile values were then smoothed using a 40-point (~5 mm) sliding mean and normalized between 1 (maximum smoothed fluorescence) and 0 (minimum smoothed fluorescence). With respect to the soma edge, delineated at the axo-somatic vertex, ankG and NaV1.6 proximal (start) and

distal (end) positions were obtained at points where the profiles reached thresholds of 0.33 and 0.5 relative to maximum fluorescence, respectively. These optimal threshold values were determined empirically and varying ± 0.2 did not change the overall pattern of results.

Quantification of perisomatic bouton density

The total number of GAD67+ and GAD67+/PV+ puncta were quantified along the perisomatic domain of YFP+ intact pyramidal neurons within layer 5 of S1BF. Single optical slices (0.9 μm thick) were captured using a 63× objective at 3× zoom (512 pixels × 512 pixels, 45 μm × 45 μm; resolution = 0.088 μm/pixel) using sequential scanning and a single laser intensity for each channel for all samples. Confocal images were imported to Fiji (a distribution of ImageJ) then processed and analyzed using custom written macros for automated analyses. YFP images were converted into binary images to segment the pyramidal neuron profile, which was then dilated and eroded to generate a 2 μm thick band approximating the perimeter/perisomatic domain. Quantification of puncta within this band was performed using both gray scale and segmented/binary images. Specifically, perisomatic GAD67+ puncta in gray scale (8-bit) images were quantified using the 'Find Maxima' function. To quantify perisomatic GAD67+/PV+ puncta, profiles in each channel were segmented from background subtracted 8-bit images by converting into binary using a minimum gray-value threshold. Varying the threshold ±10 gray-values did not change the overall pattern of results. GAD67+/PV+ colocalized populations were isolated using the 'Image Calculator' function. The 'Particle Analysis' function with appropriate size and shape exclusion filters was used to determine the total number of objects per unit area (FOV). GAD67+ (PV+) puncta within this band were

quantified and normalized by dividing by the area of the band to determine perisomatic bouton density, summarized as puncta per 100 μm^2.

Computational Modeling

Simulations in Neuron v7.1 used a previously published realistic model for AP initiation (Hallermann et al., 2012). Specifically, the model of a neocortical layer 5 pyramidal neuron was based on Neurolucida reconstructions using ion channel properties determined from experimental recordings. Simulations were executed using default setting with the exception of AIS ion channel densities and length modifications based on our experimental observations. Specifically, the default AIS length (63 μm) in this model was ~60% longer than our experimental measurements. To compare the effect of AIS length using our experimentally observed values, the peak sodium density at the AIS was increased proportionally from the default value of 7,000 to 11,200 pS μm^{-2}, which was still within the working range used by Hallermann and colleagues. Default current-clamp parameters were used to evoke an AP within 5 ms of injection. Overall, simulations resulted in AP waveforms that were similar to those produced using default settings and also our electrophysiological recordings. This allowed us to investigate the role of AIS length using experimentally observed differences and the effect of NaV density on AP kinetics.

Electrophysiology

In addition to the above, a separate cohort of sham-injured (n = 3) and mTBI (n = 4) mice were anesthetized with isoflurane and decapitated for quick brain removal 2 d postinjury. The brains were immediately chilled in ice-cold oxygenated sucrose-modified artificial cerebral spinal fluid (aCSF) slicing solution (mM: 2.5 KCl, 10 $MgSO_4$, 0.5 $CaCl_2$, 1.25

NaH_2PO4, 234 sucrose, 11 glucose, and 26 $NaHCO_3$). Using a Leica VT 1200 slicer (Leica Microsystems, Wetzlar, Germany) brains were coronally sectioned at 300 μm and then incubated for 30–45 min at 34 ºC in an oxygenated aCSF (mM: 126 NaCl, 3.5 KCl, 1 $MgSO_4$, 1.2 $CaCl_2$, 1.25 NaH_2PO_4, 10 glucose, and 26 $NaHCO_3$). Thereafter, slices remained at room temperature until placed in the recording chamber maintained at 32 ± 0.5 ºC.

As previously described (Sun and Jacobs, 2016), whole-cell patch-clamp recordings were performed under infrared Dodt contrast microscopy (Zeiss AxioExaminer). A 60× water-immersion objective was used to visually identify YFP+ layer 5 pyramidal neurons of S1BF with axons descending into the white matter (intact) or ending with an axonal swelling (DAI) deep to the surface of the slice to avoid those transected by the vibratome. We have shown previously that these morphologies are easily identified in the living slice for YFP+ layer 5 pyramidal neurons (Greer et al., 2012). Only these intact YFP+ pyramidal neurons were chosen for recording in both sham and mTBI slices. All layer 5 YFP+ neurons in the YFP-H line are expected to be pyramidal neurons and in all cases, an apical dendrite was apparent, confirming that they were pyramidal neurons. The slices were continuously perfused with aCSF solution that was saturated with 95% O_2 and 5% CO_2. Patch electrodes (final resistances, 2–4 MΩ) were pulled from borosilicate glass (World Precision Instruments, Sarasota, FL, USA) on a horizontal Flaming-Brown microelectrode puller (Model P-97, Sutter Instruments). The intracellular solution contained (in mM): 130 K-gluconate, 10 Hepes, 11 EGTA, 2.0 $MgCl_2$, 2.0 $CaCl_2$, 4 Na-ATP, and 0.2 Na-GTP. Electrode capacitance was electronically compensated. Data were acquired by MultiClamp 700B (Molecular Devices, Sunnyvale,

CA, USA) amplifier and digitized at 200 kHz with a Digidata 1440A and pClamp software (Molecular Devices). Whole-cell patch-clamp was approached under voltage-clamp mode with cell clamped at –65 mV. After 2–5 min stabilization, APs were recorded in current-clamp mode to obtain intrinsic property measurements. Pipette Capacitance Neutralization was set at 9.6 pF, Bessel Filter at bypass, auto Bridge Balance, and Gain at one. APs were evoked with 10 depolarizing steps (30 ms) beginning with a 100 pA step, and increased by 10 pA every 5 s while neurons were maintained at –60 mV. Access resistance was continuously monitored and rechecked after each recording. If the series resistance increased by 20% at any time, the recording was terminated. Previously we showed that there was no significant difference between the results for naïve and sham animals (Greer et al., 2012). Despite this similarity, for added rigor the control group contained only age- and survival time-matched shams-injured animals.

In this report, we use a newly implemented protocol for intrinsic property analysis that allows us to measure the first AP on each sweep (5 sweeps per cell). To analyze the AP specifically at the AIS, we calculated the second derivative of the membrane voltage. Specifically, the first and second peak in the plot of the second derivative of the membrane voltage corresponds to AP acceleration at the AIS and somas, respectively (Khaliq and Raman, 2006; Meeks and Mennerick, 2007). First we applied three successive seven-point boxcar filters to the membrane voltage, and then calculated the first and second derivatives. All neurons from sham and mTBI mice resulted in two peaks. These peak amplitudes were measured for each of five APs per cell. The number of recorded cells per animal (range = 2–6) between sham and mTBI was similar (X^2 =

0.5283, $p = 0.4673$). For statistical analysis, every action potential was analyzed; wherein the first AP on each of the five sweeps was nested within each cell (Sham = 13 cells from 3 mice, 63 AP total; mTBI = 14 cells from 4 mice, 70 AP total).

Statistics

Statistical analysis of data sets was performed using JMP Pro version 12.2.0 (a distribution of SAS). Data sets were assessed for normality using quantile (QQ) plots and the Shapiro-Wilk test. For all analyses, the variance in data between sham and mTBI groups was not significantly different ($p > 0.05$, Brown-Forsythe test). We employed multilevel analysis of mixed models with nested data sets (Aarts et al., 2014) that controlled for intra- and inter-animal variability within an individual group (random effect) and between sham vs. mTBI groups (fixed effect). Additionally, this statistical method can control for potential covariates and decreases both Type I and II error. Data are summarized using mean ± SEM. All statistical tests were two-tailed with a significance threshold set to $\alpha = 0.05$.

RESULTS

Intraoperative physiology was normal and consistent with previous reports on mice under isoflurane anesthesia (Cesarovic et al., 2010; Ewald et al., 2011; Hånell et al., 2015c). Specifically, mean ± SEM of arterial oxygen saturation (sham = 97.9 ± 0.2%; mTBI = 97.8 ± 0.1%), heart rate (sham = 510 ± 19 BPM; 2 d mTBI = 518 ± 16 BPM), and respiratory rate (sham = 72 ± 8 RPM; 2 d mTBI = 66 ± 9 BRPM) were similar between groups. The LORR duration (mean ± SEM) was significantly greater ($t_{16} = 7.44$, $p < 0.0001$; unpaired *t*-test) in mTBI mice (4.7 ± 0.24 min) compared to shams (1.2 ± 0.42

min) and consistent with our previous reports. Additionally, mTBI mice for confocal and electrophysiological studies had similar LORR ($t_8 = –0.31$, $p = 0.7639$; unpaired *t*-test). Importantly, signs of hypoxia/apnea were not observed during surgical preparation or post-injury. Overall, these physiological assessments did not show any evidence of confounding mechanisms that play a role in secondary insults.

Macroscopically, both sham and mTBI brain tissue appeared normal without evidence of surgically induced lesions (Figure 1D,E), as previously reported. Post-mTBI tissue sections revealed no macroscopic change (Figure 2) consistent with the mild and diffuse nature of cFPI. Importantly, the dorsal neocortex underneath the craniectomy site did not show evidence of focal contusion, cavitation, or overt subarachnoid hemorrhage induced by the fluid pressure wave (Figure 2B). Overall, the brain parenchyma was devoid of overt hemorrhage, the ventricular system maintained a regular contour, with no evidence of trauma-related ventricular enlargement. Taken together these data support our premise that cFPI in YFP-H mice is a reproducible model of mTBI.

YFP+ Pyramidal Neuron DAI

Consistent with previous studies utilizing YFP-H strain (Feng et al., 2000; Greer et al., 2011; Hånell et al., 2015c), we observed YFP+ pyramidal neurons in sham and mTBI mice primarily within layer 5 neocortex. Following sham-injury, we did not observe any YFP+ axonal swellings or morphological irregularities indicative of axonal damage within neocortex or underlying SCWM (Figure 2A). Descending axons from YFP+ pyramidal neurons in shams demonstrated a continuous trail from their soma of origin to the SCWM interface. Following cFPI, all tissue sections processed for YFP visualization

and parallel immunohistochemical analyses revealed a pattern of microscopic change consistent with that routinely described in rat and mouse cFPI models. Despite the overall preservation of brain parenchymal integrity typical of a mild diffuse TBI in both humans and rodents, the fluid pressure wave consistently evoked YFP+ axonal swellings indicating DAI. At 2 d post-mTBI, comparable to previous reports, we observed pathologic YFP+ axonal profiles in continuity with their cell bodies of origin (Figure 2B, 4A) and their detached axonal segments distributed throughout layer 5/6 of the dorsolateral neocortex corresponding to S1BF (Figure 2B). Underscoring the diffuse nature of mild cFPI, the distribution of YFP+ pyramidal neurons proximal and distal axonal swellings were interspersed among numerous YFP+ profiles showing no morphological evidence of either primary axonal injury or retrograde neuronal involvement. Similar to shams, we readily identified these non-DAI/intact YFP+ pyramidal neurons via tracing YFP+ axons continuously from the edge of soma of origin to the SCWM interface (Figure 2C). Importantly, we observed consistent YFP+ pyramidal neuron axonal injury within the same neocortical regions of all mTBI mice, indicating a generalized diffuse response to cFPI-induced mTBI in mice rather than an isolated focal event.

Intact YFP+ Pyramidal Neuron Responses

AIS Structural Plasticity

To estimate AIS position and length (Figure 6), we quantified immunofluorescent profiles of ankG, a key structural protein underpinning AIS function. Consistent with previous reports from our lab and others (Clark et al., 2016; Greer et al., 2013; Gutzmann

et al., 2014), ankG labeling throughout the neocortex was restricted to the AIS and nodes of Ranvier (Figure 3B). Importantly, ankG labeling of intact YFP+ pyramidal neurons clearly delineated the AIS in sections from both sham and mTBI mice (Figure 6B,E). For ankG quantitative analysis, the intact YFP+ pyramidal neuron sample distribution with respect to the SCWM interface was symmetrical between sham and mTBI (Figure 5). Quantitative analysis confirmed no significant difference in distribution ($p = 0.8585$) between (mean ± SEM) sham (372 ± 14 μm) and mTBI (368 ± 14 μm). The AnkG (mean ± SEM) start position of sham (2.1 ± 0.16 μm) and mTBI (2.2 ± 0.16 μm) were not significantly different ($p = 0.7957$) in the intact YFP+ pyramidal neuron population. In contrast, the ankG end position in sham (26.6 ± 0.42 μm) and mTBI (24.8 ± 0.42 μm) were significantly different ($t_{7.4} = –3.08$, $p = 0.0167$; $R^2 = 0.14$). Overall, this resulted in a 7.4% decrease (1.8 μm) in ankG length from the distal end, which was significantly different ($t_{7.4} = –3.74$, $p = 0.0066$; $R^2 = 0.28$) between shams (24.4 ± 0.33 μm) and mTBI (22.6 ± 0.35 μm). Because layer 5 pyramidal neurons are heterogeneous (Chagnac-Amitai et al., 1990; Hattox and Nelson, 2007; Le Bé et al., 2007), varying structurally and functionally with cortical depth (e.g. layer 5a vs. 5b), we controlled for this potential confound in analyzing plasticity (Jacob et al., 2012) by measuring the AIS distance from SCWM. Multilevel analysis revealed that distance from SCWM is a significant covariate of ankG length ($t_{79.0} = 4.52$, $p < 0.0001$). Specifically, ankG length is directly proportional to distance from SCWM (Figure 6I). The equal slopes of the best-fit lines for ankG length as a function of distance to SCWM indicated that there was no interaction with experimental groups ($p = 0.5512$). Importantly, accounting for this covariate resulted in a 72% increase in the R^2 value (0.16 to 0.28). While this reduction in

ankG length is relatively modest, multilevel modeling revealed that mTBI accounted for almost 30% of the variability between data sets, and the effect size was robust (Cohen's *d* = 0.76). Further, the shortening of ankG occurred within the distal AIS microdomain that contains the 'trigger zone' for AP firing, where a high density of voltage-gate sodium channels set the threshold for AP initiation (Adachi et al., 2014).

To estimate the distal AIS 'trigger zone' position and length (Figure 8), we quantified immunofluorescent profiles of NaV1.6. Consistent with previous reports from other labs (King et al., 2014; Lorincz and Nusser, 2008a), NaV1.6 labeling throughout the neocortex was restricted to the distal AIS and nodes of Ranvier (Figure 3C). Importantly, NaV1.6 labeling of intact YFP+ pyramidal neurons clearly delineated the distal AIS in sections from both sham and mTBI mice (Figure 7B,E). For NaV1.6 analysis, intact YFP+ pyramidal neurons sample distribution with respect to the SCWM interface appeared slightly asymmetrical between sham and mTBI (Figure 7). Specifically, mTBI (384 ± 15 μm) samples had a greater distribution in upper layer 5 compared to sham (339 ± 16 μm). However, quantitative analysis showed no significant difference in distribution ($p = 0.0761$) between groups. NaV1.6 (mean ± SEM) start position of sham (11.0 ± 0.28 μm) and mTBI (11.0 ± 0.32 μm) were not significantly different ($p = 0.8708$). Similarly, AIS end position in sham (26.0 ± 0.61 μm) and mTBI (27.0 ± 0.59 μm) were not significantly different ($p = 0.2876$).

Consistent with ankG findings (Figure 6I), multilevel analysis also revealed that distance from SCWM is a significant covariate of NaV1.6 length ($t_{59.9} = 3.38$, $p = 0.0013$; Figure 8I). Hence, AIS length is directly proportional to distance from SCWM, wherein upper versus lower pyramidal neurons have longer and shorter AIS, respectively.

Specifically, the statistical model predicts AIS length from distal end increases ~0.2 μm for every 10 μm from SCWM (Figure 6I,8I). Considering layer 5 S1BF is ~300 μm thick, this corresponds to a 6 μm difference in length between upper and lower pyramidal neuron populations. In light of the magnitude of this dependency, we tested the effect of controlling for AIS distance from SCWM on NaV1.6 end position. While NaV1.6 end position did not change for shams (26.1 ± 52), it decreased by ~1 μm for mTBI (26.2 ± 0.52 μm), consistent with the mean distance from SCWM of mTBI samples being ~40 μm greater than shams (Figure 7C,D). Accordingly, NaV1.6 length as a function of distance from SCWM (Figure 8I) was not significantly different ($p = 0.9663$) between sham (15.4 ± 0.54 μm) and mTBI (15.4 ± 0.56 μm). Notably, controlling for distance from SCWM increased the R^2 by 48% (0.14 to 0.27), but did not change ankG end position in shams or mTBI, consistent with their equal sample distributions (Figure 5C,D). Overall, the controlled end position of ankG in shams (26.6 ± 0.39 μm) was similar to NaV1.6 in both sham (26.1 ± 0.52 μm) and mTBI (26.2 ± 0.51 μm). In contrast, the controlled end position of ankG in mTBI (24.9 ± 0.40 μm) was 1–2 μm shorter than sham ankG, and both sham and mTBI NaV1.6 end positions. Taken together, these data show ankG and NaV1.6 uncoupling following mTBI, and reveal a novel AIS property within the intact YFP+ pyramidal neurons in layer 5 S1BF.

Perisomatic GABAergic Bouton Density

In addition to intrinsic/postsynaptic AIS structural plasticity, probing afferent inputs surrounding the perisomatic domain revealed evidence for extrinsic/presynaptic change (Figure 9). Immunolabeling GAD67, the GABA-synthesizing enzyme enriched in PV+ presynaptic boutons (Fish et al., 2011) allowed us to conduct a high precision quantitative

analysis of the major source of inhibitory input at the perisomatic domain, which strongly regulates AIS activity. We quantified perisomatic GABAergic bouton density of only intact YFP+ pyramidal neurons in S1BF using the same sampling method for AIS studies (Figure 5 and 7). Using two different quantitative methods, we found a significant decrease in perisomatic GABAergic density in both GAD67+ immunoreactivity profiles (mean ± SEM of puncta/100 μm^2: Sham = 13.0 ± 0.57; mTBI = 10.9 ± 0.57) in gray-scale images (Figure 9J) and colocalized PV+/GAD67+ puncta (Sham = 12.0 ± 0.55; mTBI = 8.7 ± 0.56) in binary images (Figure 9K). Additionally, the magnitudes of change were similar between gray and binary quantitative methods, with intact YFP+ pyramidal neuron perisomatic GABAergic bouton density decreasing by 16% (95% CI: 2–31%) and 24% (95% CI: 10–43%), respectively. Importantly, the cumulative distribution plot of the size of PV+/GAD67+ puncta (segmented particles in binary images) showed that the greatest decrease occurred in particles that were the average size (~1 μm^2) of GABAergic puncta (Figure 9L).

AIS Functional Plasticity

Electrophysiological recordings of layer 5 intact YFP+ pyramidal neurons in S1BF in revealed no overt changes in AP waveform following mTBI (Figure 10A), consistent with the diffuse nature of mTBI pathophysiology. Neurons generate AP at the AIS, which then travels distally along the axon and also back-propagates to the soma (Hu et al., 2009). Recordings of AP using whole-cell patch-clamp at the soma showed two peaks in the plot of the second derivative of membrane voltage (Figure 10B). The first and second peaks in this plot correspond to the AP at the AIS and soma, respectively (Khaliq and Raman, 2006; Meeks and Mennerick, 2007). Compared to sham (5203 ± 308 $mV/\mu s^2$) the

amplitude of the first peak was significantly reduced by 21% ($t_{25} = –2.57$, $p = 0.0164$) after mTBI (4104 ± 296 mV/μs^2). In contrast, the amplitude of the second peak was not significantly different ($p = 0.5701$). These data reveal AP generated by intact YFP+ pyramidal neurons are significantly attenuated specifically at the AIS.

Layer 5 Pyramidal Neuron Modeling

While AIS excitability varies with axial geometry such as length (Kuba et al., 2010), voltage-gated ion channel density is a critical determinant of intrinsic properties (Kole et al., 2008). To investigate the functional consequences of AIS structural plasticity and explore the effect varying NaV density we used an anatomically and physiologically accurate computational model of a layer 5 pyramidal neuron (Hallermann et al., 2012). This computational model allowed us to probe AP dynamics specifically at the AIS. The AP waveforms in the model (Figure 10E) were similar to those observed experimentally (Figure 10A). Comparing the effect of AIS length differences based on our experimental observations of ankG immunofluorescent profiles, we found that shortening the length by 7% resulted in a 19% decrease in the peak of the second derivative of membrane voltage, reflecting attenuated AP acceleration (Figure 10F). To help elucidate potential functional consequences of ankG and NaV1.6 uncoupling we evaluated the effect of a proportionate decrease in NaV density at the distal AIS. Without changing AIS length, a 7% decrease in NaV density at the distal AIS also attenuated AP acceleration by 10%. Thus, AP kinetics at the AIS depends on both geometry and density of intrinsic structural-functional components. Collectively, these morphological and computational findings suggest that even subtle AIS changes may alter neuronal excitability.

DISCUSSION

This study provides compelling evidence of intact pyramidal neuron AIS structural and functional plasticity after clinically relevant mTBI in mice. Consistent with human mTBI, midline cFPI reproducibly evoked DAI without mass lesions, neocortical contusion, and/or overt cell death (Andriessen et al., 2010; Bigler and Maxwell, 2012; Mittl et al., 1994; Saatman et al., 2008; Shultz et al., 2016; Yuh et al., 2013). Exploiting restricted YFP expression in a discrete subset of layer 5 pyramidal neurons and an established AIS marker (ankG), we confirmed subcellular structural plasticity within the non-DAI/intact population. In this mTBI-mediated response, the decrease in GABAergic presynaptic boutons surrounding the perisomatic domain of this intact pyramidal neuron population suggested compromised PV+ interneuron inhibition of their AIS. Consistent with AIS structural change, patch-clamp recordings of intact YFP+ layer 5 pyramidal neurons revealed slower AP acceleration. This finding was further supported by simulations using a realistic layer 5 pyramidal neuron model that showed even a subtle decrease in AIS length or NaV1.6 density attenuates AP acceleration. Taken together, these findings demonstrate significant structural and functional changes of both intrinsic and extrinsic/synaptic components that are major regulators of AIS activity. The conclusions of this study depart from current thought on mTBI, which has been based primarily on the role of structural disconnection of white matter tracts (Sharp et al., 2014; Sharp and Ham, 2011). Collectively, the novel neuronal and physiologic substrates identified in this study significantly extend our knowledge of cortical network dysfunction following mTBI.

Several features of our cFPI model underscore its clinical relevance and utility for evaluating DAI in cortical networks after mTBI. We used LORR as a surrogate for LOC to assess injury severity. The duration of LORR in mice was similar to LOC in humans following mTBI, ranging 3–5 min (Malec et al., 2007; Schrader et al., 2009; Shaw, 2002). While this was our only behavioral assessment, we monitored arterial oxygen saturation, heart rate, respiratory rate, and core body temperature in all mice used for structural and functional studies. Specifically, all mice were in physiological homeostasis. Importantly, evaluating these parameters help distinguish our work from most other investigators who do not perform routine physiologic monitoring to exclude secondary insults, which could severely confound the assessment of network disruption via diffuse structural and functional changes.

Capitalizing on restricted neuronal labeling with YFP including the total axonal length, readily traceable within the neocortical gray, allowed the unequivocal identification of mTBI-induced DAI vs. non-DAI/intact populations in both fixed tissue sections and live slices. Specifically, intact pyramidal neurons were readily identified by following YFP+ axons from their soma of origin to the SCWM interface. Previously, we reported that mTBI induces DAI primarily within the AIS of the YFP+ layer 5 pyramidal neurons (Greer et al., 2013). Additionally, in a former publication we showed that the most commonly used DAI marker did not colocalize with YFP axons in either the SCWM or corpus callosum (Hånell et al., 2015c). Taken together, these findings strongly support the premise that virtually all YFP+ pyramidal neuron DAI occurs within the neocortical gray. Based on this premise, YFP+ pyramidal neurons undergoing DAI can

be reliably identified by examining their axonal segment spanning neocortical layers 5/6 to the SCWM interface.

Pyramidal neurons are the major excitatory component in cortical networks (DeFelipe and Fariñas, 1992; Somogyi et al., 1998). Previously we showed that intact YFP+ pyramidal neurons intrinsic and extrinsic/synaptic properties were altered post-mTBI and developed over time (Sun and Jacobs, 2016). Initially after mTBI, the intrinsic properties of intact pyramidal neurons paralleled that found in the DAI population, suggesting that ion and/or neurotransmitter imbalance had an indiscriminant overriding effect on currents (Greer et al., 2012). However, by 2 d post-mTBI a functional divergence was identified wherein the intact pyramidal neuron population showed distinct electrophysiological changes implicating AIS structural-functional alteration. These changes occurred in parallel with overall increased network excitability (Hånell et al., 2015b). Collectively, these previous findings by our lab formed the basis of the current study focusing on the effect of mTBI on intrinsic structure and function of the AIS as well as the extrinsic/synaptic GABAergic inputs that control its output (Wefelmeyer et al., 2015). For structural studies, we employed ankG as a surrogate marker of AIS position and length. Specifically, we found that while there was no change in position with respect to the soma of origin, the length significantly decreased from the distal end. This finding departs from a previous study, which found a global decrease in neocortical AIS length in rats 2 weeks after blast wave-induced mTBI (Baalman et al., 2013). The important distinction in the current report is that we detected a decrease in AIS length within 2 d after cFPI-induced mTBI specifically within the layer 5 pyramidal neuron populations with no overt structural axonal abnormalities and/or evidence of DAI.

Building upon our previous studies in YFP-H mice we succeeded in conducting a highly detailed analysis within these pyramidal neurons. This was a crucial component of our study since the AIS ion channel distribution differs across neuronal subtypes (Lorincz and Nusser, 2008a), and even within a neuronal subtype there is substantial variability in position and length (Bender and Trussell, 2012; Kuba, 2012). Further, because DAI affects only a small fraction of neurons within a pyramidal neuron population (Greer et al., 2011) that represent 80% of all neocortical neurons (DeFelipe, 1997), quantification of such heterogeneous population (Molnár and Cheung, 2006) remains a confound. Our previous reports underscore this issue, showing that the neocortical pyramidal neuron AIS has a predilection for DAI (Greer et al., 2013). Additionally, in our previous report and the current study we show DAI occurring within the AIS severely disrupts ankG and NaV1.6 expression (Figure 4). Hence, even a 5% burden of DAI (Greer et al., 2011) causing AIS disruption would substantially contribute to data variability. To the best of our knowledge, this is the first study to account for these issues by examining only intact, Thy1-expressing, layer 5 pyramidal neurons. An unexpected finding in the current study that followed from our *a priori* control parameters was that AIS length from the distal end varied with neocortical depth, a finding confirmed using both ankG and NaV1.6 quantitative analyses. Although not previously appreciated, this observed variance is consistent with known properties of layer 5 pyramidal neurons which are subdivided into layer 5a and 5b and populated by multiple subtypes characterized by different morphological and electrophysiological properties (Chagnac-Amitai et al., 1990; Hattox and Nelson, 2007; Le Bé et al., 2007). Additionally, this is consistent with recent reports from other labs showing that in rodent neocortex, AIS length from the distal end appears

to be more dynamic than position with respect to the soma of origin (Cruz et al., 2009; Evans et al., 2015; Gutzmann et al., 2014; Hamada and Kole, 2015; Hinman et al., 2013; Kaphzan et al., 2011; Kuba et al., 2010, 2014). Lastly, another novel finding in this study is the reported structural uncoupling between ankG and NaV1.6 distributions, unlike the majority of reports on AIS plasticity (Adachi et al., 2014; Yamada and Kuba, 2016; Yoshimura and Rasband, 2014), which demonstrate parallel changes in scaffold proteins and ion channels. In the current study, we did not observe a decrease in NaV1.6 length that paralleled with ankG distribution. Notwithstanding these morphological findings, electrophysiological assessments revealed decreased AP acceleration at the AIS, but not the soma. All together, these data reflect slower NaV activation specifically at the AIS. Computer simulations using a realistic model of a layer 5 pyramidal neuron supported this premise. Specifically, decreasing either AIS length by experimentally observed values or NaV density by the same proportion also decreased AP acceleration, consistent with the data reported by Hallerman and associates (2012) in their characterization of this layer 5 pyramidal neuron model. Based on this, we now posit that at 2 d post-mTBI the AIS is in a state of flux, wherein the initial ankG structural remodeling precedes the NaV1.6 change that elicits decreased length. Alternatively, a decrease in ankG length could elicit a decrease NaV1.6 density (Gasser et al., 2012; Hedstrom et al., 2008), thus offering a potential mechanism for the structural reorganization underlying functional alterations discussed below.

The essential function of the AIS is to integrate synaptic input (excitatory and inhibitory) and determine whether to fire an AP (Kole and Stuart, 2012). The dynamics between extrinsic/synaptic and intrinsic AIS properties underlie neuronal coding,

whereby analog signal inputs are propagated via digital output (Ainsworth et al., 2012; Gerstner et al., 1997; Gütig and Sompolinsky, 2009; Shu et al., 2003). A critical feature of the interplay between synaptic transmission and intrinsic neuronal excitability is perisomatic inhibitory input (Freund and Katona, 2007), which strongly regulates pyramidal neuron AIS output (Pouille et al., 2013). Several reports demonstrate how changes in presynaptic input/activity can induce AIS structural and functional plasticity (Evans et al., 2015; Grubb and Burrone, 2010a; Kuba et al., 2010). Specifically, Kuba and associates (2010) showed that cochlear deprivation, which decreased presynaptic excitatory input, results in postsynaptic AIS elongation correlated with increased neuronal excitability. Further, Gutzmann and colleagues (2010) demonstrated AIS length dynamics in the visual cortex during the critical period in visual development could be altered by ocular deprivation. In the neocortex, the balance of excitation/inhibition is regulated by PV+ interneurons that are highly interconnected with local pyramidal neurons (Douglas and Martin, 2004; Haider et al., 2006; Haider and McCormick, 2009; Hu et al., 2014; Raichle, 2010; Scholl et al., 2015). This proximity of PV+ terminals to the AIS allows for strong inhibitory control over AIS output (Kepecs and Fishell, 2014). In light of the known features of AIS structure-function and that mTBI-induced abnormal network activity is associated with imbalanced excitation/inhibition (Bashir et al., 2012; Beamer et al., 2016; Cohen et al., 2007; Cole et al., 2010; Fagerholm et al., 2015; Guerriero et al., 2015; Paterno et al., 2016; Sponheim et al., 2011; Tremblay et al., 2011; Wolf and Koch, 2016b), we also evaluated extrinsic/synaptic structural changes in concert with our AIS investigations. Our previously reported electrophysiological studies revealed increased network excitability and the production of powerful intact pyramidal

neurons that have both increased intrinsic and synaptic excitability at 2 d after mTBI (Hånell et al., 2015b). In addition to revealing the excitatory substrates, this previous study also supported the premise that changes in inhibition may contribute to overall network hyperexcitability. In the current study, this issue was addressed by examining inhibitory structural synaptic connectivity. As noted in our results, quantitative analysis of intact layer 5 pyramidal neuron perisomatic GAD67+ and PV+/GAD67+ puncta revealed a significant decrease. While determining the actual functional consequences of this structural finding is beyond the scope of the current study, this parallel observation to our AIS findings provides additional evidence that local neocortical disruption is a consistent feature of mTBI. In future studies, it would be important to determine if such loss in presynaptic inhibitory input elicits postsynaptic AIS shortening to decrease pyramidal neuron excitability to restore network homeostasis after mTBI. Such a finding would add further validity to the work of Kuba and others (2010) who have shown that decreasing presynaptic excitatory input may result in postsynaptic AIS elongation associated with increased excitability as a compensatory response to overall network hypoexcitability. While the mechanism underlying PV+ interneuron terminal loss was not addressed in the current study, in a previous report from our lab we showed ultrastructural evidence of terminal degeneration along the perisomatic domain of healthy layer 5 pyramidal neurons within neocortical regions sustaining DAI after mTBI (Singleton et al., 2002). This provokes the question whether locally projecting GABAergic interneurons can also undergo DAI to cause disconnection of their axons resulting in presynaptic terminal loss/deafferentation at target sites of postsynaptic neurons.

The AIS is a highly complex and dynamic domain (Yamada and Kuba, 2016). Intrinsically linked structure-function relationships between scaffolding proteins and ion channels (Gasser et al., 2012; Hedstrom et al., 2008) are a crucial for AIS activity (Kole and Stuart, 2012). In this way, the neocortical pyramidal neuron AIS is a major determinant of network function and homeostatic plasticity. This premise has been evaluated in several studies showing AIS disruption associated with multiple disease states involving an imbalance of network function (Clark et al., 2016; Hamada and Kole, 2015; Hinman et al., 2013; Howard et al., 2005; Lewis, 2011; Schafer et al., 2009). The findings of this study broaden the cortical landscape affected by mTBI, emphasizing the role of postsynaptic functional disruption of intact neurons. Based on the current data, we posit that AIS plasticity may constitute a compensatory response to mTBI. However, future studies are needed to determine whether AIS structural-functional plasticity is adaptive or maladaptive, which has important implications for restoring excitatory/inhibitory balance in cortical networks disrupted by mTBI.

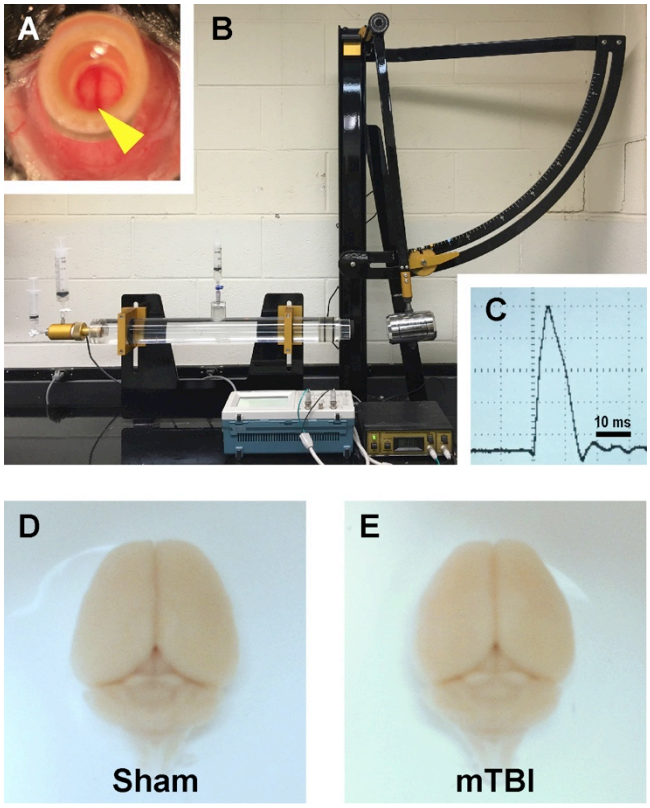

Figure 2.1. Mouse model of mTBI via midline central fluid percussion injury. **A,** Dorsal view showing craniectomy site with the dura intact. The superior sagittal sinus (yellow arrowhead) can be seen through the saline-filled hub. **B,** Fluid percussion injury device with the pendulum in the cocked position. Severity of injury is determined by arc height. After releasing the trigger the pendulum strikes a piston in a cylinder reservoir generating a fluid pressure wave. The mouse cranium is attached to the cylinder at the opposite end via the installed hub, forming a closed mechanical system. **C,** A representative fluid pressure wave that is transmitted directly onto the intact dura. **D,E,** Representative images of dissected brains perfused 2 d after cFPI-induced mTBI. Sham (**D**) and mTBI (**E**) brains show no evidence of surgically-induced damage. After cFPI, there is no evidence of mass lesions and/or contusion. There is no focal damage at the craniectomy site where the pressure wave entered the cranium.

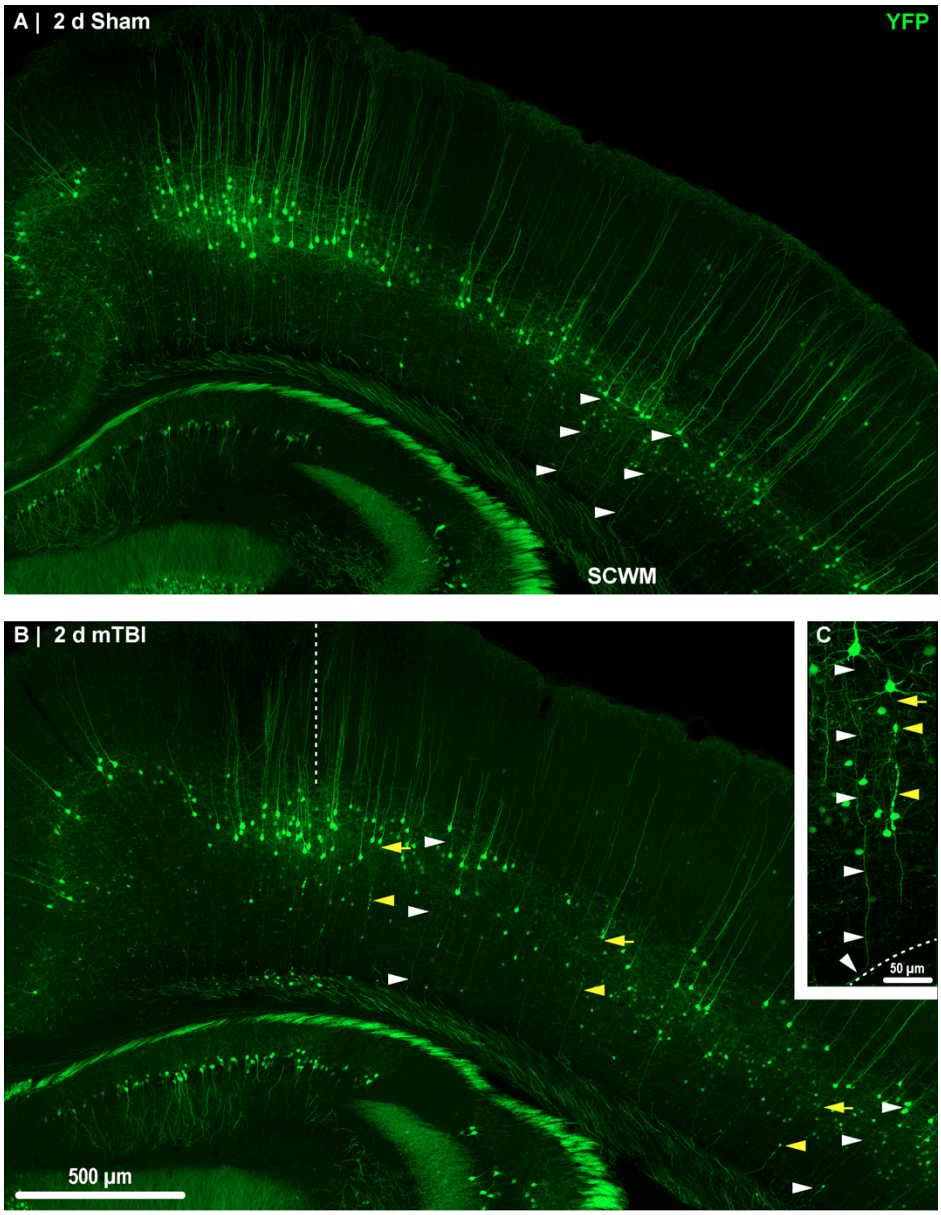

Figure 2.2. YFP expression in neocortical layer 5 pyramidal neurons. Representative images of sections from sham (A) and mTBI (B) brains shown in Figure 1. Thy1 driven YFP expression results in restricted labeling of a discrete subset of layer 5 pyramidal neurons. **A–C,** The selective YFP expression allows identification of individual axons that be traced from their soma of origin to the SCWM (white arrowheads). **B,** 2 d after mTBI, evidence of DAI indicated by YFP+ axonal swellings is seen dispersed across the dorsolateral neocortex (yellow arrowheads). The craniectomy boundary is depicted by the vertical dashed line. No evidence of focal injury is observed under the craniectomy site. **C,** A representative intact YFP+ pyramidal neuron juxtaposed by an injured axon. The intact axonal profile can be continuously traced from the soma of origin to where it enters the SCWM (dashed line), indicated by the acute change in trajectory.

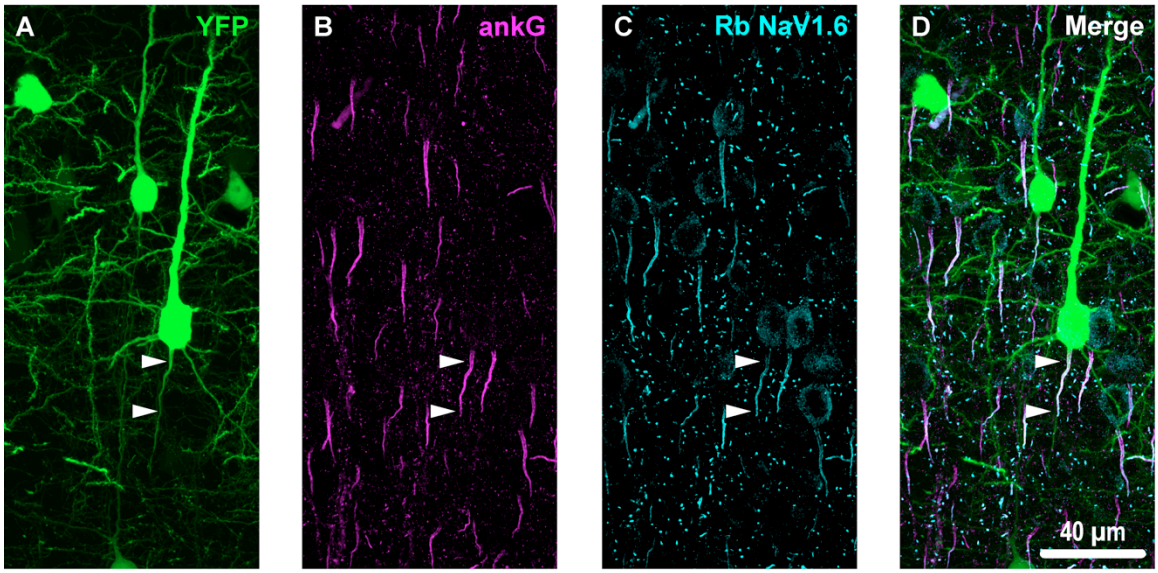

Figure 2.3. Overview of ankG and NaV1.6 immunofluorescent profiles in YFP mice. **A,** Neocortical layer 5 YFP+ pyramidal neurons (green). **B,** AnkG immunoreactivity visualized using Alexa Fluor 568 (magenta) shows characteristic tapered morphology. **C,** NaV1.6 immunolabeled with a polyclonocal rabbit (Rb) antibody visualized using Alexa Fluor 633 (cyan) reveals shorter profiles corresponding to the distal AIS. Punctate profiles indicate Nodes of Ranvier. **D,** Composite image clearly demonstrating the utility of ankG as an AIS marker. The proximal axon of the YFP+ pyramidal neuron in the center of the FOV colocalizes with ankG and NaV1.6, which is expressed at the distal AIS. Several ankG+ profiles highlight NaV1.6 expression at the distal AIS.

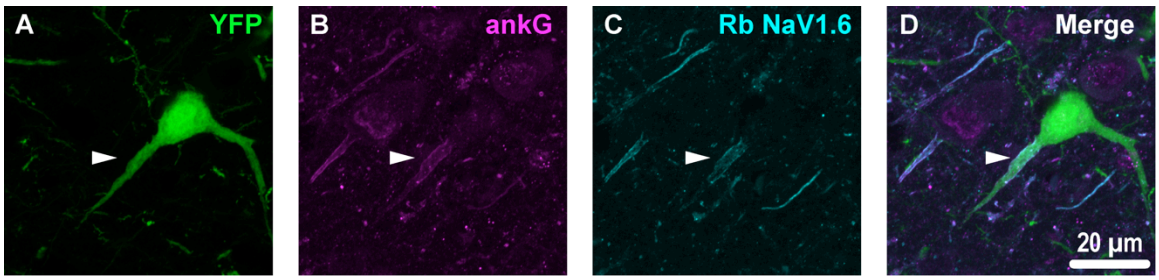

Figure 2.4. YFP+ pyramidal neuron axonal injury attenuates ankG and NaV1.6 expression at the AIS. **A–C,** Representative images of YFP (**A**) ankG (**B**) and NaV1.6 (**C**). **A,** Evidence of DAI occurring at the AIS of a YFP+ pyramidal neuron (green) is indicated by a severely swollen proximal segment (arrowhead). **B,C,** AnkG (magenta) and NaV1.6 (cyan) expression persists, but is substantially attenuated with abnormal morphology after mTBI-induced AIS injury. **D,** Composite image showing ankG and NaV1.6 within the swollen AIS of a YFP+ pyramidal neuron.

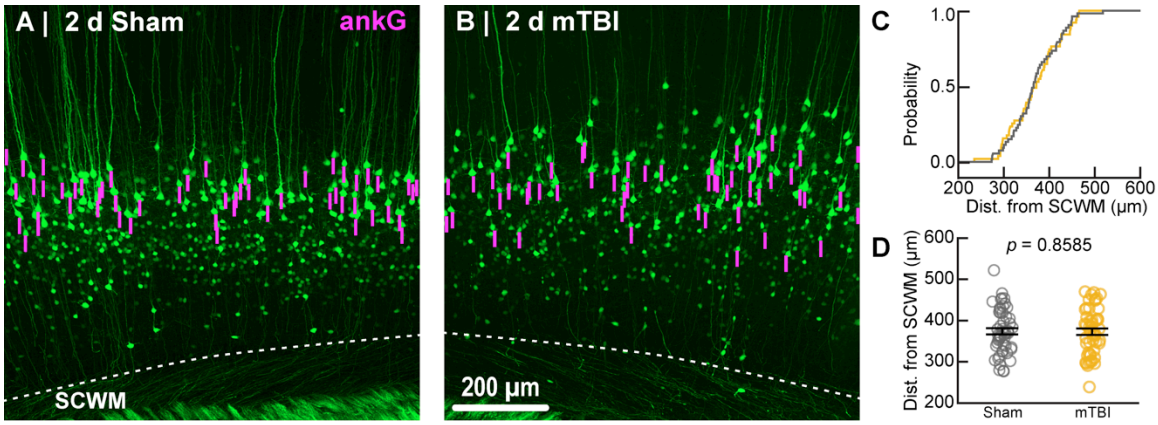

Figure 2.5. Sampling distribution of intact YFP+ pyramidal neurons for ankG quantitative analysis. **A,B,** Superimposed maximum intensity projections of 10x overview images for sham (**A**) and mTBI (**B**). The intact YFP+ pyramidal neuron sampling distribution (magenta bars) is symmetric with respect to the SCWM. **C,** Cumulative frequency distribution plot shows a high degree of overlap between sham (gray) and mTBI (gold). **D,** Quantitative analysis confirmed no sampling difference. Statistics: Multilevel analysis with animals as a random variable. Data summarized with means and SEM error bars.

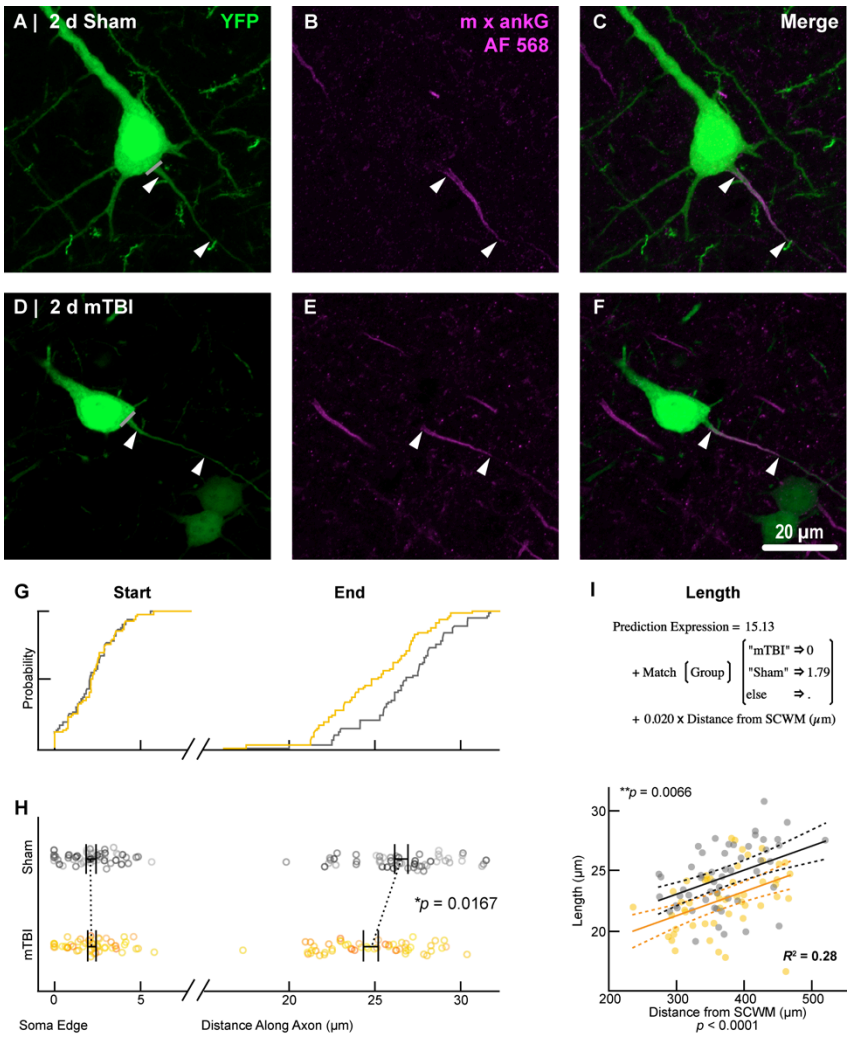

Figure 2.6. AnkG length decreases from the distal AIS after 2 d post-mTBI. Representative images of sham (**A–C**) and mTBI (**D–F**) of YFP (**A,D**; green) and ankG (**B,E**; magenta). **C,F,** Composite image showing YFP+ axon colocalization with ankG, demarcating the AIS. YFP traces were taken from the line drawn across the ado-somatic vertex (**A,D**), through and past the region of the AIS (**C,F**). **G–I** Quantitative analysis of ankG profiles of sham (gray) and mTBI (gold). **G,** Cumulative frequency distribution plots showing overlap in start position but a proximal shift in mTBI end position. **H,** Multilevel analysis of start and end positions with animals as a random variable depicted by different shades. Data summarized with means and SEM error bars. Note that there is no change in ankG start position; however, there was a significant decrease in the end position. This resulted in an overall decrease in length from the distal AIS. **I,** Multilevel analysis of ankG length with animals as a random variable and distance from SCWM as a covariate. Plot of ankG length as a function of distance from SCWM (solid lines) with 95% CI (dashed lines) for sham and mTBI. Note that distance from SCWM is a significant covariate of ankG length, but there is no interaction with experimental groups indicated seen as a parallel shift in lines.

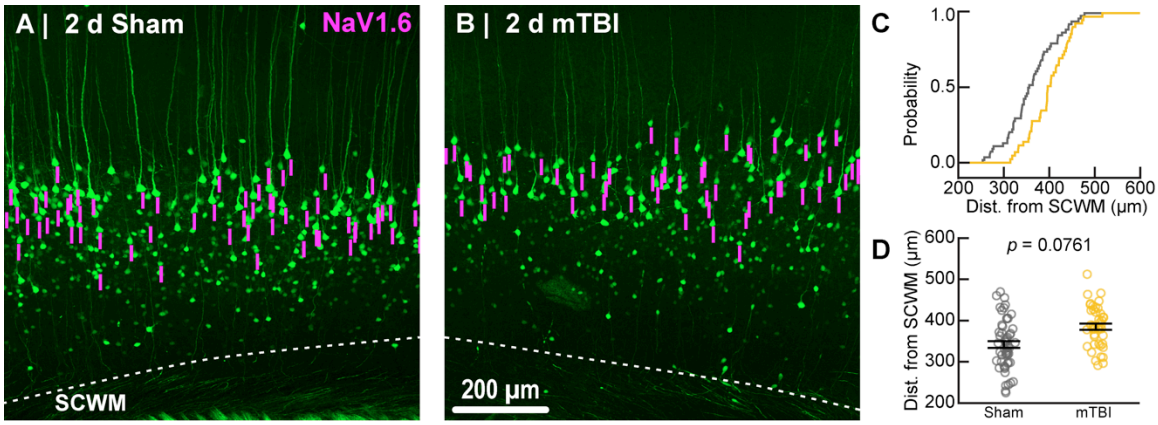

Figure 2.7. Sampling distribution of intact YFP+ pyramidal neurons for NaV1.6 quantitative analysis. **A,B,** Superimposed maximum intensity projections of 10x overview images for sham (**A**) and mTBI (**B**). The intact YFP+ pyramidal neuron sampling distribution (magenta bars) with respect to the SCWM appeared slightly asymmetric, with mTBI having several samples located more superficially (upper right aspect). **C,** Cumulative frequency distribution plot showing mTBI (gold) samples are shifted toward increased distance from SCWM compared to sham (gray). **D,** Quantitative analysis confirmed revealed there was no statistically significant difference in sampling. Statistics: Multilevel analysis with animals as a random variable. Data summarized with means and SEM error bars.

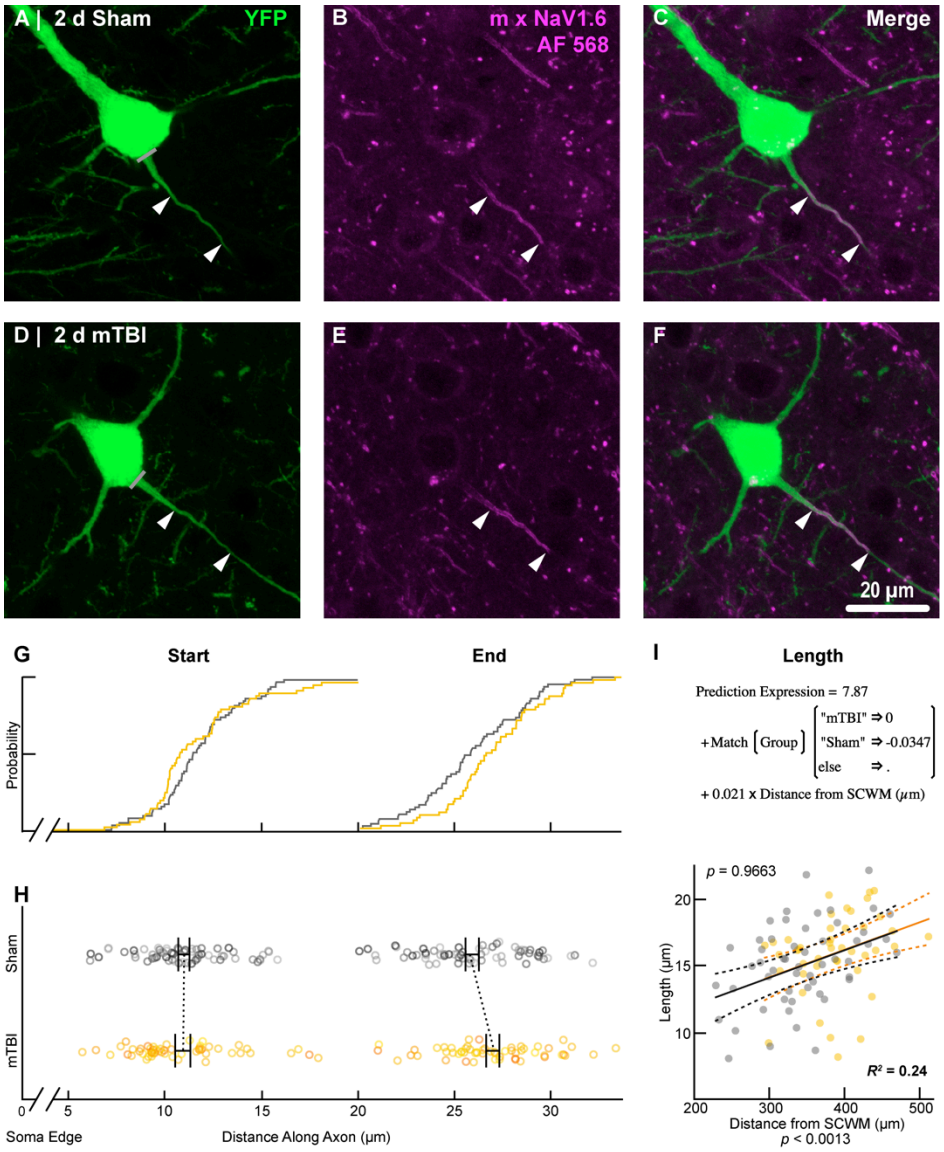

Figure 2.8. NaV1.6 geometry does not change after mTBI. Representative images of sham (**A–C**) and mTBI (**D–F**) of YFP (**A,D**; green) and NaV1.6 (**B,E**; magenta). **C,F,** Composite image showing YFP+ axon colocalization with NaV1.6, demarcating the distal AIS. **G–I**, Quantitative analysis of NaV1.6 profiles of sham (gray) and mTBI (gold). **G,** Cumulative frequency distribution plots showing overlap in start position but a distal shift in mTBI end position. **H,** Multilevel analysis of start and end positions with animals as a random variable depicted by different shades. Data summarized with means and SEM error bars. Note that there was no change in NaV1.6 start or end position. **I,** Multilevel analysis of NaV1.6 length with animals as a random variable and distance from SCWM as a covariate. Plot of NaV1.6 length as a function of distance from SCWM (solid lines) with 95% CI (dashed lines) for sham and mTBI. Distance from SCWM is a significant covariate of NaV1.6 length. This accounted for the overlap in sham and mTBI plots compared to the shift seen in the uncorrected distribution of the end position (G).

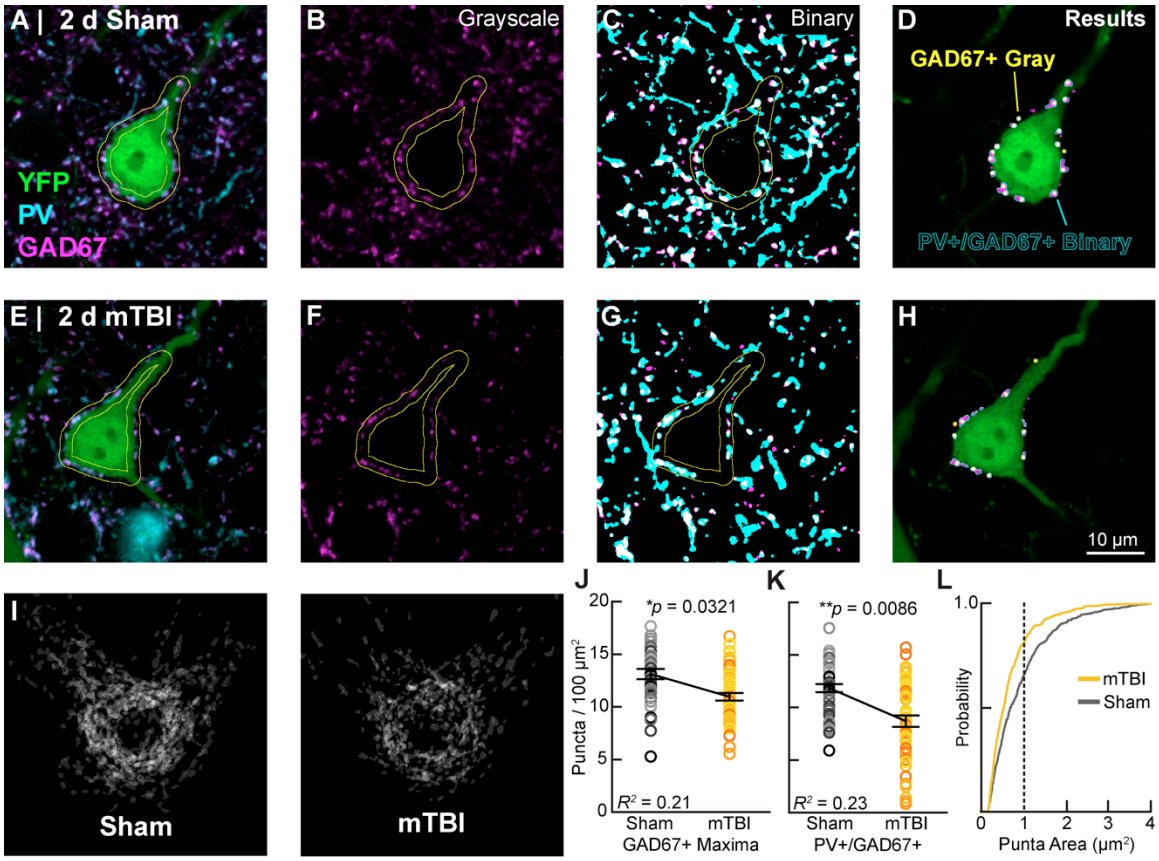

Figure 2.9. Intact YFP+ pyramidal neuron perisomatic GABAergic bouton density decreases 2 d post-mTBI. Representative images of sham (**A–D**) and mTBI (**E–H**) GAD67+ (**B,F**; magenta) and PV+ (**A,C,E,G**; cyan) punch along the perimeter of YFP+ pyramidal neurons (**A,E,D,H**; green). Perisomatic bouton density was quantified in 8-bit gray scale images of GAD67 expression (**B,F,J**) and also binary images of colocalized PV+/GAD67+ puncta (**C,G,I,K,L**). **D,H,** Outcome of automated quantification using gray scale and binary images was comparable. Perisomatic GAD67 expression (magenta) and result of gray scale analysis (yellow dots) largely overlapped with results of PV+/GAD67+ binary image analysis (cyan outlines). **I,** A qualitative decrease in perisomatic GABAergic bouton density is seen in superimposed images of binary PV+/GAD67+ profiles. **J,K** Multilevel analysis with animals as a random variable depicted by different shades for sham (gray) and mTBI (gold/orange). Data summarized with means and SEM error bars. GAD67+ maxima in grayscale images and PV+/GAD67 puncta in binary images were both significantly reduced in mTBI vs. sham. The absolute values as well as relative decrease were similar between grayscale and binary image analyses. **L,** Cumulative frequency distribution of PV+/GAD67+ puncta area. Vertical line at 1 µm2 corresponds to average size of a GABAergic presynaptic bouton. This shift in the mTBI plot shows that PV+/GAD67+ puncta approximating the average area of a GABAergic bouton accounting for the majority of the loss.

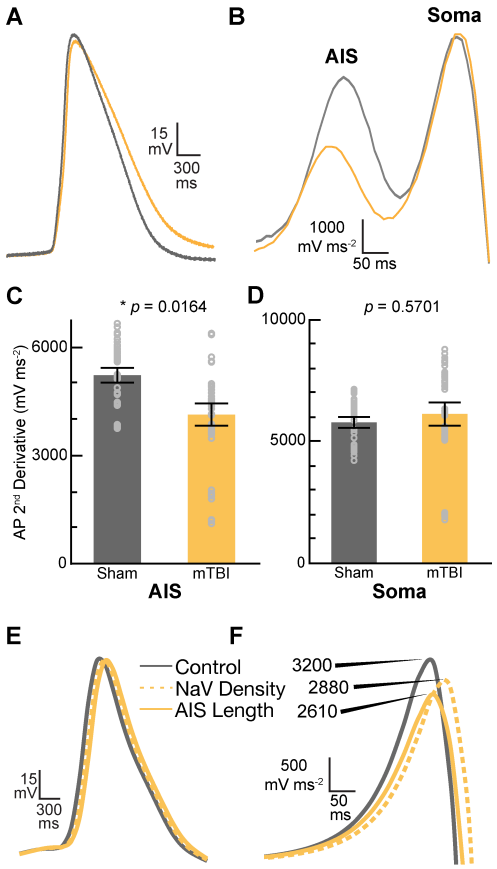

Figure 2.10. AP acceleration at the AIS is reduced 2 d post-mTBI. **A–C**, Electrophysiological analysis of layer 5 intact YFP+ pyramidal neurons in sham (gray) and mTBI (gold) live slices. Representative traces of AP (**A**) and second derivative of membrane voltage (**B**). **A,** AP between sham and mTBI were similar. **B,** In contrast, second derivative plots revealed the peak amplitude is reduced at the AIS but not the soma. **C,D,** Multilevel analysis of the second derivative with animals as a random variable and accounting for the 5 recorded AP nested within each neuron. Data summarized with means and 95% CI error bars. **C,** The peak amplitude at the AIS was significantly reduced, reflecting attenuated AP acceleration. **D,** In contrast, there was no change in the peak amplitude at the soma. **E,F**, Computational modeling of a layer 5 pyramidal neuron. Evoked AP waveforms in simulations (**E**) using experimentally observed AIS lengths were similar to AP recorded from intact YFP+ pyramidal neurons (**A**). Overall, changing AIS length or NaV density at the distal AIS by 7% did not have an overt effect on AP waveform. **F,** The plots of computationally derived second derivatives of membrane voltage were also comparable to experimental observations (**B**). Modeling data showed that a 7% decrease in AIS length or NaV density at the distal AIS both decrease peak amplitude of the second derivative plot.

AUTHOR CONTRIBUTIONS

MV, KMJ, and JTP contributed to the design of the experiments. MV performed all surgeries and confocal imaging. JS collected all electrophysiological data. Both MV and MB performed statistical data analyses. MV, JS, KMJ, and JTP contributed to writing of the manuscript.

CHAPTER THREE

MILD TBI INDUCES STRUCTURAL AND FUNCTIONAL DISCONNECTION OF LOCAL NEOCORTICAL INHIBITORY NETWORKS VIA PARVALBUMIN INTERNEURON DIFFUSE AXONAL INJURY

Michal Vascak, Xiaotao Jin, Kimberle M. Jacobs, John T. Povlishock

ABSTRACT

Diffuse axonal injury (DAI) plays a major role in cortical network dysfunction posited to cause excitatory/inhibitory imbalance after mild traumatic brain injury (mTBI). Current thought holds that white matter is uniquely vulnerable to DAI. However, clinically diagnosed mTBI is not always associated with white matter DAI. This suggests an undetected neocortical pathophysiology, implicating GABAergic interneurons. To evaluate this possibility, we used mild central fluid percussion injury to generate DAI in mice with Cre-driven tdTomato labeling of parvalbumin interneurons. We followed tdTomato+ profiles using confocal and electron microscopy, together with patch-clamp analysis to probe for DAI-mediated neocortical GABAergic interneuron disruption. Within 3h post-mTBI tdTomato+ perisomatic DAI (PSAI) was found across somatosensory layers 2–6. The DAI marker amyloid precursor protein colocalized with

GAD67 immunoreactivity within tdTomato+ PSAI, representing the majority of GABAergic interneuron DAI. At 24h post-mTBI we used phospho-c-Jun, a surrogate DAI marker, for retrograde assessments of sustaining somas. Via this approach we estimated DAI occurs in ~9% of total tdTomato+ interneurons, representing ~14% of pan-neuronal DAI. Patch-clamp recordings of tdTomato+ interneurons revealed decreased inhibitory transmission. Overall, these data show that parvalbumin interneuron DAI is a consistent and significant feature of experimental mTBI with important implications for cortical network dysfunction.

INTRODUCTION

Traumatic brain injury (TBI) is a serious global healthcare problem (Langlois et al. 2006). Recent attention is on mild TBI (mTBI) that represents almost 90% of all TBIs (Cassidy et al. 2004; Mannix et al. 2016). Cognitive impairments are common sequelae of mTBI and extract a substantial toll on society (McAllister 1992; CDC 2003). Compared to moderate-to-severe TBI involving mass lesions, contusion, and overt cell death, mTBI pathology is undetectable using routine CT/MRI (Mittl et al. 1994; Povlishock and Katz 2005). However, converging evidence now suggests that more subtle structural and functional disconnection of cortical networks underlies cognitive impairment seen after mTBI (Sharp et al. 2014; Fagerholm et al. 2015; Wolf and Koch 2016).

Although mTBI pathophysiology remains unclear, it is now recognized that microscopic diffuse axonal injury (DAI) contributes to mTBI morbidity (Povlishock and Katz 2005; Johnson et al. 2013; Smith et al. 2013). Previously, we showed that DAI is a

progressive axonopathy leading to overt structural disconnection followed by widespread terminal loss and Wallerian degeneration (Povlishock et al. 1983; Erb and Povlishock 1991; Povlishock 1993; Christman et al. 1994). Although studying diffuse changes in the fine-scale structure of neocortex is difficult (Crick 1979; Povlishock and Christman 1995), emerging evidence supports that widespread terminal loss/deafferentation of cerebral networks contributes to mTBI morbidity and sets the stage for subsequent adaptive or maladaptive plasticity (Povlishock et al. 1992; Christman et al. 1997; Phillips and Reeves 2001; Huang et al. 2009; Marquez de la Plata et al. 2011; Patel et al. 2016; van der Horn et al. 2016). It has been assumed that this DAI elicits cortical network disconnection primarily via the white matter (WM) tracts' vulnerability for deformation (Adams et al. 1989, 1991). This belief arose primarily from human post-mortem examinations (Strich 1956; Adams et al. 1982; Blumbergs et al. 1995) and was later reinforced with diffusion tensor imaging (DTI) of patients with TBI (Salmond et al. 2006; Bazarian et al. 2007; Kraus et al. 2007), which both revealed DAI signatures in the subcortical WM (SCWM), corpus callosum, and other deep WM tracts. While across the spectrum of TBI severity WM involvement cannot be dismissed (Mayer et al. 2010; Kinnunen et al. 2011), this presumption remains controversial in mTBI (Dodd et al. 2014). Several groups reported clinically diagnosed mTBI marked by substantial cognitive impairment without significant WM involvement (Zhang et al. 2010; Mac Donald et al. 2011; Ilvesmäki et al. 2014; Wäljas et al. 2014). This suggests an undetected structural-functional pathophysiology within neocortical gray matter (GM), where local (intrinsic) network processing relies on balanced excitatory/inhibitory neural activity (Aron 2007; Fries 2009; Haider and McCormick 2009; Raichle 2010).

Supporting this possibility, studies measuring neocortical metabolic (fMRI) and electrophysiological (EEG, MEG) change, revealed a wide range of intrinsic neocortical network dysfunction involving abnormal spontaneous, rhythmic, and excitatory/inhibitory activity (Mayer et al. 2011; Sponheim et al. 2011; Tremblay et al. 2011; Bashir et al. 2012; De Beaumont et al. 2012; Luo et al. 2013; Huang et al. 2016; Palacios et al. 2017). Additionally, recent DTI studies of neocortical GM have detected reactive changes suggesting that mTBI disrupts local structural connectivity (Newcombe et al. 2011; Bouix et al. 2013; Ling et al. 2013). Collectively, these clinical findings strongly implicate that mTBI disrupts structural and functional connectivity in local neocortical networks formed by excitatory (glutamatergic) pyramidal neurons and inhibitory (GABAergic) interneurons (Somogyi et al. 1998; McCormick 2003; Douglas and Martin 2007).

Both clinical and experimental methodologies used to investigate neocortical GM excitatory/inhibitory networks have limitations. Advanced structural and functional neuroimaging in mTBI patients cannot resolve the specific neuronal and physiologic substrates of neocortical GM disruption (Logothetis 2008; Delouche et al. 2015). Further, in both human (Gentleman et al. 1993; Blumbergs et al. 1994; Sherriff et al. 1994) and animal investigations (Stone et al. 2000; Mac Donald et al. 2007) DAI is typically identified via amyloid precursor protein (APP) immunohistochemistry, which transiently accumulates at sites of impaired axonal transport following TBI (Maxwell et al. 1997; Smith et al. 2013). While APP+ accumulations (swellings) distal aspect demarcates the site of axonal disconnection (Greer et al. 2011; Wang et al. 2011), this strategy fails to provide retrograde information (e.g. glutamatergic vs. GABAergic) on the soma of origin

(Büki et al. 2000; Povlishock and Stone 2001). Moreover, in the experimental setting excitatory/inhibitory cortical network disruption has mostly been assessed in animal models that evoke cell death (Carron et al. 2016) and/or mass lesions involving neocortical contusion (Kobori and Dash 2006; Cantu et al. 2014; Hsieh et al. 2016), which typically do not occur in mTBI associated with DAI (Povlishock and Katz 2005; Parikh et al. 2007; Andriessen et al. 2010).

To critically address these issues, we developed a clinically relevant, well-controlled transgenic mouse model of mTBI uncomplicated by mass lesions/contusion and cell death (Greer et al. 2011). Exploiting cytosolic fluorescent protein expression we conducted structural and functional assessments within neocortical GM of both DAI and non-DAI (intact) populations in a discrete subset (Thy1-expressing) of long-distance projecting excitatory pyramidal neurons. We reported that DAI within this pyramidal neuron subset primarily occurred near the soma of origin (Greer et al. 2013). We also found that this same perisomatic axonal injury (PSAI) was unresponsive to therapeutic targeting that proved neuroprotective within the underlying SCWM and corpus callosum (Hånell, Greer, McGinn, et al. 2015). Importantly, these findings suggested DAI within neocortical GM vs. the underlying WM tracts involved different pathophysiological mechanisms. In concert with neocortical DAI we also observed widespread electrophysiological abnormalities among intact pyramidal neurons associated with local network hyperexcitability post-mTBI (Greer et al. 2012; Hånell, Greer, and Jacobs 2015; Sun and Jacobs 2016). Since GABAergic interneurons regulate neocortical network activity (Isaacson and Scanziani 2011), these findings strongly implicated inhibitory interneuron disruption (Zhou et al. 2009; Yizhar et al. 2011; Lazarus et al. 2015).

While excitatory pyramidal neurons comprise 80% of neocortical neurons, their activity is controlled by the remaining 20% of inhibitory interneurons (DeFelipe and Fariñas 1992; Markram et al. 2004). The largest neocortical GABAergic interneuron subclass is genetically/molecularly characterized by parvalbumin (PV) expression and physiologically via their fast-spiking action potentials (Kawaguchi and Kubota 1997; Rudy et al. 2011). The extensive axonal arbor of a single PV+ interneuron can innervate up to a thousand neighboring postsynaptic neurons (Packer and Yuste 2011). In turn, PV+ interneurons receive converging inputs from excitatory pyramidal neurons and other PV+ interneurons (Gulyás et al. 1999), forming highly interconnected local neocortical networks that underlie gamma oscillations seen during cognitive loading (Howard 2003; Buzsáki and Wang 2012; Hu et al. 2014). Both clinical (Sponheim et al. 2011) and experimental (Paterno et al. 2016) mTBI studies have shown changes in these local neocortical firing patterns, which reflects changes in excitatory/inhibitory balance (Atallah and Scanziani 2009). Based on previous clinical observations, our own findings, and these PV+ interneuron properties, we questioned whether mTBI induces structural and functional disconnection via DAI within local neocortical inhibitory networks.

To address this issue, we further refined our mTBI model by employing Cre/lox mice (Madisen et al. 2010) to genetically label the total PV+ interneuron population (Hippenmeyer et al. 2005). Specifically, we relied on Cre-driven expression of the red fluorescent protein (RFP) tdTomato within PV+ interneurons, coupled with immunohistochemical strategies for optimal structural assessment of potential DAI via confocal and ultrastructural analysis. Additionally, we performed targeted patch-clamp analysis of neocortical fast-spiking tdTomato+ interneurons to functional assess

inhibitory transmission within pharmacologically isolated local GABAergic networks. Using this multifaceted approach we show for the first time that GABAergic interneurons undergo DAI, preferentially involving PV+ interneuron PSAI. Additionally, we report a concurrent reduction of inhibitory transmission within local neocortical PV+ interneuron networks. Together, these findings have major implications in neocortical network dysfunction following mTBI.

METHODS AND MATERIALS

Animals

The Virginia Commonwealth University Institutional Animal Care and Use Committee approved all protocols involving animal maintenance and experimentation. Homozygous PV-Cre [B6;129P2-Pvalbtm1(cre)Arbr/J; Stock No. 008069, (Hippenmeyer et al. 2005)] and reporter line Ai9 [B6.Cg-Gt(ROSA)26Sortm9(CAG-tdTomato)Hze/J; Stock No. 007909, (Madisen et al. 2010)] breeding pairs were directly received from Jackson Laboratory. We generated experimental animals (PV-Cre;Ai9 mice) by crossing homozygous male PV-Cre mice with female Ai9 tdTomato reporter mice. In the F1 progeny hemizygous at both alleles, Cre-driven recombination occurs in greater than 90% of Pvalb-expressing neurons (Taniguchi et al. 2011). This resulted in selective tdTomato labeling of neocortical PV+ interneurons.

Experimental Design

A total of 38 male PV-Cre;Ai9 mice were randomly assigned to either sham-injury (control) or mTBI experimental groups. For confocal and electron microscopy (EM) studies, a total of 20 mice (8.7–10.9 weeks; 21.1–29.8 grams) were surgically prepared

for either sham-injury (N = 5) or mTBI (N = 15) induction. Three mTBI mice were excluded for not meeting previously established criteria (Greer et al. 2011). Based on our previous work we assessed DAI and downstream structural-functional changes at 3 h and 24 h post-mTBI, respectively (Greer et al. 2011; Hånell, Greer, McGinn, et al. 2015). At 3 h post-mTBI, we probed for DAI in PV-Cre;Ai9 mice by analyzing tdTomato+ axonal profiles via parallel confocal microscopy (n = 5) and EM (n = 3). To further confirm DAI we compared tdTomato+ axonal profiles against endogenous PV protein and APP immunoreactivity. In a complementary confocal analysis we tested whether the GABA vesicular transporter (VGAT) and synthesizing enzyme (GAD67) also delineate DAI. As previously reported, between 3 h and 24 h post-mTBI in mice, the distal disconnected axonal segment undergoes Wallerian degeneration, increasing axonal debris. In contrast, by 24 h post-mTBI proximal axonal swelling contiguous with soma of origin begins to resorb, decreasing APP immunoreactivity (Hånell, Greer, McGinn, et al. 2015). Therefore, to comprehensively study the anterograde and retrograde sequelae of tdTomato+ DAI we temporally assessed the relation of the observed axonal debris to nuclear responses in their sustaining somas. Specifically, to identify tdTomato+ somas sustaining DAI while evaluating their fate, we used a previously developed strategy based on retrograde activation of c-Jun via phosphorylation (p-c-Jun), a nuclear transcription factor associated with cell survival and axonal regeneration (Raivich et al. 2004; Greer et al. 2011; Wang et al. 2013). We also employed p-c-Jun as a parallel somatic DAI marker to estimate overall burden of injury in PV-Cre;Ai9 mice at 24 h post-mTBI (n = 4). For all qualitative and quantitative confocal assessments sham mice (3 h: n = 2; 24 h: n = 3) did not reveal any significant differences ($0.5 < p \leq 1.0$;

Wilcoxon test). Therefore, 3 h and 24 h sham mice were considered as a single control group (n = 5) for quantitative analyses of temporal changes following mTBI. Lastly, to probe for any functional correlates of our structural findings we recorded in slice preparations electrophysiological data from a total of 18 PV-Cre;Ai9 mice (6.0–8.4 weeks; 20.0–26.8 grams) at 24 h following sham-injury (N = 8) of mTBI (N = 10).

Surgical Preparation for cFPI

To model mTBI we used midline cFPI first described by Dixon et al., (1987) using rats, which our lab modified for mice as described previously (Greer et al. 2011). Briefly, anesthetized mice were surgically prepared for cFPI induction by installing a hub surrounding a craniectomy centered on the superior sagittal suture, midway between bregma and lambda. Intraoperative rectal temperature was maintained at 37 ± 0.2°C using a thermostatically controlled heating pad (Harvard Apparatus). Additionally, heart rate (BPM), respiratory rate (RPM), and arterial blood oxygenation (SpO2) were monitored using a thigh-clamp pulse oximeter sensor (MouseOx; STARR Life Sciences) to ensure maintenance of physiological homeostasis. After a post-operative recovery (~1.5 h), mice were re-anesthetized and then connected to the fluid percussion apparatus (Custom Design & Fabrication, Virginia Commonwealth University) forming a closed mechanical system. Releasing the pendulum, striking the piston in the fluid percussion apparatus generated a mild pressure wave transient (~20 msec; mean peak = 1.6 ± 0.02 SEM atmospheres) that was delivered onto the intact dura. This action simulates human brain inertial loading during trauma-induced rapid acceleration-deceleration causing diffuse brain injury. The pressure wave (mean peak = 1.6 ± 0.02 SEM atmospheres) was measured by a transducer and displayed on an oscilloscope (Tektronix TDS 210). For

sham-injury, an identical procedure was used with the exception of the pendulum's release. Mice were disconnected from the apparatus immediately after injury and visually monitored while removing the hub, suturing the incision, and checking reflexes. None of the mice showed signs of seizure or apnea. Severity of injury and duration of loss of righting reflex (LORR), a rodent behavioral surrogate of loss of consciousness (LOC), were recorded for each animal (Grimm et al. 2015). We determined the degree of mTBI by comparing LORR duration with shams (Morehead et al. 1994). After recovering from LORR animals were transferred to a warmed cage to maintain normothermia and monitored before returned to the vivarium.

Perfusion and Tissue Processing

Mice received a lethal dose of sodium pentobarbital (1.6 mg/g IP) 3 h or 24 h survival. After loss of pain reflexes mice were transcardially perfused, first with heparinized (10 units/ml) saline for 1 min then 4% paraformaldehyde in Millonig's buffer pH 7.4 for 10–20 min. Brains were dissected and immersed in the same fixative overnight at 4°C. Mice for EM studies were perfused with 4% paraformaldehyde in Millonig's buffer pH 7.4 supplemented with 0.2% glutaraldehyde. Brains were then section coronally at 40 µm using a vibratome (Leica VT1000S). Sections directly below the craniectomy (bregma level −0.58 to −2.5 mm) were collected in 24-well plates filled with Millonig's buffer pH 7.4. Each well had two sections, one rostral from the first series of 24 sections collected and one caudal from the second series of 24 sections (i.e. sections 25–48). Serial sections within a single column were spaced 240 µm apart. For all quantitative studies we randomly sampled from caudal sections (1.5–2.5 posterior to bregma) due to the

consistency with which our mTBI model generates DAI within a well-defined region of neocortical GM containing S1 (Greer et al. 2011).

Immunohistochemistry

Free-floating sections were rinsed with PBS. Heat-induced epitope retrieval was performed by incubating sections in 10 mM sodium citrate buffer pH 8.5 for 10 min in an 80°C water bath (Jiao et al. 1999). After cooling to room temperature sections were rinsed with PBS then incubated for 1 h at room temperature with 10% normal goat serum, 2% fish skin gelatin, and 0.5% Triton X-100 in PBS. To mask any potential endogenous mouse immunoglobulin, the blocking buffer was supplemented with Mouse-on-Mouse reagent (MOM; Vector Laboratories, MKB-2213). Then, sections were rinsed with 1% normal goat serum, 1% fish skin gelatin, and 0.5% Triton X-100 in PBS (working buffer). Primary antibody solutions were prepared by diluting with working buffer and the sections were incubated overnight at 4°C. Specifically, we used antibodies against PV (mouse IgG1, 1:2000, PV235; rabbit, 1:2000, PV27; Swant), RFP (mouse IgG2a, clone 8E5.G7, 1:1000, 200-301-379; rabbit, 1:1000, 600-401-379; Rockland), APP (rabbit, 1:500, Invitrogen, 51-2700; mouse IgG1, clone 22C11, 1:500, Millipore, MAB348), VGAT (polyclonal rabbit, 1:1000; Synaptic Systems, 131 013), GAD67 (mouse IgG2a, clone 1G10.2, 1:1000; Millipore, MAB5406), and p-Ser63 of c-Jun (rabbit, 1:100; Cell Signaling Technology). The following day, sections were rinsed with working buffer and incubated with appropriate goat-derived secondary antibodies conjugated to Alexa Fluor 488, 568, or 633 (1:500: ThermoFisher Scientific) for 2 h at room temperature. After final rinses using working buffer then PBS, sections were mounted on glass slides and

cover-slipped using non-hardening Vectashield ± DAPI (Vector Laboratories, H-1000 or H-1200). Note, when labeling p-c-Jun PBS was replaced with TBS.

Mouse immunoglobulin isotype-specific secondary antibodies were used in all studies to optimize the signal-to-noise ratio (Manning et al. 2012). Parallel control studies were conducted to ensure both primary and secondary antibody fidelity (Lorincz and Nusser 2008). In all cases, primary antibody omission abolished immunoreactivity. Secondary antibody specificity evaluated via cross-reactivity showed no signal between all possible primary × secondary host and/or isotype combinations. Also, tdTomato signal photostabilization was achieved using primary RFP antibodies reacted with secondary antibodies conjugated to Alexa Fluor 568.

Confocal Microscopy

Image acquisition was performed using a laser-scanning confocal microscope (LSM 710, Carl Zeiss). Adhering to stereological principles including random sampling, in all quantitative studies the investigator was blinded from the experimental/dependent variable channel while choosing the region-of-interest visualized under epifluorescence. Using a 10× objective (low-power) the field-of-view (FOV) was centered over the primary somatosensory cortex (S1) along the dorsolateral edge of the hippocampus. For equal representation of each neocortical layer 2–6, we used continuous laser scanning to guide rotation of the FOV until it was orthogonal to the underlying subcortical white matter. Images were acquired with optimal Nyquist sampling using Plan-Apochromat 10×/0.45 NA (XY = 0.41 μm/pixel; Z = 5.8 μm), 20×/0.8 NA (XY = 0.152 μm/pixel; Z = 0.94 μm), and 40×/1.4 (XY = 0.094 μm/pixel; Z = 0.47 μm) oil immersion object lenses. All multichannel images were acquired using sequential scanning at the lowest possible

last power to avoid crosstalk (488 Argon, 561 DPSS, and 633 HeNe). Gain and offset were adjusted for optimal signal range. The pinhole was set to 1.0 ± 0.3 Airy units to maintain identical optical slice thickness in multichannel images. Images for quantitative analysis were acquired using identical settings across samples. For qualitative DAI analyses, z-stack images captured the entire dimensions of perisomatic/proximal axonal swellings contiguous with the soma of origin, and the also the distal disconnected axonal segment up to the initial branch point when possible.

Electron Microscopy

Ultrastructural analysis of tdTomato+ DAI at 3 h post-mTBI mice was conducted as described previously by our lab (Greer et al. 2011; Hånell, Greer, McGinn, et al. 2015). To confirm the fidelity of tdTomato labeling PSAI we performed photoconversion to follow the same fluorescently labeled profile from confocal imaging to an electron dense reaction product with EM. First, sections were wet-mounted for confocal imaging and then refloated in PBS for EM processing. To immunolabel tdTomato in sections for EM, we employed the same monoclonal RFP antibody (1:1000) used for photostabilization as described above. We converted the fluorescent signal into an electron dense product via routine peroxidase-based immunoreaction visualized using 3,3-diaminobenzidine. Regions containing confocal-identified tdTomato+ PSAI profiles were located in plastic embedded tissue sections using standard light microscopy. These regions were removed and used for sectioning. One thick section (0.5–1 μm) was cut before collecting thin serial sections (70 nm) and saved to guide location of the labeled neuron of interest. Ultrastructural analysis was performed using a JEM-1230 transmission electron

microscope (JEOL-USA) equipped with an Ultrascan 4000SP and Orius SC1000 CCD cameras (Gatan).

Quantitative Confocal Image Analysis

An investigator blinded to experimental/dependent variables performed all quantitative image analyses. Confocal images were imported to Fiji (ImageJ) then processed and analyzed using custom written macros. For automated analyses, objects were segmented from background subtracted 8-bit images by converting into binary using a minimum gray-value threshold. Varying the threshold ±10 gray-values did not change the overall pattern of results. For colocalization studies we isolated spatially overlapping objects (Ch1+/Ch2+) using the 'Image Calculator' function. The 'Particle Analysis' function with appropriate size and shape exclusion filters was used to determine the total number of objects per unit area (FOV). To determine the appropriate statistical unit for continuous data we analyzed the means of the differences between images of ipsi- and contra-lateral hemispheres within each individual group, and also across different experimental groups. There were no statistically significant differences (p-values ranging from 0.1250–1.0000; Wilcoxon Signed Rank test); therefore, we considered the statistical unit as a single section. To determine the total count per section, we summed the number of objects (particles) per FOV of ipsi- and contra-lateral hemispheres. We divided the sum of particles per section by the combined area to yield a normalized density reported as particles/mm^2.

We used pixel-based intensity correlation to assess the overlap of tdTomato expression with PV and RFP immunoreactivity specifically in axons and dendrites. A

minimum and maximum thresholds were applied to subtracted background and exclude the high-intensity signals from neuronal somas, respectively. The 'Colocalization Finder' function was used to measure pixel intensity spatial correlation, which yields a Pearson's Correlation Coefficient (Rr). The percentage of soma overlap and the Pearson's Rr were then averaged for each group (tdTomato/PV: n = 6 FOV from 3 mice; tdTomato/RFP: n = 4 FOV from 2 mice).

GABAergic Markers of DAI

Currently, there are no neuronal class-specific DAI markers. To establish a GABAergic-specific DAI marker we performed a two-part (visual and automated) quantitative colocalization analysis. From each animal (n = 5) four serial sections starting at a random well (#1–6) were double labeled for GAD67 and APP. The first section from each series was saved for a pilot study described below and the remaining sections were used for quantitative colocalization analyses. Low-magnification (10× objective) full-section z-stacks captured GAD67 and APP immunoreactive profiles in S1 layers 2–6. Visual analysis of low-magnification images yielded 97% accuracy of identifying GAD67+/APP+ axonal swellings (N = 183) from GAD67+ profiles (N = 189). To quantitatively assess colocalization with native tdTomato expression single optical slices through the center of each GAD67+/APP+ axonal swelling were acquired using a 20× objective at 3× zoom. We estimated the percentage of neocortical GABAergic DAI represented by PV+ interneurons from the frequency of GAD67+/APP+ axonal swellings that were tdTomato+ (N = 158) and tdTomato– (N = 25) and compared the proportions that occurred in the perisomatic domain.

Further, we performed quantitative colocalization analysis to determine if GAD67+ accumulations (particles) are a positive predictor of APP+ axonal swellings at 3 h post-mTBI. Automated object-based colocalization analysis of maximum intensity projections segregated the population of GAD67+ particles that were and were not colocalized with APP. We determined the optimal threshold area of axonal swellings by analyzing GAD67+ particle size distribution varying as a function of APP colocalization in the first serial section from each animal. From these subpopulations we determined maximum (30 μm2) and minimum (5 μm2) threshold areas to minimize quantification of individual and/or clusters of GAD67+ presynaptic boutons, respectively. We found that a GAD67+ particle size threshold of 10 μm2 predicted APP colocalization with a 76% sensitivity and 96% specificity. Using the remaining serial sections we determined the frequency of GAD67+ particles with areas above (N = 138) and below (N = 799) the 10 μm2 threshold and compared the proportions that colocalized with APP+ axonal swellings.

p-c-Jun Expression following tdTomato+ Interneurons PSAI

Continuous tdTomato+ PSAI profiles traceable back to the soma of origin provided a unique opportunity to follow retrograde changes. We evaluated p-c-Jun expression at 3 h post-mTBI, when tdTomato+ PSAI was readily identified. Randomly selected single sections per animal (n = 5) were labeled for p-c-Jun. To attain a sufficient sample size while retaining adequate resolution we used a 20× objective to acquire full-section z-stacks. The FOV was centered in S1 layer 5, which has highest density of PV+ interneurons (Rudy et al. 2011; Pfeffer et al. 2013). All tdTomato+ interneurons were counted to ensure the samples were representative. First, an investigator blinded to the p-

c-Jun channel visually identified and marked tdTomato+ somas with PSAI morphological profiles within a 20 μm radius (N = 22). The remaining unmarked tdTomato+ interneurons were considered non-PSAI/intact (N = 497). Object-based colocalization analysis isolated tdTomato+/p-c-Jun+ somas and the proportions overlapping with marked (PSAI morphology) and unmarked (non-PSAI/Intact) profiles were compared.

Anterograde and Retrograde Sequelae of tdTomato+ Interneuron PSAI

Previously we showed anterograde changes following PSAI involve rapid axonal disconnection and Wallerian degeneration (Kelley et al. 2006), which is associated with widespread terminal loss (Erb and Povlishock 1991; Povlishock et al. 1992). Also, we reported that the retrograde consequences of DAI do not involve cell death (Singleton et al. 2002). Rather, DAI neurons express p-c-Jun (Greer et al. 2011; Wang et al. 2013), a nuclear transcription factor associated with cell survival and axonal regeneration (Raivich et al. 2004). Here, we quantitatively analyzed the densities of tdTomato+ axonal debris and tdTomato+/p-c-Jun+ interneurons in mice following sham-injury (n = 5), 3 h mTBI (n = 5) and 24 h mTBI (n = 4). Based on mean ± SD of pilot data we determined one randomly selected section per animal would be sufficient to detect a significant difference in tdTomato+/p-c-Jun+ density between sham and 24 h post-mTBI. During immunohistochemical processing one of the 3 h mTBI sections was lost to damage. Automated object-based analysis was used to quantify the density of axonal debris, tdTomato+/p-c-Jun+ interneurons, and total tdTomato+ and p-c-Jun+ populations. The numbers of tdTomato+/p-c-Jun+ somas were used to estimate overall burden of injury with respect to the total tdTomato+ interneuron population and pan-neuronal DAI (pyramidal and interneuron) p-c-Jun+ nuclei population.

Electrophysiology

To determine functional correlates of tdTomato+ interneuron PSAI we probed for disruption of GABAergic transmission in local neocortical inhibitory networks. In a separate cohort of mice, acute slice preparation, patch-clamp recordings, and data analysis were performed as described in our previous reports (Hånell, Greer, and Jacobs 2015; Sun and Jacobs 2016). Briefly, we recorded spontaneous inhibitory postsynaptic currents (sIPSC) in tdTomato+ interneurons within layer 5 of S1BF in ex vivo coronal slices 24 h after sham-injury (N = 8) or mTBI (N = 10). To isolate sIPSC from excitatory currents, the normal aCSF bathing medium was supplemented with glutamate receptor antagonists (50 mM APV and 20 mM DNQX). The intracellular solution (ECl- = –15 mV) contained (in mM): 70 K-gluconate, 70 KCl, 10 Hepes, 4 EGTA, 4 Na-ATP, and 0.2 Na-GTP, and 0.05-0.2% biocytin conjugated to Alexa Fluor 488 (ThermoFisher Scientific). IPSCs were recorded from tdTomato+ interneurons held 3 min under voltage-clamp at –60 mV and data having more than 200 events were analyzed. Action potentials were recorded using current-clamp of tdTomato+ interneurons maintained at –60 mV and analyzed from individual sweeps with eight or more events. For post hoc morphological analysis sections were immersed in 4% paraformaldehyde pH 7.4 in PBS for 2 h at room temperature and then stored in PBS. Immunohistochemistry for p-c-Jun was performed as described above. Biocytin was reacted with streptavidin conjugated to Alexa 488 (1:1000; ThermoFischer Scientific) during the secondary antibody incubation step. Electrophysiological recordings were acquired from a total of 46 tdTomato+ fast-spiking PV+ interneurons (Sham n = 18; mTBI n = 28). Individual neurons were considered as the statistical unit.

Statistics

Data analysis was performed using JMP Pro version 12.2.0 (SAS Institute) software. Continuous data sets were assessed for normality using quantile (QQ) plots and the Shapiro-Wilk test. Normal data are summarized using mean ± standard deviation (SD) with corresponding 95% confidence intervals (CI). Significant differences in normally distributed data were determined using parametric tests. In all analyses the variance did not significantly different between groups ($p > 0.05$, Brown-Forsythe test). Statistically significant differences were determined between two groups that were either independent or dependent using unpaired and paired t-test, respectively. For multiple groups, we performed one-way ANOVA followed by post hoc comparisons of all pairs using the Tukey-Kramer HSD test. Continuous data distributions deviating from normality were summarized using medians with inter-quartile range (IQR), and analyzed with non-parametric statistical tests. Statistically significant differences between two groups were determined using the Wilcoxon test. Multiple groups were statistically analyzed using the Kruskal-Wallis test followed by post hoc comparisons with control (sham-injury group) using the Dunn method for joint ranking. The Pearson and Spearman tests were used to determine significant correlations between parametric and non-parametric data sets, respectively. For categorical data the proportions of dichotomous groups were compared using 2×2 contingency analysis. Significant differences were determine using a X2 test if the expected frequencies were greater than five; otherwise, the group proportions were analyzed with the Fisher's exact test. All statistical tests were two-tailed and the significance threshold was $\alpha = 0.05$.

RESULTS

Intraoperative Physiology and Mild cFPI

Intraoperative physiology was normal and consistent with previous reports on mice under isoflurane anesthesia (Cesarovic et al. 2010; Ewald et al. 2011; Hånell, Greer, McGinn, et al. 2015). For mice used in morphological studies, mean ± SD arterial oxygen saturation (sham = 97.6 ± 0.2%; 3 h mTBI = 97.7 ± 0.5%; 24 h mTBI = 98.1 ± 0.4%), heart rate (sham = 553 ± 23 BPM; 3 h mTBI = 565 ± 17 BPM; 24 h mTBI = 536 ± 55 BPM), and respiratory rate (sham = 67 ± 9 RPM; 3 h mTBI = 62 ± 9 RPM; 24 h mTBI = 66 ± 6 RPM) were similar across all groups (arterial oxygen saturation: $F_{2,13} = 2.80$, $p = 0.1005$; heart rate: $F_{2,13} = 0.81$, $p = 0.4688$; respiratory rate: $F_{2,13} = 0.58$, $p = 0.5758$; one-way ANOVA). Similarly, in the mice used for electrophysiological analysis, arterial oxygen saturation (sham = 97.5 ± 0.7%; mTBI = 97.8 ± 0.3%), heart rate (sham = 555 ± 36 BPM; 24 h mTBI = 524 ± 44 BPM), and respiratory rate (sham = 68 ± 5 RPM; 24 h mTBI = 68 ± 6 RPM) were similar across all groups (arterial oxygen saturation: $t_{16} = 1.15$, $p = 0.2785$; heart rate: $t_{16} = -1.25$, $p = 0.2380$; respiratory rate: $t_{16} = 0.01$, $p = 0.9896$; unpaired *t*-test). Importantly, signs of hypoxia were not observed (minimal respiratory rate 50 ± 17 RPM, 95% CI: 54—69 RPM) and ≥95% oxygen saturation was maintained throughout the duration of the surgery. Overall, these physiological assessments did not show any evidence of confounding mechanisms that play a role in secondary insults.

The LORR duration was significantly greater in mTBI mice compared to shams and consistent with our previous reports (Greer et al. 2011, 2013; Hånell, Greer, McGinn, et al. 2015). For mice used in morphological studies, there was a significant difference in LORR duration between sham and mTBI groups ($F_{2,13} = 40.66$, $p < 0.0001$; one-way

ANOVA). Specifically, *post hoc* comparisons showed LORR duration of both 3 h mTBI (4.8 ± 0.8 min, 95% CI: 3.9–5.7 min) and 24 h mTBI (4.3 ± 0.9 min, 95% CI: 3.2–5.4 min) groups to be significantly longer ($p < 0.0001$; Tukey-Kramer HSD) compared to shams (1.1 ± 0.3 min, 95% CI: 0.7–1.4 min). No significant difference in LORR duration was observed between the 3 h and 24 h mTBI groups ($p = 0.4317$). Similarly, in mice used for electrophysiological analysis there was a significant difference in LORR duration between sham (1.2 ± 0.7 min, 95% CI: 0.3–2.1 min) and mTBI (5.0 ± 2.0 min, 95% CI: 3.6–6.4 min) groups ($t_{16} = 4.01$, $p = 0.0015$; unpaired *t*-test). No significant differences in LORR duration were observed between morphological and electrophysiological groups (sham: $t_{11} = -0.47$, $p = 0.6479$; mTBI: $t_{23} = -0.63$, $p = 0.5383$; unpaired *t*-test). Lastly, no animals were lost to anesthesia, surgical preparation, or mild cFPI.

Macroscopically, both sham and mTBI brain tissue appeared normal without evidence of surgically-induced lesions as previously reported (Kelley et al. 2006; Greer et al. 2011; Hånell, Greer, McGinn, et al. 2015). Post-mTBI tissue sections revealed little to no macroscopic change consistent with the mild and diffuse nature of cFPI (Dixon et al. 1987; Johnson et al. 2015; Lifshitz et al. 2016). Importantly, the dorsal neocortex underneath the craniectomy site did not show evidence of focal contusion, cavitation, or overt subarachnoid hemorrhage induced by the fluid pressure wave. Overall, the brain parenchyma was devoid of overt hemorrhage, with only isolated petechial hemorrhage observed in the corpus callosum of 8/21 mTBI mice. At all survival times, the ventricular system maintained a regular contour, with no evidence of trauma-related ventricular

enlargement. Taken together these data support our premise that cFPI in PV-Cre;Ai9 mice is a reproducible model of mTBI.

Characterization of PV-Cre;Ai9 Mice and tdTomato Photostabilization

PV-Cre;Ai9 mice provided a homogenous and reliable system to probe for PV+ interneuron DAI. To enable optimal analysis of PV+ interneuron fine axonal structure we fluorescently labeled cells by crossing PV-Cre mice with the Ai9 Cre-dependent tdTomato reporter line. PV+ interneurons were selectively labeled with tdTomato across neocortical layers 2–6, where broad colocalization with endogenous PV protein immunoreactivity was observed (Fig. 1*A*). Expression specificity between the Cre-dependent tdTomato reporter and the endogenous *Pvalb* gene was quantitatively assessed via immunofluorescence using a monoclonal antibody against PV protein (Fig. 1*B–D,J*). A high degree of expression specificity was observed using both object-based analysis of soma overlap (mean, 95% CI: 93, 89–96% of tdTomato expressing somas were PV+; and 95, 93–97% of PV+ somas expressed tdTomato) and pixel intensity spatial correlation of dendrites and axons (Pearson's $Rr = 0.81$). To stabilize the tdTomato fluorescent signal and increase the visibility of slender axonal fibers (Fig. 1*H*), we used an additional approach that employed primary antibodies against RFP that recognize tdTomato (Fig. 1*E–G*). Specificity of RFP antibodies used throughout this study was tested via immunoreaction with sections from PV-Cre;Ai9 (positive control; Fig. 1*E–G*) and wild-type C57BL/6 (negative control; Fig. 1*I*) mice, the background strain for both the PV-Cre and Ai9 knock-in gene targeted mice (Hippenmeyer et al. 2005; Madisen et al. 2010). In the PV-Cre;Ai9 positive control (Fig. 1*E,F*), immunoreaction with RFP antibodies was visualized using secondary antibodies conjugated to Alexa Fluor 488 (Fig. 1*F*), revealing

broad colocalization with tdTomato expression (Fig. 1*E–G*). Similar to PV immunoreactivity (Fig. 1*J*), a high degree of RFP antibody specificity was observed using both object-based analysis of soma overlap (mean, 95% CI: 93, 87–98% of tdTomato expressing cells were RFP+; and 97, 93–100% of RFP immunoreactive cells were tdTomato+) and pixel intensity spatial correlation (Pearson's $Rr = 0.83$). However, in the parallel negative control reaction, no RFP immunoreactivity was observed in wild-type C57BL/6 sections (Fig. 1*I*). The robust and reliable expression of tdTomato as well as its intrinsic brightness, coupled with its photostabilization, allowed for detailed, high fidelity analysis of the fine axonal structure of PV+ interneurons.

Evidence for PV+ Interneuron DAI Demonstrated by tdTomato Expression

PV-Cre;Ai9 mice following sham or mTBI showed major differences in their tdTomato+ profiles. No tdTomato+ profiles indicative of DAI were observed in shams (Fig. 1*D,G*). Axons arising from tdTomato+ somas were fine caliber (~0.5 μm). With respect to the soma of origin, tdTomato+ axons could be traced approximately 30 μm distally to their initial branch point where secondary fibers then became difficult to follow (Fig. 1*H*). Following mTBI, despite the macroscopic preservation of brain parenchymal integrity, cFPI consistently evoked microscopic tdTomato+ axonal pathology revealing DAI throughout the dorsolateral neocortex (Fig. 2). At 3 h post-mTBI PV-Cre;Ai9 mice showed readily identified tdTomato+ axonal swellings (~5 μm in diameter) proximal to their soma of origin (within 20 μm) scattered across S1 layers 2–6 (Fig. 2*A–F*). Most of these tdTomato+ axonal swellings were in continuity with their soma of origin, consistent with PSAI described in our previous communications (Singleton et al. 2002; Kelley et al. 2006; Greer et al. 2013; Hånell, Greer, McGinn, et al. 2015). Axonal segments between

perisomatic swellings and their somas retained a normal caliber (Fig. 2*F*). The majority of tdTomato+ PSAI coursed toward the cortical pial surface (Fig. 2*A–F*), consistent with PV+ interneuron morphological characteristics (Markram et al. 2004). Less frequently, smaller isolated tdTomato+ globular profiles were found, suggesting potential sites of axonal injury remote from their soma of origin. The tdTomato+ distal axonal segments disconnected from their perisomatic/proximal axons revealed anterograde change reflected in bulbous, multilobular varicosities (Fig. 2*F*). Typically these disconnected distal axonal segments could be traced to their initial branch point, indicating that tdTomato+ PSAI leads to disconnection and degeneration of the entire distal axonal arbor (Fig. 2*H*). At 24 h post-mTBI (Fig. 2*H–K)* the tdTomato+ PSAI profiles were difficult to identify. In contrast, readily observable were dense tdTomato+ globules ranging from 1–5 μm in diameter scattered throughout regions of neocortical DAI, again consistent with progressive anterograde degeneration of disconnected distal axonal segments (Fig. 2*I,J*) and their associated terminals (Fig. 2*K*).

The parallel use of RFP antibodies not only helped stabilize and enhance the tdTomato signal, but also allowed the confirmation of these confocal microscopy findings (Fig. 2*A–G*; Fig. 3*A,B*) with ultrastructural analysis (Fig. 3*C–E*). Photoconverting the fluorescent signal into an electron dense reaction product via routine peroxidase-based methods allowed visualization of the same tdTomato+ interneuron using both confocal (Fig. 3*A,B*) and EM (Fig. 3*C–E*). At 3 h post-mTBI, ultrastructural analysis of a tdTomato+ PSAI interneuron revealed a proximal axonal swelling, contiguous its soma, that was laden with organelles and vesicles (Fig. 3*E*), pathognomonic of focal impaired axonal transport (Povlishock 1993). The associated disconnected distal segment showed

evidence of cytoskeletal disorganization and the rapid onset of Wallerian degeneration (Fig. 3*D*).

APP Expression after mTBI: Linkage to tdTomato+/PV+ Interneuron Axonal Changes

Neocortical tdTomato+/PV+ interneuron DAI was also confirmed using APP immunofluorescence. The focal intra-axonal vesicle accumulations seen in EM images (Fig. 3*E*) were detected indirectly using confocal microscopy by targeting APP (Fig. 4*B,F,J*). At 3 h post-mTBI, APP+ axonal swellings were observed across S1 layers 2–6 as well as the underlying subcortical white matter (SCWM; Fig. 5*A*). To confirm neocortical PV+ interneuron DAI, we labeled APP to determine the extent of colocalization at sites of tdTomato+ PSAI and endogenous PV protein to verify the identity of tdTomato+ interneurons. At 3 h post-mTBI we observed elevated tdTomato expression and PV immunoreactivity within APP+ perisomatic axonal swellings (Fig. 4*A–D*). APP immunoreactivity was restricted to the evolving perisomatic/proximal axonal swelling, with the distal surface demarcating the site of disconnection (Fig. 4*B*). In contrast, the disconnected distal axonal segments were always devoid of APP immunoreactivity, consistent with previous findings from our lab using transgenic mice (Greer et al. 2011; Wang et al. 2011; Hånell, Greer, McGinn, et al. 2015). Characteristic of DAI, we found these APP+ axonal swellings juxtaposed non-DAI (intact) tdTomato+/PV+ axonal profiles (Fig. 4*A–D*). Similar to observations in shams (Fig. 1*H*), intact tdTomato+ axons could be followed up to approximately 30 µm distal to their soma of origin (Fig. 4*C*) and in the absence of any pathologic morphology there was also no detectable intra-axonal APP immunoreactivity (Fig. 4*B*). Based on our quantitative

analysis of tdTomato/PV overlap (Fig. 1*J*) and the demonstration of tdTomato+/PV+ PSAI colocalizing with APP+ swellings (Fig. 4*A–D*) we considered tdTomato and parvalbumin proteins as synonymous molecular interneuron markers for subsequent studies described below.

Complementary Approaches Employing GABAergic Markers to Further Validate PV+ interneuron DAI

Based on our finding of APP+ immunoreactivity in tdTomato+ PSAI, we tested whether VGAT and GAD67, vesicle-associated proteins (Kanaani et al. 2010) found in presynaptic boutons (Fish et al. 2011), would also accumulated at sites of impaired axonal transport. Qualitative (Fig. 4) and quantitative (Fig. 5) analyses were conducted at 3 h post-mTBI due to the ease with which PSAI/DAI could be identified via tdTomato expression and APP immunoreactivity. S1 layers 2–6 demonstrating APP+ axonal swellings also revealed VGAT (Fig. 4*E–H*) and GAD67 (Fig. 4*I–L*) immunoreactive profiles that colocalized with tdTomato+ PSAI. These VGAT+ or GAD67+ accumulations were dramatically larger than the surrounding immunoreactive presynaptic boutons (0.5–2.5 μm in diameter) and overlapped with APP+ axonal swellings. Signal intensity of GAD67+ (Fig. 4*C*) accumulations were comparable to tdTomato+ PSAI (Fig. 4*G*) and showed a better signal-to-noise than VGAT immunoreactive swellings (Fig. 4*E*) with respect to surrounding presynaptic boutons.

Low-magnification overview images further demonstrated the utility of targeting GAD67 to not only identify GABAergic DAI but also provide a high-throughput and reliable means of quantifying the burden of injury, wherein the nearest neighboring axonal swelling could be several hundred microns away (Fig. 5*A*). In low-magnification

(10× objective) z-sacks images, 183/189 visually identified GAD67+ profiles colocalized with APP+ axonal swellings verified in higher-magnification (20× objective) single optical slice images. Visual quantification of GAD67+/APP+ axonal swellings in S1 Layers 2–6 (Fig. 5*A*, arrows) yielded a mean density (swellings/mm^2) of 8.4 (95% CI: 6.4–10.5). The majority of GAD67+/APP+ axonal swellings (mean ± SD) colocalized with tdTomato (88 ± 7%, 95% CI: 84–92.0%), which was significantly greater (t_{14} = 19.83, $p < 0.0001$; paired *t*-test) than the tdTomato– population (12 ± 7%, 95% CI 8–16%). To confirm the association between GAD67+ axonal swellings with APP immunoreactivity, we quantified the overlap between the spatial distributions with respect to the size of GAD67+ and APP+ axonal swellings via automated object-based analysis (Fig. 5*A,* outlines). Automated quantitation yielded a density (swellings/mm^2: 8.1, 95% CI: 6.2–10.0) almost identical to the visual approach ($t_{14} = 0.67$, $p = 0.5117$; paired t-test), and displayed a strong significant correlation (Pearson's $r = 0.82$, $p = 0.0002$). Having established a consistent and systematic method of quantifying the total number of axonal swellings, we then compared the size distributions of GAD67+ accumulations (Fig. 5*C*) and found a statistically significant difference with respect colocalization with APP+ axonal swellings ($p < 0.0001$). Approximately 82% of GAD67+ profiles with areas greater than 10 μm^2 (approximately 3.5 μm in diameter) colocalized with APP+ axonal swellings, which was nearly 10-fold more than profiles below this size threshold (Fig. 5*C*). Accordingly, our results show that GAD67 immunoreactivity is a positive predictor of APP+ axonal swellings with sensitivity = 66% (95% Score CI: 57–71%), specificity = 97% (95% Score CI: 95–98%), and odds ratio = 54 (95% CI: 32—89).

PV+ Interneuron DAI Occurs Primarily within the Perisomatic Domain

The majority of tdTomato+ DAI occurred within 30 μm from the soma of origin. Relative to the terminal tdTomato+ axonal swelling, the non-injured proximal axonal segment could be continuously traced back to the soma of origin (Fig. 2*F*). Less frequently, isolated DAI remote from the soma of origin was identified via colocalization of GAD67 and APP immunoreactivity (Fig. 5*B,* bottom row). To validate our qualitative findings, we performed a complementary quantitative analysis determining whether the same population of visually identified GAD67+/APP+ axonal swellings analyzed above was significantly correlated with tdTomato+ PSAI (Fig. 5*B*, top row). Corroborating our qualitative observations, GAD67+/APP+/tdTomato+ swellings were significantly associated with the PSAI ($p < 0.0001$), representing approximately 78% of total tdTomato+ DAI (Fig. 5*D*), and accounting for 98% (123/124) of the total GAD67+/APP+ PSAI population (Fig. 5*B,* top and middle rows). Qualitative inspection of the ~22% remote swellings demonstrated several tdTomato+ profiles that appeared to be disconnected from their somas of origin, which were either likely outside the optical plane, or a relatively small (about 2–3 μm diameter) subpopulation that was often located in neocortical layer 6, near the subcortical white matter interface. Taken together, these approaches demonstrate that visual detection of PV+ interneuron PSAI via tdTomato+ profiles is reliable, affording us the unique opportunity to assess retrograde consequences.

Anterograde and Retrograde Sequelae of PV+ interneuron PSAI

Our results also confirm that tdTomato+ interneuron PSAI is significantly associated with retrograde p-c-Jun nuclear expression. Importantly, in shams tdTomato+ abnormalities

and p-c-Jun immunoreactivity were virtually absent (Fig. 7*A*). In contrast, within 3 h post-mTBI the occurrence of tdTomato+ PSAI coincided with increased p-c-Jun expression throughout S1 layers 2–6 (Fig. 7*B*). These tdTomato+ PSAI profiles could be traced back to the soma of origin (Fig. 6*A*), providing a unique opportunity to follow retrograde changes. Quantitative analysis of visually identified PSAI profiles showed that 64% of tdTomato+ somas colocalized with nuclear p-c-Jun immunoreactivity, reflecting a significant ($p < 0.0001$) and rapid retrograde response (Fig. 6*A,B*). In contrast, only 1.6% of tdTomato+ somas with no apparent PSAI overlapped with p-c-Jun+ profiles. *Post hoc* inspection of tdTomato PSAI+/p-c-Jun– (false positive; Fig. 6*C*) and tdTomato PSAI–/p-c-Jun+ (false negative; Fig. 6*D*) subsets revealed tdTomato+ profiles that were more likely perisomatic dendritic branch points and subtle PSAI obscured by surrounding neurites, respectively. Accordingly, our results show that nuclear p-c-Jun expression is a retrograde surrogate marker of tdTomato+ PSAI with sensitivity = 64% (95% Score CI: 43–80%), specificity = 98% (95% Score CI: 97–98%), and odds ratio = 107 (95% CI: 35—326). Validating nuclear expression of p-c-Jun as a reliable surrogate tdTomato+ PSAI marker and establishing fluorescent-based methodologies for assessing axonal morphology, allowed use to follow both retrograde and anterograde changes over time, respectively (Fig. 7).

Retrograde p-c-Jun nuclear expression and anterograde disconnected distal axon degeneration evolved rapidly over time leading to a substantial tdTomato+ burden of injury (Fig. 7*A–C*). As described above, we showed tdTomato+ interneuron involvement following mTBI by examining nuclear changes in somas connected to PSAI. Consistent with distal axon degeneration following disconnection from perisomatic/proximal axonal

swellings, the densities of tdTomato+ debris and tdTomato+/p-c-Jun+ somas, respectively, were significantly correlated (Spearman $\rho = 0.74$, $p < 0.0041$). Temporal analysis showed the densities of tdTomato+ axonal debris ($p = 0.0291$; Fig. 7*D*) and tdTomato+/p-c-Jun+ somas ($p = 0.0053$; Fig. 7*E*) were significant different between sham, 3 h mTBI, and 24 h mTBI groups. Specifically, at 24 h post-mTBI, the densities of tdTomato+ axonal debris and tdTomato+/p-c-Jun+ somas were both significantly different from sham ($p = 0.0381$ and $p = 0.0034$, respectively). Notably, between 3 h and 24 h post-mTBI tdTomato+/p-c-Jun+ density increased five-fold (Fig. 7*H*). Despite cFPI consistently evoking widespread tdTomato+ axonal pathology that evolved over time along with increased p-c-Jun expression, overt tissue damage and tdTomato+ interneuron loss ($p = 0.4401$; Fig. 7*G*) were not observed. However, the overall DAI burden (median, IQR) with respect to the total population of tdTomato+ interneurons and p-c-Jun+ nuclei (i.e. total population of neocortical neuron DAI) was substantial. At 24 h post-mTBI we found 8.7, 4.6–13.2% tdTomato+ interneurons expressed p-c-Jun (Fig. 7*H*), representing 13.7, 8.4–28.6% of the total population of p-c-Jun+ nuclei (pyramidal and interneuron; Fig. 7*I*).

Together, these data highlight the vulnerability of locally projecting PV+ interneurons to mild cFPI. We found compelling evidence that PV+ interneuron PSAI is not an isolated phenomenon. Rather, PV+ interneuron PSAI comprises almost 70% of all GABAergic DAI and is a significant component of mTBI pathology. Furthermore, p-c-Jun early expression and rapid increase within the PV+ interneuron PSAI population in the absence of neuronal loss provides evidence for acute retrograde genetic responses in the sustaining somas attendant with widespread anterograde axonal terminal loss.

Reduced Inhibitory Transmission within PV+ Interneurons

Our finding of widespread tdTomato+ axonal/terminal debris at 24 h post-mTBI (Fig. 7*C*) prompted us to assess local inhibitory networks for functional disconnection. Whole-cell patch clamp recordings from tdTomato+ interneurons within S1 layer 5 demonstrated fast-spiking action potentials (Fig. 8*A*), a physiologic marker of PV+ interneurons (Kawaguchi and Kubota 1997). This included brief action potentials and little adaptation during sustained depolarization. The medians (IQR) of intrinsic properties between sham and mTBI were similar [*F-I* slope (Hz/pA): sham = 1.0 (0.8–1.4), mTBI = 0.9 (0.7–1.3), $X^2 = 1.08$, $p = 0.2982$; Adaptation Ratio: sham = 1.1 (0.9–1.3), mTBI = 1.2 (1.1–1.3), $X^2 = 3.69$, $p = 0.0547$; action potential half-width (msec), sham = 0.52 (0.50–0.57), mTBI = 0.55 (0.50–0.69), $X^2 = 1.22$, $p = 0.2691$; Wilcoxon test]. Considering PV+ interneurons strongly and selectively inhibit one another (Pfeffer et al. 2013) and our observation that the majority of GABAergic DAI is represented by tdTomato+ interneuron PSAI (Fig. 5*D*), disconnecting the entire distal axonal arbor (Fig. 2*F*), we expected an alteration of inhibitory transmission at 24 h post-mTBI. We found sIPSC (median, IQR) frequency (Fig. 8*E*) significantly decreased by 60% in (6.0, 4.0–9.0 Hz) compared to sham (14.5, 10.4–19.4 Hz). The sIPSC amplitude (Fig. 8*F*) also significantly decreased by 23% (sham = 29.3, 25.5–49.3 mV; mTBI = 22.6, 18.7–30.9 mV). Consistent with an overall reduction of inhibitory input to tdTomato+ interneurons, the sIPSC event area (charge transfer; Fig. 8*G*) following mTBI (76.3, 60.2–92.6 pA□msec) significantly decreased by 32% compared to sham (112.7, 72.6–187.5 pA□msec). Collectively, our structural and functional data demonstrate the impact of mTBI on local inhibitory networks embedded

within neocortical GM, where reduced inhibitory transmission occurred in concert with PV+ interneuron PSAI and widespread terminal degeneration.

DISCUSSION

This study provides compelling evidence of structural and functional disconnection of local neocortical inhibitory networks via DAI in well-characterized PV-Cre;Ai9 mice after clinically relevant mTBI. Exploiting Cre-driven tdTomato expression in PV+ interneurons coupled with detailed confocal and ultrastructural analysis, we show for the first time that mTBI induces GABAergic interneuron DAI across neocortical layers 2–6. Consistent with human mTBI, midline cFPI reproducibly evoked DAI without mass lesions, neocortical contusion, and/or cell death. Using established markers of impaired axonal transport (APP) and neuronal stress (p-c-Jun) we confirmed DAI within GABAergic interneurons that comprise only a small fraction of neocortical neurons. Further, in this mTBI-mediated response, colocalization of GABAergic and DAI markers revealed a disproportionate involvement of PV+ interneurons and vulnerability for PSAI. Patch-clamp recordings of tdTomato+ fast-spiking interneurons showed reduced inhibitory transmission. Taken together, these findings demonstrate significant structural and functional disconnection of local inhibitory neocortical networks independent of excitatory input from WM tracts. Our results depart from current thought on mTBI, which has been based primarily on the presumption of WM tract vulnerability without any consideration of neocortical involvement. Collectively, the novel neuronal and physiologic substrates identified in this study significantly extend our knowledge of cortical network dysfunction following mTBI.

Several features of our cFPI model underscore its clinical relevance and utility for evaluating DAI in neocortical networks after mTBI (Lifshitz et al. 2016; McGinn and Povlishock 2016). We used LORR as a surrogate for LOC to assess injury severity (Morehead et al. 1994). The duration of LORR in mice was similar to LOC in humans following mTBI, ranging 3–5 min (Malec et al. 2007). While this was our only behavioral assessment, we monitored arterial oxygen saturation, heart rate, respiratory rate, and core body temperature in all mice used for structural and functional studies. Specifically, all mice were in physiological homeostasis, with no evidence of any mass lesions, neocortical contusion, and/or cell death, a finding entirely consistent with human mTBI (Andriessen et al. 2010; Blyth and Bazarian 2010). Importantly, evaluating these parameters help distinguish our study from most other investigations, which do not perform routine physiologic monitoring to exclude secondary insults that could severely confound the assessment of network disruption via diffuse structural and functional changes. Although other investigations have shown neocortical GABAergic interneuron changes, these were in the context of cell death using models of blunt-force trauma (Carron et al. 2016) or more severe TBI involving mass lesions/contusion (Cantu et al. 2014; Hsieh et al. 2016) to model epileptogenesis (Pitkänen and McIntosh 2006; Hunt et al. 2013), which is not an outcome of clinical or experimental mTBI (Alexander 1995; Shaw 2002; Blyth and Bazarian 2010). Further, while cell death was for many years viewed as the primary contributor to morbidity after TBI, it is now recognized that mTBI pathophysiology conditions ensue without neuronal loss (Farkas and Povlishock 2007).

The markers previously used to understand DAI pathogenesis and its implications for network disconnection had several limitations. Specifically, APP accumulates at focal

sites of impaired axonal transport, which can be readily observed in dense WM tracts, but cannot be used to trace long-distance projections back to the soma of origin (Büki et al. 2000). Further complicating this issue is that not all injured axons develop swellings (Stone et al. 2001). Lastly, APP is ubiquitously expressed by neocortical neurons (Bahmanyar et al. 1987) and cannot provide information on the type of fiber system involved (e.g. glutamatergic or GABAergic). Since WM tracts are composed of axons projecting from excitatory pyramidal neurons that represent ~80% of total neocortical neurons (DeFelipe and Fariñas 1992), this has contributed to the long-held misconception that only long-distance fibers are vulnerable to traumatic forces (Adams et al. 1989, 1991). Further complicating this issue is that WM axon density is in the realm of two orders of magnitude greater than neocortical GM (Zhang and Sejnowski 2000; Carlo and Stevens 2013; Walhovd et al. 2014). Hence, a disproportionately higher burden DAI based on APP immunoreactivity would be expected. This has not been considered in any studies to date and thus it remains unknown whether DAI vulnerability varies between WM tract and neocortical GM.

To dissect specific neuronal components of local neocortical network dysfunction we employed Cre/lox mice to genetically label the total population of PV+ interneurons. As only ~20% of neocortical neurons are GABAergic, we chose to probe PV+ interneurons, which are the largest subclass representing 40–50% of total inhibitory interneurons (Rudy et al. 2011). While Cre/lox mice have become an essential tool for studying neocortical structure and function, caution must be exercised when labeling specific neuronal populations (Taniguchi et al. 2011). In our hands, quantitative analysis showed >90% colocalization between Cre-driven tdTomato expression and endogenous

PV immunoreactivity. Thus, PV-Cre;Ai9 animals enabled axon identification based on tdTomato+ profiles alone, while also allowing us to follow the same interneuron from confocal to electron microscopy via antibodies targeting tdTomato. With confocal microscopy, we routinely identified DAI in a population that represented ≤10% of total neocortical neurons. Ultrastructural analysis of tdTomato+ PSAI revealed vesicle/organelle-laden swellings pathognomonic of impaired axonal transport (Povlishock 1993; Christman et al. 1994). The distal disconnected segment was disorganized indicating rapid onset of Wallerian degeneration (Kelley et al. 2006). To unequivocally demonstrate PV+ interneuron DAI we immunolabeled endogenous PV and APP and showed that immunoreactive accumulations of these proteins mapped to tdTomato+ swellings. Similarly, we further confirmed GABAergic DAI by targeting GAD67, which also undergoes fast anterograde transport (Koo et al. 1990; Kanaani et al. 2010) and accumulates within APP+ axonal swellings. Capitalizing on the utility of GAD67 as a reliable DAI marker, we determined that PV+ interneuron DAI represented almost 90% of all GABAergic DAI, suggesting limited involvement of other inhibitory interneuron subclasses. This observed preferential involvement of PV+ interneurons may be due to the 'metabolic hypothesis' that postulates that their fast-spiking behavior creates a high-energy demand in both their soma and axonal domains (Kann 2016). Indeed, PV+ interneurons have the highest concentration of axonal mitochondria compared to other neurons (Kann et al. 2014) and local ongoing neocortical activity consumes the majority of brain energy (Buzsáki et al. 2007). The use of GAD67/APP to identify GABAergic DAI also confirmed that the vast majority of tdTomato+ swellings demonstrated PSAI. Previously, we showed that mTBI induced DAI primarily within the

axon initial segment (AIS) of excitatory pyramidal neurons (Greer et al. 2013), where action potentials are generated (Kole and Stuart 2012). The currently observed PV+ interneuron PSAI, together with the previously observed pyramidal AIS involvement, suggests that perisomatic/AIS vulnerability may be a distinguishing neocortical DAI feature (Stone et al. 1999; Farkas and Povlishock 2007). The AIS is a conserved structure with a highly developed subaxolemmal cytoskeleton integrated with a unique extracellular matrix via cell adhesion molecules (Grubb and Burrone 2010). A recent review (Hemphill et al. 2015) underscores the concept that physical forces are transmitted across all spatial scales (Van Essen 1997) suggesting that the relatively gross tissue deformation used to describe WM tract vulnerability may not account for the forces exerted on the underlying cellular structures in different brain regions. Thus, the perisomatic/AIS domain may represent a structural vulnerable domain on a much finer scale, where mechanotransduction through the neuronal microenvironment may be a potential mechanism underlying neocortical PSAI (Hemphill et al. 2015).

The anterograde and retrograde sequelae of PV+ interneuron PSAI involved both structural and functional changes. In the current study, the observed PV+ interneuron PSAI evolved rapidly following mTBI. Similar to previous findings, by 24h post-mTBI identifying tdTomato+ PSAI became difficult, likely due to anterograde transport suspension/reversal (Povlishock and Stone 2001). Circumventing this limitation, we used a previously established strategy incorporating p-c-Jun, a nuclear transcription factor (Raivich et al. 2004), as a surrogate DAI marker (Greer et al. 2011; Wang et al. 2013) to spatiotemporally assess retrograde changes in the sustaining somas of origin. Nuclear expression of p-c-Jun increased within 3h post-mTBI and was consistently associated

with tdTomato+ PSAI, thus reaffirming our previous findings and further supporting the use of p-c-Jun as a pan-neuronal DAI marker. Temporal assessment of tdTomato+ profiles also showed a strongly correlated, dramatic increase in anterograde axonal debris and retrograde p-c-Jun expression, thereby supporting their linkages with these anterograde changes most likely reflecting widespread axon terminal degeneration concomitant with deafferentation of target neurons (Erb and Povlishock 1991; Povlishock et al. 1992; Patel et al. 2016). Importantly, this neuropathology evolved without evidence of neuronal loss, consistent with the observation of tdTomato+ interneuron PSAI associated with retrograde p-c-Jun nuclear expression, indicating activation of genetic programs involving cell survival and axonal regeneration (Christman et al. 1997; Raivich et al. 2004; Greer et al. 2011; Wang et al. 2013; Patel et al. 2016). Based on the robust expression of p-c-Jun at 24h post-mTBI, we determined that ~9% of tdTomato+ interneurons underwent DAI. Previously, we estimated ~5% of Thy1-expressing layer 5 pyramidal neurons undergo DAI (Greer et al. 2011). To our knowledge these two studies are the only quantitative estimates of the proportion of neocortical DAI following experimental mTBI in mice. Further, we estimate that of the total population of p-c-Jun+ population (pyramidal and interneuron DAI), ~14% is accounted by tdTomato+ interneurons. This suggests that ~86% of neural DAI is represented by pyramidal neurons, which is consistent with that fact that this is approximately the same percentage of pyramidal neurons comprising the total neocortical neuron population. Overall, both our qualitative and quantitative data validate that neocortical PV+ interneuron PSAI is not an isolated phenomenon. Rather, it is a consistent and significant component of mTBI-induced pathology, with major functional implications for postsynaptic neurons.

GABAergic interneuron structure reflects function (Hangya et al. 2014; Kepecs and Fishell 2014). Specifically, the expansive axonal arbors of PV+ interneurons highlight their role in balancing neocortical excitation/inhibition to synchronizing neuronal ensembles (Bartos et al. 2007; Buzsáki and Wang 2012; Hu et al. 2014), which play major roles in plasticity and behavior (Kuhlman et al. 2013; Doron et al. 2014). Operationally, the strong and selective connectivity between PV–PV interneurons (Pfeffer et al. 2013) leads to disynaptic disinhibition forming powerful local neocortical networks that generate gamma oscillations during cognition (Howard 2003; Cardin et al. 2009; Sohal et al. 2009). Hence, PV+ interneuron firing is a 'pulse' of local excitatory/inhibitory network activity (Scholl et al. 2015; Trachtenberg 2015). Accordingly, the impact of mTBI on local neocortical inhibitory networks via PV+ interneuron PSAI also involved functional disconnection. Applying ionotropic glutamate receptor antagonist pharmacologically isolated local neocortical inhibitory networks from excitatory WM tract (extrinsic) and collateral (intrinsic) inputs. Patch-clamp recordings of tdTomato+ interneurons showed fast-spiking action potentials characteristic of PV+ interneurons (Kawaguchi and Kubota 1997). Importantly, PV+ interneuron intrinsic properties were similar between shams and mTBI. This supported that tdTomato+ interneurons in mTBI slices were healthy, consistent with our observation that ~9% of PV+ interneurons underwent DAI. Notwithstanding this relatively subtle burden of injury, inhibitory transmission in PV+ interneurons was compromised following mTBI, marked by a 60% and 32% decrease in sIPSC frequency and event area (charge transfer), respectively. Such a drastic decrease in inhibitory transmission is consistent with known properties of PV+ interneurons described above and our findings that PSAI disconnects

the distal axonal arbor causing widespread axonal degeneration and terminal loss/deafferentation of postsynaptic neurons in local neocortical networks. Since PV+ interneurons strongly inhibit one another via perisomatic innervation (Tamás et al. 2000) and inhibitory presynaptic discharge does not saturate all postsynaptic $GABA_A$ receptors (Perrais and Ropert 2000), this may potential explain the subtle decrease in sIPSC amplitude (Williams and Mitchell 2008). IPSCs play a major role in local (intrinsic) neocortical networks (Hasenstaub et al. 2005), which can operate independent of sensory (extrinsic) inputs via ongoing spontaneous activity (Haider and McCormick 2009; Raichle 2010). In such a scenario local network dysfunction elicited by DAI within neocortical GM could provide a potential mechanism of clinically significant mTBI without WM tract involvement (Zhang et al. 2010; Wäljas et al. 2014). While our electrophysiological assessments were not comprehensive, the paucity of information on the role of GABAergic interneurons in neocortical network dysfunction following mTBI adds importance to our findings and warrants future investigations. Taken together, our electrophysiological findings show that even a small fraction of PV+ interneuron PSAI is enough to cause substantial reduction of GABAergic transmission within local neocortical inhibitory networks following mTBI.

Converging evidence provided by our lab and others underscores that TBI involves both excitatory and inhibitory systems (Reeves et al. 1997; Cohen et al. 2007; Cole et al. 2010; Gupta et al. 2012; Guerriero et al. 2015; Beamer et al. 2016). This forces reconceptualization of the anatomical structures vulnerable to DAI and the impact of specific neuronal subtypes on cortical network dysfunction following TBI (Sharp et al. 2014). In an earlier report, we showed ultrastructural evidence of terminal degeneration

along the perisomatic domain of pyramidal neurons within layer 5 neocortex, suggesting anterograde synaptic loss following PV+ interneuron PSAI (Singleton et al. 2002). More recently, within this same anatomical locus we also reported hyperexcitability of pyramidal neurons and also the local neocortical network (Greer et al. 2012; Hånell, Greer, and Jacobs 2015; Sun and Jacobs 2016). Focusing on PV+ interneurons, the current report's structural and functional data from layer 5 neocortex corroborates our previous findings and implicates GABAergic loss as a contributor to abnormal excitatory pyramidal neuron activity and local neocortical excitatory/inhibitory imbalance. Similarly, PV+ interneuron PSAI in layers 2/3 and 4 could also implicate altered intra-cortical and thalamocortical input processing, respectively (Gentet 2012).

In light of converging evidence showing cortical network dysfunction is a preeminent sequelae of mTBI, the structural and functional data provided in this investigation has major implications for both the initial posttraumatic morbidity and any subsequent neuronal reorganization/repair. Although clinical studies indirectly support mTBI-induced neocortical inhibitory network disruption, to the best of our knowledge, the current report provides the only direct evidence of the specific neuronal and physiologic substrates involved. Further, this study dismisses the notion that only axons within WM tracts are susceptible to mTBI forces. Considering the neocortical column as the fundamental computational unit for higher-order information processing, understanding such inhibitory interneuron pathophysiology may be crucial for therapy development from a local network perspective (Douglas and Martin 2004; Bullmore and Sporns 2009; Zhang and Raichle 2010). Ultimately, this study reshapes our knowledge of the cerebral landscape affected by mTBI in both animals and humans.

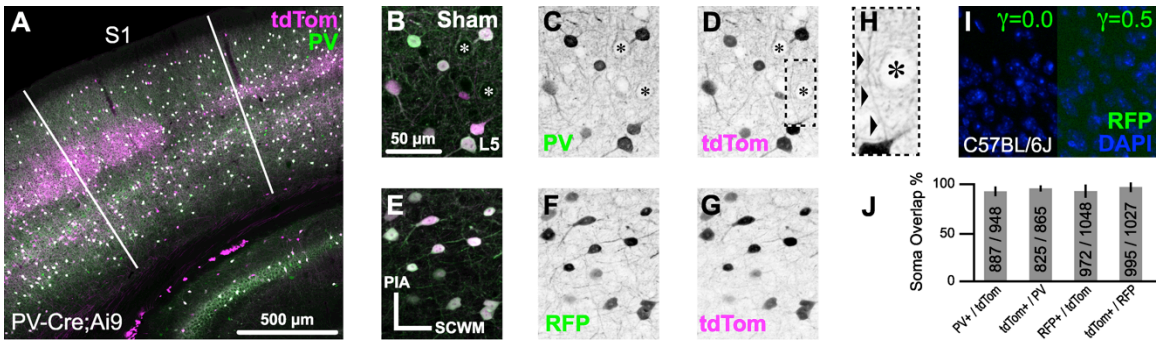

Figure 3.1. Characterization of PV-Cre;Ai9 mouse and RFP antibody for enhanced visualization of tdTomato expression. ***A–H,*** Representative maximal intensity projections from sham-injured PV-Cre;Ai9 mice that express tdTomato (tdTom) in PV+ interneurons. All images are oriented perpendicular to the subcortical white matter (SCWM, ***E***). ***A,*** Overview image of a coronal section showing broad overlap between native tdTomato expression and endogenous PV immunoreactivity with S1 delineated. ***B–G,*** Higher-magnification images showing colocalization of tdTomato with PV (***B–D***) and immunoreaction using antibodies against RFP (that recognize tdTomato; ***E–G***) within layer 5 neocortex. ***B–D,H,*** Typical profiles of tdTomato+/PV+ perisomatic innervation of a layer 5 pyramidal neurons (asterisks). ***H***, Zoomed image of box in ***D***, showing an ascending axonal projection (arrowheads) juxtaposed by tdTomato+ presynaptic terminals with characteristic 'basket' morphology. Note the fine diameter of the axon (~0.5 µm), which could be followed for ~30 µm distal to the soma of origin. ***E–G,*** Colocalization of tdTomato with RFP immunoreactivity, which was visualized using secondary antibodies conjugated to Alexa Fluor 488 (***F***). Parallel anti-RFP reaction in a C57BL/6J (WT) tissue section (***I***), the background strain of PV-Cre and Ai9 mice, did not reveal evidence of non-specific binding. ***J***, Summary data (mean with 95% CI error bars and cell counts) from quantitative colocalization analysis of expression specificity between Cre-driven tdTomato and endogenous PV (n = 6 FOV from 3 animals) and native tdTomato signal with RFP immunoreactivity (n = 4 FOV from 2 animals) within neocortical layers 2–6.

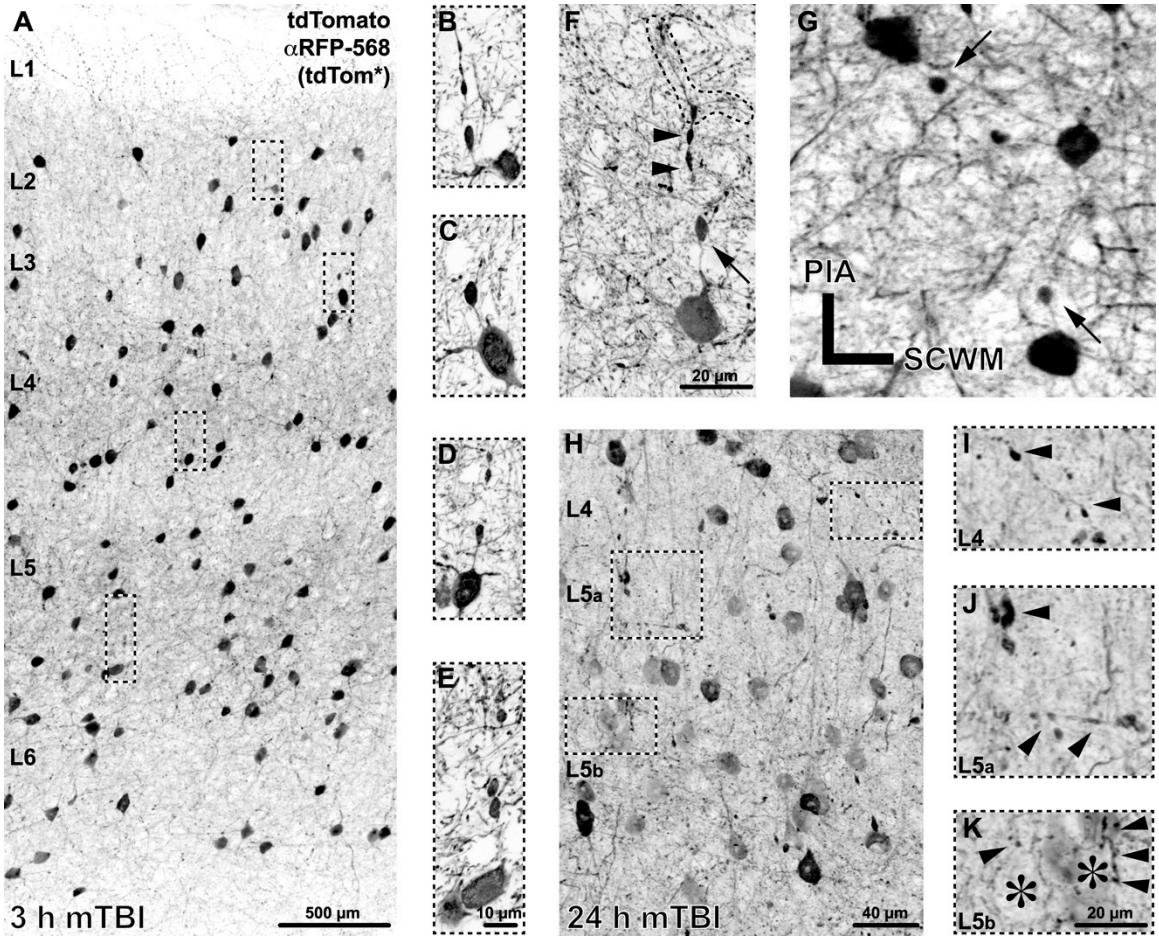

Figure 3.2. Repertoire of tdTomato+ neuropathology following mTBI. Representative images of tdTomato+ morphological changes at 3 h (***A-G***) and 24 h (***H–K***) post-mTBI. ***A–E***, Within 3 h post-mTBI, tdTomato+ axonal swellings, occurring near the soma of origin, were observed across S1 layers 2–6. ***F,*** A representative tdTomato+ interneuron showing a perisomatic axonal swelling (arrow, oriented toward pia) and the distal disconnected axonal segment with lobular/varicose morphology (arrowheads) that can be traced to the initial branch point (outline). While the majority of tdTomato+ perisomatic axonal swellings were oriented toward the pia (***A–F***), occasionally profiles with descending and/or lateral trajectories were found (***G***). ***H–K,*** At 24 h post-mTBI, perisomatic axonal swellings were difficult to identify; however, widespread tdTomato+ axonal debris was readily observable. ***I–K,*** Zoomed images corresponding to insets in ***H,*** reflecting progressive tdTomato+ anterograde changes (arrowheads) likely associated distal disconnected axonal arbor (***F***) degeneration. ***K,*** Layer 5 pyramidal neuron silhouettes (asterisks) showing evidence of tdTomato+ axonal terminal degeneration, ranging from punctate (left arrow) to varicose (right arrows) profiles.

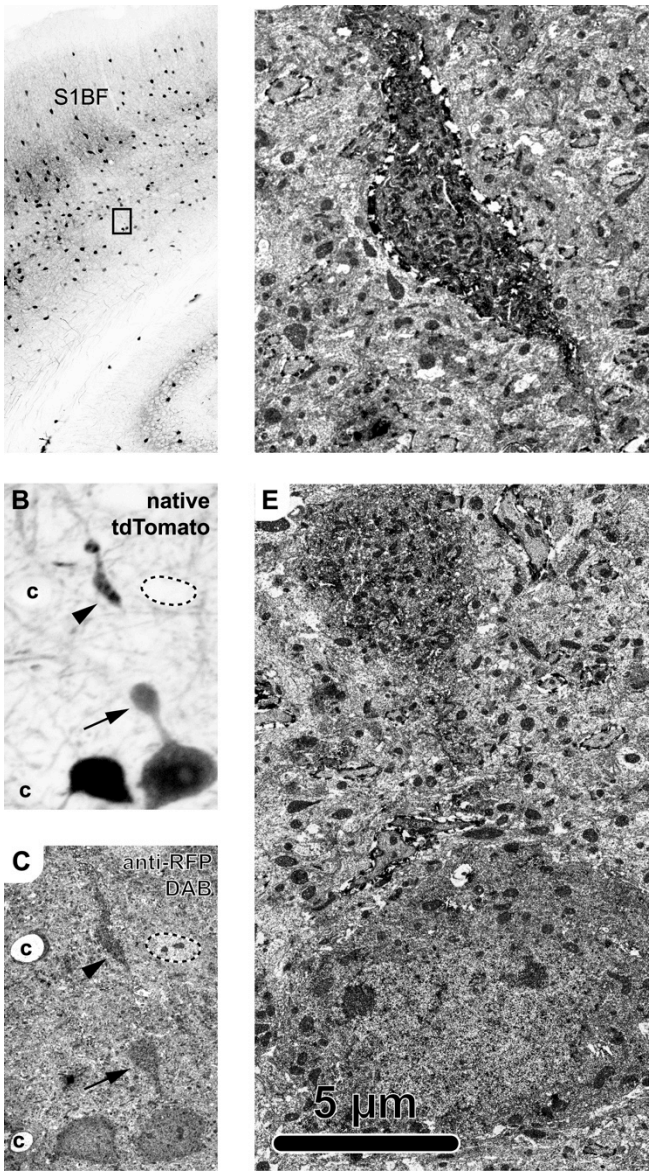

Figure 3.3. Ultrastructural analysis of tdTomato+ perisomatic axonal injury identified via confocal microscopy. The same tdTomato+ profile was followed from the light (***A,B***) to electron (***C–D***) microscopy level at 3 h post-mTBI. ***A,B***, Confocal images capturing native tdTomato signal. ***A,*** Overview image of S1BF with inset in layer 5 corresponding to tdTomato+ neuron in ***B,*** showing PSAI (arrow, oriented toward pia) and related disconnected distal segment (arrowhead). Employing the same RFP antibodies used for photostabilizing allowed use to follow the same tdTomato+ neuron from confocal (***B***) to electron (***C–E***) microscopy level. ***C***, The tdTomato+ neuron was identified based on morphology, including the perisomatic axonal swelling (arrow) and disconnected distal axonal segment (arrowhead), as well as other fiduciary markers including an adjacent tdTomato+ neuron (left), nearby capillaries (c), and a non-tdTomato expressing neuron adjacent to the tdTomato+ disconnected distal axonal segment (outline, upper right). ***D–E,*** Ultrastructural analysis of the tdTomato+ distal disconnected segment (***D***) showed disorganized cytoskeleton consistent with the onset of Wallerian degeneration and the perisomatic swelling (***E***) laden with organelles and vesicles, indicating a focal site of impaired axonal transport.

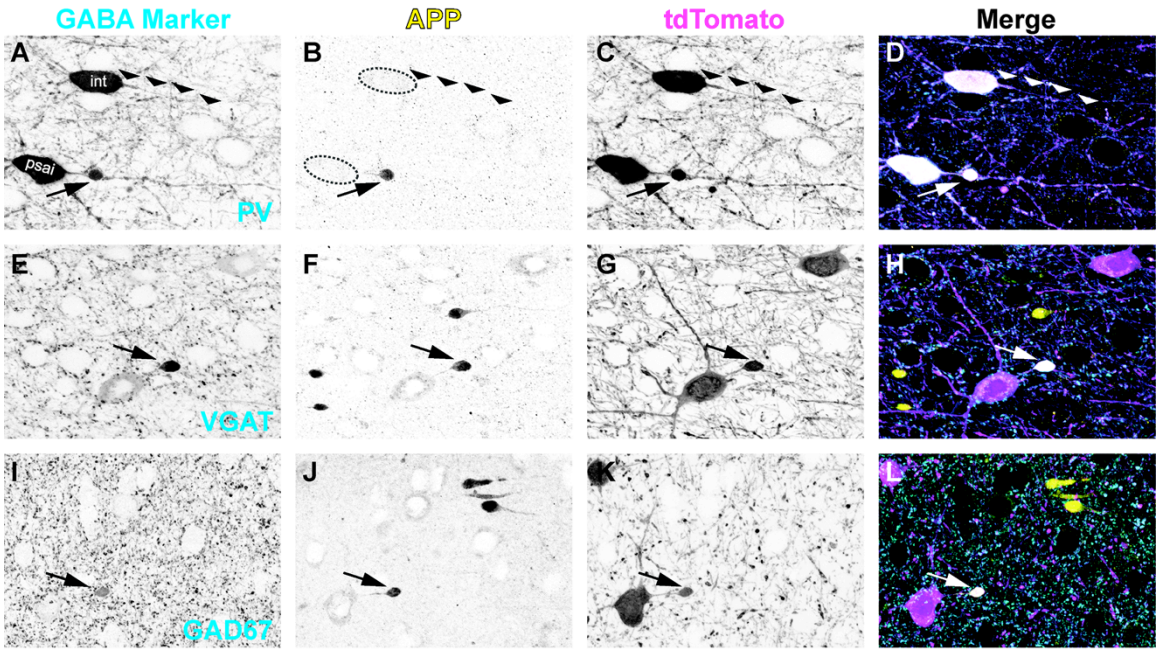

Figure 3.4. GABAergic markers accumulate in APP+/tdTomato+ perisomatic axonal swellings. Representative images at 3 h post-mTBI showing GABAergic markers (***A,E,I***) with respect to APP immunoreactivity ***(B,F,J)***, which accumulates at focal sites of impaired axonal transport (arrows). Colocalization of tdTomato+ PSAI with PV (***A–D***), VGAT (***E–H***), and GAD67 (***I–L***) immunoreactivity confirms GABAergic interneuron axonal injury. ***A,*** Normal uninjured intact (int) axonal profile (wide arrowheads) juxtaposed by PV+ interneuron PSAI (arrow). ***B,*** APP is not detected within the intact axonal profile, while robust APP immunoreactivity colocalizes with tdTomato+/PV+ interneuron PSAI (***C,D***). Within sites of tdTomato+ PSAI (***C,G,K***), the immunoreactive profiles of VGAT (***E***) and GAD67 (***I***) are similar to APP+ axonal swellings (***F*** and ***J***, respectively). Qualitatively, the GAD67+ axonal swelling profile (***I,L***) has a better signal-to-noise than VGAT (***E,H***). Note non-GABAergic APP+ axonal swellings have opposite trajectories.

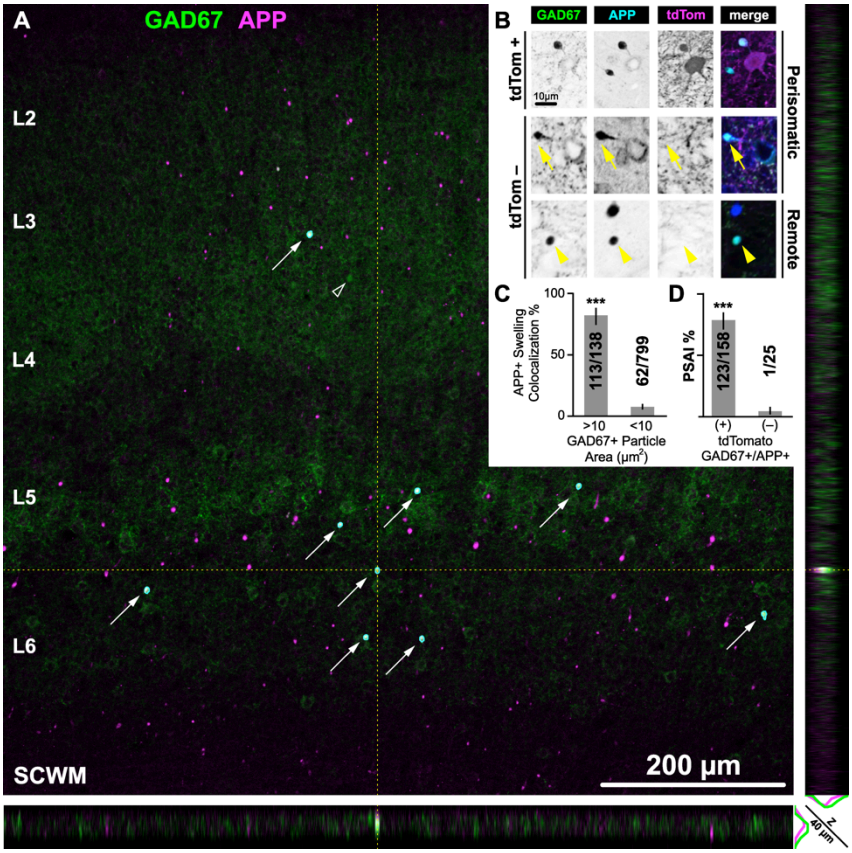

Figure 3.5. Quantitative analysis of GABAergic DAI at 3 h post-mTBI. ***A,*** Representative low-magnification (10× objective) maximum intensity projection of S1 layers 2–6, with corresponding XZ (bottom) and YZ (right) planes through the center of a GAD67+/APP+ axonal swelling, which can be readily identified visually (arrows) and also using automated image analysis (cyan outlines). Note the scattered distribution of APP+ axonal swellings across the XY plane of S1 layers 2–6 and the sparse distribution of the APP+/GAD67+ subpopulation. XZ and YZ planes highlight GAD67 colocalization with APP is not an artifact of flattening z-stacks. ***B,*** Representative higher-magnification (20× objective) single optical slices through the center of visually identified GAD67+/APP+ axonal swellings. Top and middle panels show tdTomato+ and tdTomato– PSAI (yellow arrow), respectively. Bottom panel shows an isolated/remote tdTomato– axonal swelling (yellow arrowheads). ***C,*** Summary of quantitative data reported as mean percentage with 95% CI error bars. *LEFT*, GAD67+ accumulations are a positive predictor of APP+ axonal swellings. The proportion of GAD67+ profiles with areas >10 µm^2 that colocalized with APP+ axonal swellings (0.819, 95% CI: 0.746–0.874) was significantly greater (X_1^2 = 426, ***p < 0.0001) than the proportion of GAD67+ profiles with areas <10 µm^2 (0.078, 95% CI: 0.061–0.98). *RIGHT*, The majority of GABAergic DAI is represented by tdTomato+ PSAI. The proportion of tdTomato+ PSAI (0.779, 95% CI: 0.708–836) was significantly greater (X_1^2 = 53.88, ***p < 0.0001) than the proportion of tdTomato– axonal injury (0.040, 95% CI 0.007–0.195). Statistics: Chi-squared test used to determine significance. Counts obtained from n = 15 sections from 5 mice.

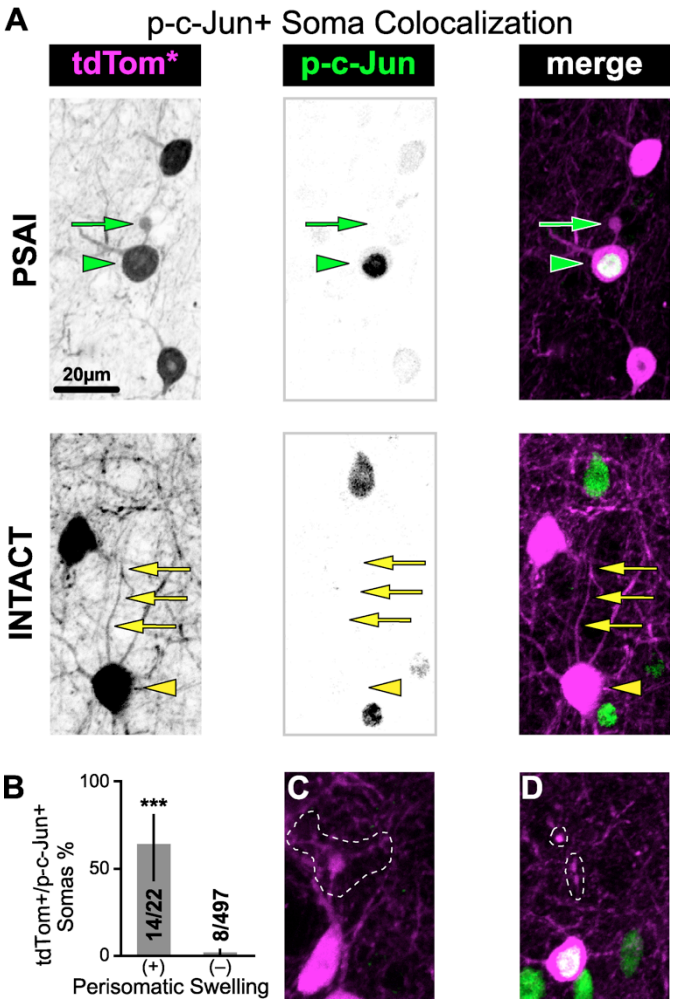

Figure 3.6. tdTomato+ interneuron PSAI is associated with retrograde nuclear expression of p-c-Jun within 3 h post-mTBI. ***A,*** Representative images of two distinct tdTomato+ somas within a field of p-c-Jun+ nuclei in S1 layer 5. *TOP,* tdTomato+/p-c-Jun+ soma (green arrowhead) contiguous with PSAI (green arrow). *BOTTOM,* tdTomato+/p-c-Jun– soma (yellow arrowhead) with an intact axon (yellow arrows). ***B,*** Summary data reported as mean percentage with 95% CI error bars. The proportion of tdTomato+/p-c-Jun+ somas with perisomatic swellings (PSAI: 0.636, 95% CI: 0.430–80.3) was significantly greater ($p < 0.0001$; Fisher's exact test;) than the proportion with intact profiles (0.016, 95% CI: 0.008–0.031%). Counts obtained from a single sections taken from $n = 5$ mice.

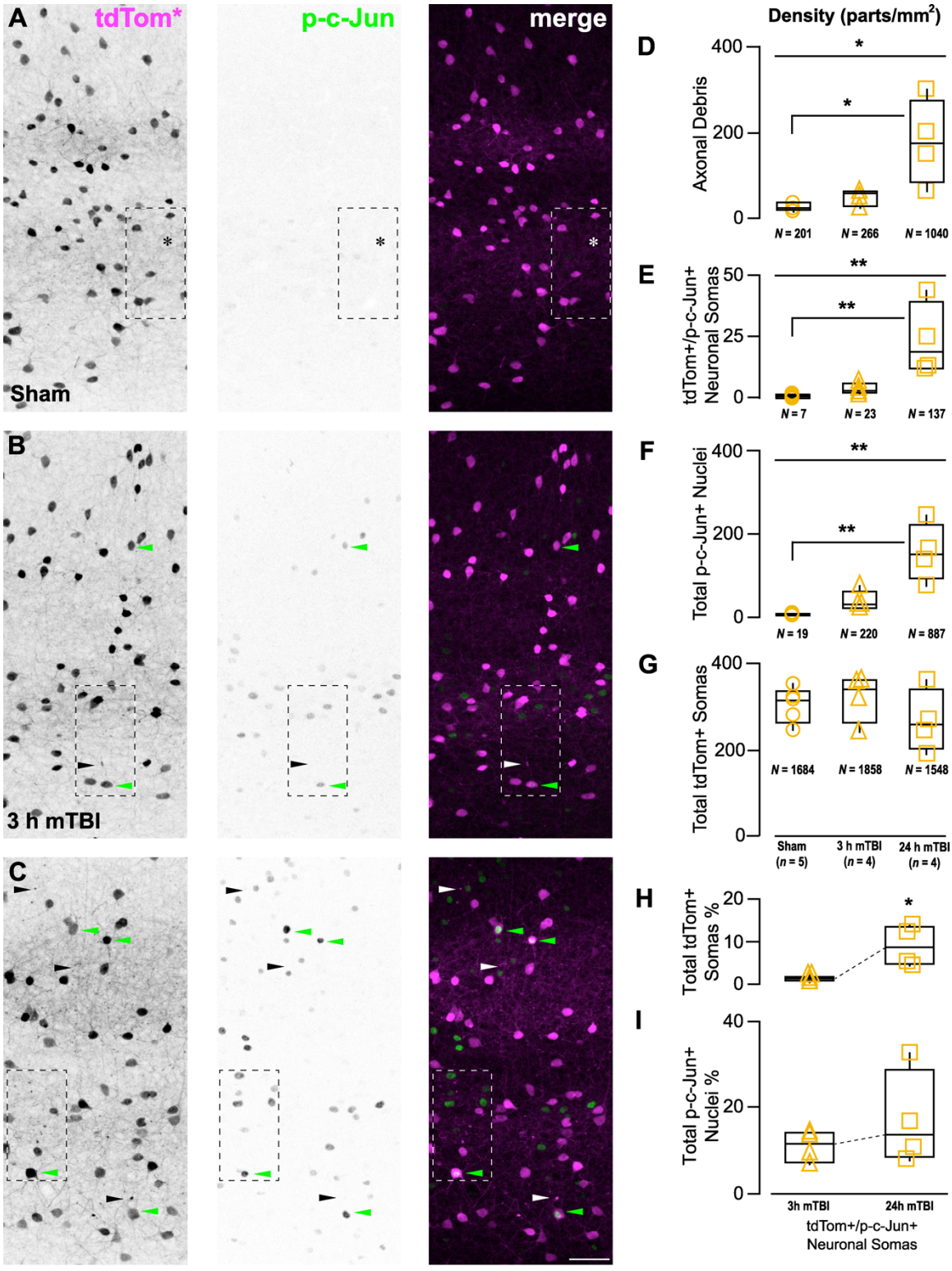
A
tdTom*
p-c-Jun
merge
Sham
B
3 h mTBI
C
D
Density (parts/mm²)
Axonal Debris
400
200
0
*
*
N = 201
N = 266
N = 1040
E
tdTom+/p-c-Jun+ Neuronal Somas
50
25
0
**
**
N = 7
N = 23
N = 137
F
Total p-c-Jun+ Nuclei
400
200
0
**
**
N = 19
N = 220
N = 887
G
Total tdTom+ Somas
400
200
0
N = 1684
N = 1858
N = 1548
Sham (n = 5)
3 h mTBI (n = 4)
24 h mTBI (n = 4)
H
Total tdTom+ Somas %
20
10
0
*
I
Total p-c-Jun+ Nuclei %
40
20
0
3h mTBI
24h mTBI
tdTom+/p-c-Jun+ Neuronal Somas

Figure 3.7. Anterograde axonal degeneration and retrograde p-c-Jun nuclear expression progresses rapidly following mTBI. ***A–C,*** Representative maximum intensity projections showing mTBI-induced changes in tdTomato+ profiles and p-c-Jun immunoreactivity across S1 layers 2–6. ***A,*** Sham-injury did not induce any tdTomato+ neuropathology and p-c-Jun immunoreactivity was virtually absent. ***B,*** Within 3 h post-mTBI tdTomato+ axonal debris (black/white arrowheads) is seen near a tdTomato+/p-c-Jun+ neuronal soma (green arrowhead). ***C,*** At 24 h post-mTBI the density of tdTomato+ axonal debris and p-c-Jun+ nuclei increase drastically. ***D–G,*** Quantitative data summarized using median, IQR, and min/max values. The density of tdTomato+ axonal debris (***D***), tdTomato+/p-c-Jun+ somas (***E***), and total p-c-Jun+ nuclei (***F***) were significantly different across experimental groups (X_2^2 = 8.61, *p = 0.0135 and X_2^2 = 10.48, **p = 0.0053, respectively; X_2^2 = 10.68, **p = 0.0048). *Post hoc* analyses revealed significant increases in at 24 h post-mTBI compared to sham (***D,*** tdTomato+ axonal debris: *p = 0.0381; ***E,*** tdTomato+/p-c-Jun+ somas: **p = 0.0034; ***F,*** total p-c-Jun+ neurons: **p = 0.0031). ***G,*** tdTomato+ soma density did not change over time (X_2^2 = 1.64, p = 0.4401). ***H,I,*** Overall burden of injury, estimated as percentage of tdTomato+/p-c-Jun+ somas, with respect to total tdTomato+ somas (***H***) significantly increased overtime (X_1^2 = 5.33, *p = 0.0209), while there was no change with respect to total p-c-Jun+ nuclei (X_1^2 = 0.75, p = 0.3865). Statistics: Significant differences were determined using Kruskal-Wallis test followed by *post hoc* pair-wise comparisons using Dunn's method with control (sham) for joint ranking (***D–G***) and Wilcoxon test (***H,I***). Each data point (statistical unit) corresponds to a single section per animal (n). The total counts per group (N) are denoted underneath each graph.

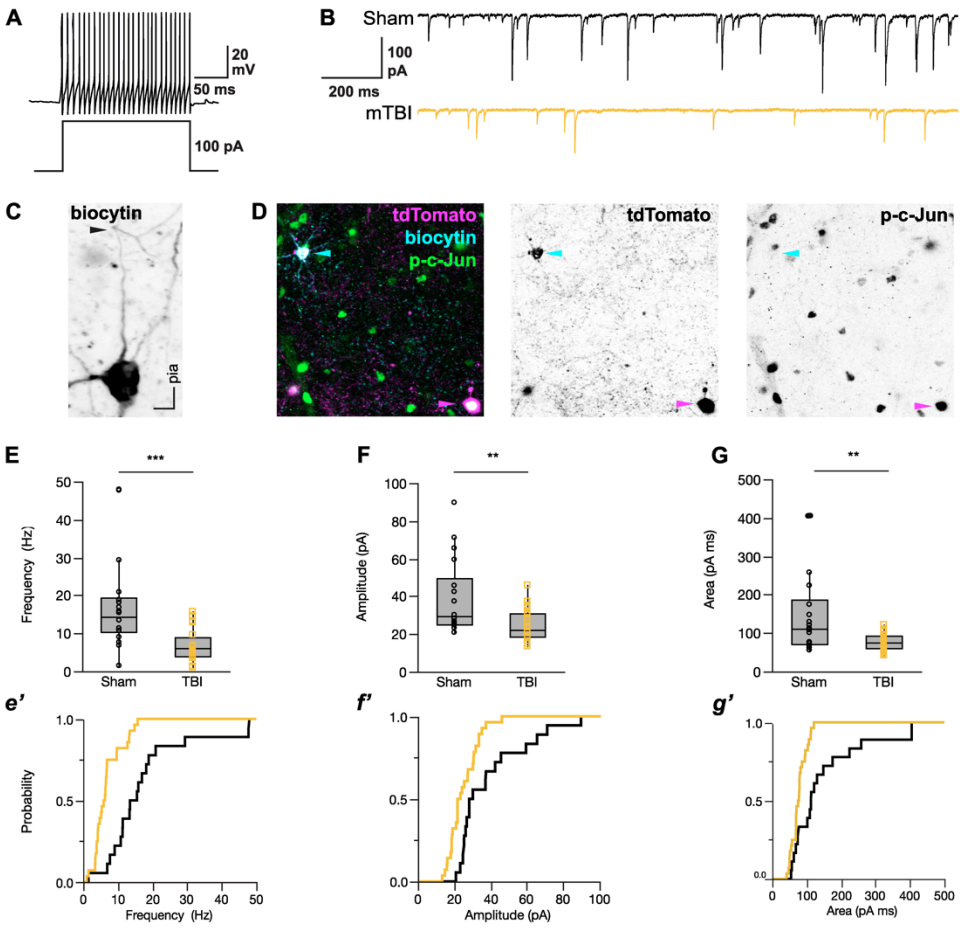

Figure 3.8. IPSC are reduced in tdTomato+ fast-spiking interneurons 24 h post-mTBI. ***A,B,*** Representative traces of whole-cell patch clamp recordings made in S1BF layer 5 showing a fast-spiking action potentials characteristic of PV+ interneurons (***A***), and sIPSCs from sham-injury (black) and mTBI (gold) mice (***B***). ***C,*** A representative biocytin-filled tdTomato+ interneuron from a mTBI animal revealing an ascending intact axon that can be continuously traced distally through and past the initial branch point (arrowhead). ***A–C,*** Representative images showing a fast-spiking firing pattern characteristic of PV+ interneurons (***A***), sIPSCs from sham-injury (black) and mTBI (gold) mice (***B***), and a biocytin-filled recorded neuron from a mTBI animal (***C***). The biocytin-filled ascending intact axon can be continuously traced distally through and past the initial branch point (arrowhead). ***D,*** *Post-hoc* confocal image showing a biocytin-filled tdTomato+ interneuron (top left, cyan arrowhead) within a field of diffuse p-c-Jun immunoreactivity (green). Note the tdTomato+/p-c-Jun+ PSAI neuron (bottom right, magenta arrowhead). ***E–G,*** sIPSC recordings summarized using median, IQR, and min/max values. At 24 h post-mTBI, there was a significant decrease in frequency (***E,*** X_1^2 = 17.15, ***$p < 0.0001$), amplitude (***F,*** X_1^2 = 8.56, **$p = 0.0034$), and event area/charge transfer (***G,*** X_1^2 = 8.17, **$p = 0.0043$; ***G***) of IPSCs compared to shams. Statistics: Data. Individual tdTomato+ interneurons were considered as the statistical unit (Sham: $n = 18$ from 9 mice; mTBI: $n = 28$ from 12 mice). Significant difference determined using Wilcoxon test.

AUTHOR CONTRIBUTIONS

MV, KMJ, and JTP contributed to the design of the experiments. MV performed all surgeries and confocal imaging. XJ collected all electrophysiological data. MV performed statistical data analyses. MV, XJ, KMJ, and JTP contributed to writing of the manuscript.

CHAPTER FOUR

DISCUSSION

Synopsis

This study provides compelling evidence of structural and functional disruption of local excitatory-inhibitory networks after clinically relevant mTBI in transgenic/knock-in gene mice. Consistent with human mTBI, midline cFPI reproducibly evoked DAI without mass lesions, neocortical contusion, and/or overt cell death. In Chapter 2, exploiting restricted YFP expression in a discrete subset of layer 5 pyramidal neurons and an established AIS marker (ankG), we confirmed subcellular structural plasticity within the non-DAI/intact population. In this mTBI-mediated response, the decrease in GABAergic presynaptic boutons surrounding the perisomatic domain of this intact pyramidal neuron population suggested compromised PV+ interneuron inhibition of their AIS. Consistent with postsynaptic AIS structural plasticity, patch-clamp recordings of intact YFP+ layer 5 pyramidal neurons revealed slower AP acceleration. This finding was further supported by simulations using a realistic layer 5 pyramidal neuron model that showed even a subtle decrease in AIS length or NaV1.6 density attenuates AP acceleration. In Chapter 3, we showed compelling evidence supporting the loss of perisomatic GABAergic inhibition via DAI using cre/lox mice. Exploiting Cre-driven tdTomato expression in PV+ interneurons coupled with detailed confocal and ultrastructural analysis, we show for the first time that mTBI induces GABAergic interneuron DAI across neocortical layers 2–6. Using established markers of impaired axonal transport (APP) and neuronal stress (p-c-

Jun) we confirmed DAI within GABAergic interneurons that comprise only a small fraction of neocortical neurons. Further, in this mTBI-mediated response, colocalization of GABAergic and DAI markers revealed a disproportionate involvement of PV+ interneurons and vulnerability for PSAI. Patch-clamp recordings of tdTomato+ fast-spiking interneurons showed reduced inhibitory transmission. Taken together, these findings demonstrate significant structural and functional changes of both intrinsic and extrinsic/synaptic components in neuronal domains crucially involved in regulating excitability and excitatory-inhibitory balance. The conclusions of this study depart from current thought on mTBI, which has been based primarily on the role of structural disconnection of white matter tracts without any consideration of neocortical involvement. Collectively, the novel neuronal and physiologic substrates identified in this study significantly extend our knowledge of cortical network dysfunction following mTBI.

Neurobiological Relevance and Potential Impact on Neocortical Circuits/Networks

Several features of our cFPI model underscore its clinical relevance and utility for evaluating neocortical network disruption after mTBI (Lifshitz et al., 2016; Spain et al., 2010). The large size of the human brain makes it susceptible to inertial loading and deformation following rapid changes in acceleration/deceleration. In turn, such mechanical loading leads to shear forces, perturbing neuronal microstructure and leading to DAI (Maxwell et al., 1997; Zhang et al., 2004). While the rapid mechanical loading (<50 ms) consistent with human (closed-head) mTBI is difficult to reproduce in laboratory animals with brains smaller by orders of magnitude, employing a mouse

model provides a number of advantages. First, many inbred mouse strains are now well characterized. Therefore, comparisons between mTBI and sham mice could be made with the existence with normative data for a wide range of physiological and behavioral variables. While our mouse model of mTBI involves craniectomy, the fluid pulse is delivered into the mouse cranium using a closed mechanical system. Additionally, the duration of the fluid pulse (<20 ms) simulates rapid acceleration/deceleration mechanical loading of the human brain following trauma (Dixon et al., 1987). This form of mechanical brain injury generates neurological signs of transient behavioral suppression resembling signs of unconsciousness (LOC) in humans. Specifically, we used LORR as a surrogate for LOC to assess injury severity. The duration of LORR in mice was similar to LOC in humans following mTBI, ranging 3–5 min.

To date, human TBI across the spectrum of severity is commonly associated with DAI occurring within the corpus callosum and SCWM. The use of rodent cFPI for over 30 years has yielded hundreds of reports from our lab and others that show DAI occurring within these WM tracts, highlighting the model's consistent reproducibility of human TBI neuropathology. Additionally, experimental TBI studies have shown that DAI identified via DTI in rodents maps to APP immunoreactivity in WM tracts (Mac Donald et al., 2007). This is entirely consistent with findings from more recent DTI studies and postmortem examinations across the spectrum of human TBI severity, respectively. Hence, the finding of WM tract DAI after rodent cFPI serves as an 'internal control' for the neuropathology typically induced by the forces of TBI. Rodent cFPI also consistently generated DAI within cortical (neocortical and hippocampal), and deep gray matter as well as the optic nerve, confirming the observations of other studies, while

offering new insight into the potential neocortical involvement. Collectively, these widespread neuropathological findings suggest that experimentally induced DAI in rodents is not an epiphenomena related to the biomechanics of cFPI. Rather, the distribution of cFPI-induced neuropathology in rodents suggests that this model is representative of human mTBI.

Capitalizing on this model system we previously showed that intact YFP+ pyramidal neurons, which are the major excitatory component in neocortical networks, revealed altered intrinsic and extrinsic/synaptic properties post-mTBI that developed over time. Initially after mTBI, the intrinsic properties of intact pyramidal neurons paralleled that found in the DAI population, suggesting that ion and/or neurotransmitter imbalance had an indiscriminant overriding effect on currents. However, by 2 d post-mTBI a functional divergence was identified wherein the intact pyramidal neuron population showed distinct electrophysiological changes implicating AIS structural-functional alteration. Specifically, powerful intact pyramidal neurons were found that had both increased intrinsic and synaptic excitability at 2 d after mTBI. Additionally, these changes occurred in parallel with overall increased network excitability. Collectively, these previous findings by our lab formed the basis of the current study focusing on the effect of mTBI on intrinsic structure and function of the AIS as well as the extrinsic/synaptic GABAergic inputs that control its output.

The essential function of the AIS is to integrate synaptic input (excitatory and inhibitory) and determine whether to fire an AP (Kole and Stuart, 2012). The dynamics between extrinsic/synaptic and intrinsic AIS properties underlie neuronal coding, whereby analog signal inputs are propagated via digital output (Ainsworth et al., 2012). A

critical feature of the interplay between synaptic transmission and intrinsic neuronal excitability is perisomatic inhibitory input, which strongly regulates pyramidal neuron AIS output (Freund and Katona, 2007; Gerstner et al., 1997; Lisman and Jensen, 2013; Miller, 1996). Hence, the pyramidal neuron perisomatic domain can be viewed as an excitatory-inhibitory interface critical for regulating neuronal activity. Several reports demonstrate how changes in presynaptic input/activity can induce AIS structural and functional plasticity. Kuba and associates (2010) showed that cochlear deprivation, which decreased presynaptic excitatory input, results in postsynaptic AIS elongation, which correlated with increased neuronal excitability.

Since altered network activity and/or presynaptic input modifies AIS architecture, which in turn alters neuronal excitability, the current study sought to determine if the previously observed electrophysiological changes within intact layer 5 pyramidal neuron were related to structural and/or functional changes within this crucial subcellular domain. For structural studies, we employed ankG as a surrogate marker of AIS position and length. Specifically, we found that while there was no change in position with respect to the soma of origin, the length significantly decreased from the distal end. Electrophysiological assessments revealed decreased AP acceleration at the AIS, but not the soma. All together, these data reflect slower NaV activation specifically at the AIS. Computer simulations using a realistic model of a layer 5 pyramidal neuron supported this premise. Specifically, decreasing either AIS length by experimentally observed values or NaV density by the same proportion also decreased AP acceleration, consistent with the data reported by Hallerman and associates (2012) in their characterization of this layer 5 pyramidal neuron model (Hallermann et al., 2012).

An unexpected finding in the current study that followed from our *a priori* control parameters was that AIS length from the distal end varied with neocortical depth. Importantly, this dependency was observed in the distribution of both the ankG and NaV1.6 immunofluorescent profiles. Although not previously appreciated, this observed variance is consistent with known properties of layer 5 pyramidal neurons. Specifically, layer 5 pyramidal neurons are subdivided into layer 5a and 5b in which multiple pyramidal neuron subtypes characterized by different morphological and electrophysiological properties exist (Chagnac-Amitai et al., 1990; Le Bé et al., 2007; Schubert et al., 2001, 2006). This observation is also consistent with recent reports from other labs showing changes in AIS length but not position with respect to soma of origin (Gutzmann et al., 2014; Kuba et al., 2010).

In the neocortex, the balance of excitation-inhibition is regulated by PV+ interneurons that are highly interconnected with local pyramidal neurons (Hu et al., 2014). This proximity of PV+ terminals to the AIS allows for strong inhibitory control over AIS output. As described above, in addition to revealing the excitatory substrates, our previous study also supports the premise that changes in inhibition may contribute to overall network hyperexcitability (Hånell et al., 2015a). In light of the known features of AIS structure-function and the fact that mTBI-induced abnormal network activity is associated with imbalanced excitation-inhibition, we also evaluated extrinsic/synaptic structural changes in concert with our AIS investigations. In the current study, this issue was addressed by examining inhibitory structural synaptic connectivity. Quantitative analysis of intact layer 5 pyramidal neuron perisomatic GAD67+ and PV+/GAD67+ puncta revealed a significant decrease. While multiple mechanisms underlying PV+

interneuron terminal loss were possible, worthy of note is a previous report from our lab showing ultrastructural evidence of terminal degeneration along the perisomatic domain of healthy layer 5 pyramidal neurons within DAI areas of neocortex 2 d after mTBI (Singleton et al., 2002). In addition to the evidence provided in the current study on loss of PV+ interneuron axonal terminals, the recent advancements in neocortical mapping have led us to amend our interpretation of our previous ultrastructural data, which we then thought to be related to thalamocortical DAI. However, given the fact that the pyramidal neurons perisomatic domain is almost exclusively targeted by PV+ interneurons, and that PV+ interneurons and pyramidal neurons are highly interconnected, this suggests that our original interpretation was incorrect. Accordingly, our current findings now provide direct evidence for the disruption of a local microcircuit having major implications in both neocortical output and potential for reorganization. Taken together, these findings suggest that PV+ interneuron DAI is a more likely mechanism for anterograde synaptic loss following mTBI. Collectively, these findings provoked the question whether locally projecting GABAergic interneurons can also undergo DAI to cause disconnection of their axons resulting in presynaptic terminal loss/deafferentation at target sites of postsynaptic neurons.

To dissect specific neuronal components of local neocortical network dysfunction we employed Cre/lox mice to genetically label the total population of PV+ interneurons (Madisen et al., 2010; Taniguchi et al., 2011). As only ~20% of neocortical neurons are GABAergic, we chose to probe PV+ interneurons, which are the largest subclass representing 40–50% of total inhibitory interneurons (Rudy et al., 2011). While Cre/lox mice have become an essential tool for studying neocortical structure and function,

caution must be exercised when labeling specific neuronal populations. Similar to previous reports by other groups (Pfeffer et al., 2013), in our hands, quantitative analysis showed >90% colocalization between Cre-driven tdTomato expression and endogenous PV immunoreactivity. Thus, PV-Cre;Ai9 animals enabled axon identification based on tdTomato+ profiles alone, while also allowing us to follow the same interneuron from confocal to electron microscopy via antibodies targeting tdTomato.

With confocal microscopy, we routinely identified DAI in a population that represented ≤10% of total neocortical neurons. Ultrastructural analysis of tdTomato+ PSAI revealed vesicle/organelle-laden swellings pathognomonic of impaired axonal transport (Christman et al., 1994). The distal disconnected segment was disorganized indicating rapid onset of Wallerian degeneration. These findings are consistent with previous observations that showed ultrastructural evidence of terminal degeneration along the perisomatic domain of healthy layer 5 pyramidal neurons within neocortical regions sustaining DAI after mTBI (Singleton et al., 2002). The observed PV+ interneuron PSAI evolved rapidly following mTBI. Similar to previous findings, by 24h post-mTBI identifying tdTomato+ PSAI became difficult, likely due to anterograde transport suspension/reversal. Circumventing this limitation, we used a previously established strategy incorporating p-c-Jun, a nuclear transcription factor, as a surrogate DAI marker to spatiotemporally assess retrograde changes in the sustaining somas of origin (Greer et al., 2011). We found that nuclear expression of p-c-Jun increased within 3 h post-mTBI and was consistently associated with tdTomato+ PSAI, thus reaffirming our previous findings and further supporting the use of p-c-Jun as a pan-neuronal DAI marker. Additionally, these data show for the first time that p-c-Jun is rapidly expressed

in DAI neurons after mTBI. In our previous studies, the earliest time point showing p-c-Jun expression was 24 h post-mTBI. This suggests that retrograde signaling activates somatic genetic programs immediately following axonal failure. Specifically, these responses are thought to be associated with neuronal survival and axonal regeneration. Further, temporal assessment of tdTomato+ profiles also showed a strongly correlated, dramatic increase in anterograde axonal debris and retrograde p-c-Jun expression, thereby supporting their linkage, with these anterograde changes most likely reflecting widespread axon terminal degeneration concomitant with deafferentation of target neurons. This further supported the premise that locally projecting GABAergic interneurons can also undergo DAI to cause disconnection of their axons resulting in presynaptic terminal loss/deafferentation at target sites of postsynaptic neurons. Importantly, this neuropathology evolved without evidence of neuronal loss, consistent with our previous findings in pyramidal neurons, thalamic neurons, and retinal ganglion cells (Greer et al., 2011; Wang et al., 2013). For many years cell/neuronal death was viewed as the primary contributor to morbidity after TBI, even when mild. However, it is now recognized that mTBI pathophysiology conditions ensue without neuronal loss (Farkas et al., 2006). Our findings not only reveal a novel substrate of DAI (GABAergic interneurons), but also provide further support for this premise by showing yet another neuronal subtype in which cell death is absent.

Capitalizing on the utility of GAD67 as a reliable DAI marker, we determined that PV+ interneuron DAI represented almost 90% of all GABAergic DAI, suggesting limited involvement of other inhibitory interneuron subclasses. This observed preferential involvement of PV+ interneurons may be due to the ‘metabolic hypothesis’ that

postulates that their fast-spiking behavior creates a high-energy demand in both their soma and axonal domains (Kann et al., 2014). Indeed, PV+ interneurons have the highest concentration of axonal mitochondria compared to other neurons and local ongoing neocortical activity consumes the majority of brain energy (Buzsáki et al., 2007; Raichle, 2010). In fact, selective vulnerability of PV+ interneurons have been implicated in several other diseases including epilepsy and Alzheimer's (Hu et al., 2014; Kann, 2016; Zhang and Raichle, 2010).

The use of GAD67/APP to identify GABAergic DAI also confirmed that the vast majority of tdTomato+ swellings demonstrated PSAI. Previously, we showed that mTBI induced DAI primarily within the AIS of excitatory pyramidal neurons, where action potentials are generated (Greer et al., 2013). The currently observed PV+ interneuron PSAI, together with the previously observed pyramidal AIS involvement, suggests that perisomatic/AIS vulnerability may be a distinguishing neocortical DAI feature. The AIS is a conserved structure with a highly developed subaxolemmal cytoskeleton integrated with a unique extracellular matrix via cell adhesion molecules (Grubb and Burrone, 2010b). A recent review underscores the concept that physical forces are transmitted across all spatial scales suggesting that the relatively gross tissue deformation used to describe WM tract vulnerability may not account for the forces exerted on the underlying cellular structures in different brain regions (Hemphill et al., 2015). Thus, the perisomatic/AIS domain may represent a structural vulnerable domain on a much finer scale, where mechanotransduction through the neuronal microenvironment may be a potential mechanism underlying neocortical PSAI.

Rigor, Reproducibility, and its Relation to Previous Findings

All mice used for structural and functional studies were in physiological homeostasis, with no evidence of any mass lesions, neocortical contusion, and/or cell death, a finding entirely consistent with human mTBI. Specifically, a crucial feature in our approach is that we monitored arterial oxygen saturation, heart rate, respiratory rate, and core body temperature. Importantly, evaluating these parameters help distinguish our study from most other investigations, which do not perform routine physiologic monitoring to exclude secondary insults that could severely confound the assessment of network disruption via diffuse structural and functional changes. Therefore, we are confident that our interpretations of the observed morphological changes in axonal fluorescent protein expression profiles are associated with mechanisms with mTBI-induced DAI.

Both clinical and experimental methodologies used to investigate excitatory-inhibitory networks have limitations. Advanced structural and functional neuroimaging in mTBI patients cannot resolve the specific neuronal and physiologic substrates of neocortical gray matter disruption (Le Bihan and Johansen-Berg, 2012; Logothetis, 2008). The novel approaches enabled by the recent adoption of transgenic/knock-in gene mice into the mTBI research field highlight several features of this invaluable resource for investigating pathobiology and electrophysiology. Perhaps one of the most valuable features of mouse models is the selective expression of fluorescent proteins by discrete neuronal subsets. This allowed us to dissect specific excitatory and inhibitory components of cortical network disruption. In a pioneering study employing the Thy1-YFP-H mouse line, Greer and associates (2011)showed fluorescent protein accumulations identify sites of DAI in a discrete subset of layer 5 pyramidal neurons. This crucial

discovery enabled highly detailed structural and functional investigation of both DAI and non-DAI/intact neuronal populations. In subsequent studies, these transgenic mice were used to experimentally interrogate neocortical circuit/network disruption via procedures such as *ex vivo* electrophysiological recording, yielding real-time measurements of traumatically altered neurophysiology. In the current study, we continue in the use of these novel approaches that exploit restricted expression in the Thy1-YFP to structurally assess subcellular components critical to regulation neuronal physiology. Further, in Chapter 3, we build upon our model by employing PV-Cre;Ai9 mice to dissect structural-functional changes in neocortical GABAergic interneurons after mTBI.

As described in Chapter 2, capitalizing on restricted neuronal labeling with YFP including the total axonal length, readily traceable within the neocortical gray, allowed the unequivocal identification of mTBI-induced DAI vs. non-DAI/intact populations in both fixed tissue sections and live slices. Specifically, intact pyramidal neurons were readily identified by following YFP+ axons from their soma of origin to the SCWM interface. Previously, we reported that mTBI induces DAI primarily within the AIS of the YFP+ layer 5 pyramidal neurons (Greer et al., 2013). Additionally, in a former publication we showed that APP immunoreactive swellings did not colocalize with YFP axons in either the SCWM or corpus callosum (Hånell et al., 2015b). Taken together, these findings strongly support the premise that virtually all YFP+ pyramidal neuron DAI occurs within the neocortical gray. Based on this premise, YFP+ pyramidal neurons undergoing DAI can be reliably identified by examining their axonal segment spanning neocortical layers 5/6 to the SCWM interface. Building upon our previous studies in

YFP-H mice we succeeded in conducting a highly detailed analysis within these pyramidal neurons.

This was a crucial component of our study since the AIS ion channel distribution differs across neuronal subtypes (Lorincz and Nusser, 2008), and even within a neuronal subtype there is substantial variability in position and length, as shown in the current study. Further, because DAI affects only a small fraction of neurons within a pyramidal neuron population that represent 80% of all neocortical neurons, quantification of such heterogeneous population remains a confound. Our previous reports underscore this issue, showing that the neocortical pyramidal neuron AIS has a predilection for DAI. Additionally, in our previous report and the current study we show DAI occurring within the AIS severely disrupts ankG and NaV1.6 expression. Hence, even a 5% burden of DAI (Greer et al., 2011)(Greer et al., 2011)(Greer et al., 2011)(Greer et al., 2011)(Greer et al., 2011)(Greer et al., 2011)(Greer et al., 2011)(Greer et al., 2011)(Greer et al., 2011)(Greer et al., 2011)(Greer et al., 2011)(Greer et al., 2011)(Greer et al., 2011)(Greer et al., 2011)(Greer et al., 2011)(Greer et al., 2011)(Greer et al., 2011)causing AIS disruption would substantially contribute to data variability. To the best of our knowledge, this is the first study to account for these issues by examining only intact, Thy1-expressing, layer 5 pyramidal neurons.

For structural studies of intact YFP+ pyramidal neurons, we employed ankG as a surrogate marker of AIS position and length. Specifically, we found that while there was no change in position with respect to the soma of origin, the length significantly decreased from the distal end. This finding departs from a previous study, which found a global decrease in neocortical AIS length in rats 2 weeks after blast wave-induced mTBI (Baalman et al., 2013). The important distinction in the current report is that we detected

a decrease in AIS length within 2 d after cFPI-induced mTBI specifically within the layer 5 pyramidal neuron populations with no overt structural axonal abnormalities and/or evidence of DAI. Our novel finding of structural uncoupling between ankG and NaV1.6 distributions underscores the important of this distinction. In the current study, we did not observe a decrease in NaV1.6 length that paralleled with ankG distribution. This is unlike the majority of reports on AIS plasticity, which demonstrate parallel changes in scaffold proteins and ion channels. Further, this uncoupling of ankG and NaV1.6 (intrinsic structural plasticity) occurred in concert with loss of perisomatic GAD67+/PV+ presynaptic boutons (extrinsic structural plasticity). The perisomatic domain of (post-synaptic) pyramidal neurons is an excitatory-inhibitory interface in this neocortical microcircuit with (presynaptic) PV+ interneurons. Perisomatic GABAergic synaptic input from PV+ interneurons is a strong source of inhibition for pyramidal neuron AIS excitability/output. Hence, these presynaptic (inhibitory) structural changes are likely associated with postsynaptic (excitatory) functional changes. Further, as described in detail below, a potential mechanism resulting in the observed terminal loss is PV+ interneuron DAI.

Some of the major obstacles in the current study were limitations of the previously used markers to understand DAI pathogenesis (e.g. APP) and its implications for network disconnection. In both human postmortem and animal investigations DAI is typically identified via APP immunohistochemistry, which transiently accumulates at sites of impaired axonal transport following TBI (Sherriff et al., 1994a; Stone et al., 2000). APP+ swellings can be readily observed in dense WM tracts, wherein the distal aspect demarcates the site of axonal disconnection. However, this strategy cannot be used

to trace long-distance projections back to their origin, thus fails to provide retrograde information on the fate of the sustaining neuronal soma. Further complicating this issue is that APP is ubiquitously expressed by neocortical neurons and cannot provide information on the type of fiber system involved (e.g. glutamatergic or GABAergic). The adoption of transgenic mice into the experimental mTBI research field by Greer and colleagues (2011) has provided a novel approach to identifying DAI with high fidelity in specific neuronal subtypes. As mentioned above, Greer and associates (2011) showed that fluorescent protein accumulations map to APP+ swellings in a discrete subset of layer 5 (excitatory) pyramidal neurons. Building on this approach, in the current study unequivocally demonstrated PV+ interneuron DAI via mapping tdTomato+/PV+ profiles to APP+ axonal swellings. Similarly, we further confirmed GABAergic DAI by targeting GAD67, which also undergoes fast anterograde transport and accumulates within APP+ axonal swellings. Importantly, the detailed quantitative analysis presented in Chapter 3 established GAD67 as a novel immunohistochemical DAI marker specific to GABAergic neurons.

Although other investigations have shown neocortical GABAergic interneuron involvement, these were in the context of cell death using models of blunt-force trauma or more severe TBI involving mass lesions/contusion to model epileptogenesis (Hunt et al., 2013; Pitkänen and McIntosh, 2006)(Hunt et al., 2013; Pitkänen and McIntosh, 2006)(Hunt et al., 2013; Pitkänen and McIntosh, 2006)(Hunt et al., 2013; Pitkänen and McIntosh, 2006)(Hunt et al., 2013; Pitkänen and McIntosh, 2006)(Hunt et al., 2013; Pitkänen and McIntosh, 2006)(Hunt et al., 2013; Pitkänen and McIntosh, 2006)(Hunt et al., 2013; Pitkänen and McIntosh,

2006)(Hunt et al., 2013; Pitkänen and McIntosh, 2006)(Hunt et al., 2013; Pitkänen and McIntosh, 2006)(Hunt et al., 2013; Pitkänen and McIntosh, 2006)(Hunt et al., 2013; Pitkänen and McIntosh, 2006)(Hunt et al., 2013; Pitkänen and McIntosh, 2006), which is not an outcome of clinical or experimental mTBI. To the best of our knowledge, this is the first study to address GABAergic interneuron after mTBI. Additional strength and rigor was exercised in the current study through the targeting of p-c-Jun to estimate the burden of DAI of PV+ interneurons at 1 d post-mTBI. Based on the robust expression of p-c-Jun at 1 d post-mTBI, we determined that ~9% of tdTomato+ interneurons underwent DAI. Previously, we estimated ~5% of Thy1-expressing layer 5 pyramidal neurons undergo DAI. To our knowledge these two studies are the only quantitative estimates of the proportion of neocortical DAI following experimental mTBI in mice. Further, we estimate that of the total population of p-c-Jun+ population (pyramidal and interneuron DAI), ~14% is accounted by tdTomato+ interneurons. This suggests that ~86% of neural DAI is represented by pyramidal neurons, which is consistent with that fact that this is approximately the same percentage of pyramidal neurons comprising the total neocortical neuron population. Collectively, both our qualitative and quantitative data validate that neocortical PV+ interneuron PSAI is not an isolated phenomenon. Rather, it is a consistent and significant component of mTBI-induced pathology. Accordingly, PV+ interneuron PSAI has major postsynaptic functional implications for both microcircuits involving feedback inhibition of excitatory (intact) pyramidal neurons and also small-scale neocortical inhibitory networks as described below.

GABAergic interneuron structure reflects function (Kepecs and Fishell, 2014). Specifically, the expansive axonal arbors of PV+ interneurons highlight their role in

balancing neocortical excitation-inhibition to synchronizing neuronal ensembles, which play major roles in plasticity and behavior. Operationally, the strong and selective connectivity between PV–PV interneurons leads to disynaptic disinhibition forming powerful local neocortical networks that generate high-frequency gamma oscillations. Neocortical activity reflected as gamma oscillations observed using EEG occurs during both cognitive and resting states. Specifically, during resting-state, transient gamma oscillations emerge from spontaneous excitatory-inhibitory neuronal activity. In ferrets, it was found that inhibitory postsynaptic currents (IPSC) carry synchronized high-frequency (gamma range) information in active neocortical networks (Hasenstaub et al., 2005). Specifically, fast-spiking PV+ interneuron activity correlated with gamma oscillations. Hence, PV+ interneuron firing is a 'pulse' of local excitatory-inhibitory neocortical network activity (Trachtenberg, 2015). Accordingly, the impact of mTBI on local neocortical inhibitory networks via PV+ interneuron PSAI also involved functional disconnection.

To assess local neocortical (small-scale) networks, we used inotropic glutamate receptor antagonist to pharmacologically isolate GABAergic neurotransmission from excitatory WM tract (extrinsic) and collateral (intrinsic/recurrent) inputs. Note, extrinsic/intrinsic have different definitions for microcircuits and small-scale neocortical networks. Patch-clamp recordings of tdTomato+ interneurons showed fast-spiking action potentials characteristic of PV+ interneurons. Importantly, PV+ interneuron intrinsic properties were similar between shams and mTBI. This supported the premise that the tdTomato+ interneurons in mTBI slices were healthy, consistent with our observation that ~9% of PV+ interneurons underwent DAI. Notwithstanding this relatively subtle

burden of injury, inhibitory transmission in PV+ interneurons was compromised following mTBI, marked by a 60% and 32% decrease in sIPSC frequency and event area (charge transfer), respectively. Such a drastic decrease in inhibitory transmission is consistent with known properties of PV+ interneurons described above and our findings that PSAI disconnects the distal axonal arbor causing widespread axonal degeneration and terminal loss/deafferentation of postsynaptic neurons in local neocortical networks. PV+ interneurons powerfully inhibit one another via perisomatic innervation, reflected by the relatively large amplitude of their IPSC. Further, inhibitory presynaptic discharge does not saturate all postsynaptic $GABA_A$ receptors (Perrais and Ropert, 2000). Together, these known properties of PV+ interneurons may potentially explain the subtle decrease in sIPSC amplitude. Taken together, our electrophysiological findings show that even a small fraction of PV+ interneuron PSAI is adequate to cause a substantial reduction of GABAergic transmission within local neocortical inhibitory networks after mTBI.

Implications of Our Findings for the Formation of a Unifying Theory

Based on the data presented in Chapters 2 and 3, we believe that intact pyramidal neuron AIS plasticity is associated with PV+ interneuron DAI. Specifically, we posit that at 2 d post-mTBI, intact pyramidal neuron AIS's are in a state of flux. Our structural data suggests that initial AIS change involves ankG shortening and that AnkG remodeling may precede mechanisms that affect NaV1.6 resulting from a decreased length from the distal end. Alternatively, a decrease in ankG length could elicit a decrease NaV1.6 density. AnkG is the master scaffolding protein whose structural dynamics modulate AIS function via clustering NaV1.6 channels. In this case, ankG shortening may destabilize

NaV1.6 leading to redistribution resulting in decreased density at the distal AIS but without a change in length. This form of AIS structural reorganizations offers a potential mechanism fro the observed AIS function alterations.

This intact pyramidal neuron AIS structural-functional plasticity is highly likely to occur as a downstream consequence of PV+ interneurons PSAI. Presynaptic activity/input is known to modulate postsynaptic AIS structure-function. For example, decreased presynaptic excitatory drive induces postsynaptic AIS lengthening functionally associated with increased neuronal excitability. PV+ interneurons are known as the dominant regulators of neocortical excitatory-inhibitory balance. Several studies have shown that loss of PV+ interneuron-mediated inhibition results in neocortical network hyperexcitability. Our recent studies demonstrated that neocortical networks and intact pyramidal neurons become hyperexcitable 1–2 d post-mTBI. Here, we provide compelling evidence for loss of GABAergic mediated inhibition as a major contributor for local network disruption within 1 d post-mTBI. Taken together, these studies provide specific neuronal and electrophysiological substrates underlying neocortical excitatory-inhibitory balance. Specifically, PV+ interneurons provide strong inhibition via their GABAergic synapses distributed along the perisomatic domain of excitatory pyramidal neurons. Hence, the pyramidal neuron perisomatic domain is a crucial interface of excitatory-inhibitory interactions. Our structural data showing PV+ interneuron PSAI, which disconnects the entire distal axonal arbor with, together with the loss of perisomatic GABAergic bouton density by 1 d post-mTBI suggests that these changes in presynaptic input may drive postsynaptic AIS plasticity within intact pyramidal neurons at 2 d post-mTBI. The decrease length in ankG, consistent with AIS shortening, and

attenuated AP acceleration is consistent with a postsynaptic neuronal response to loss of perisomatic inhibition and heightened network activity. Specifically, AIS length decrease is associated with reduced neuronal excitability. Therefore, the observed structural and functional AIS plasticity among intact pyramidal neurons may be a compensatory mechanisms to help restore balance excitation-inhibition following loss of GABAergic input, a premise that will require more experimental evidence warranting future investigation.

Implications for Understanding of mTBI: Morbidity and Recovery

Recent clinical studies further support the premise that mTBI induces structural and functional disruption of local neocortical networks. Several groups reported clinically diagnosed mTBI marked by substantial cognitive impairment without significant WM involvement (Ilvesmäki et al., 2014; Mac Donald et al., 2011; Wäljas et al., 2014; Zhang et al., 2010). This suggests an undetected structural-functional pathophysiology within neocortical GM, involving recurrent microcircuits and small-scale network information processing (Aron, 2007; Fries, 2009; Haider and McCormick, 2009; Raichle, 2010). Supporting this possibility, studies measuring neocortical metabolic (fMRI) and electrophysiological (EEG, MEG) change, revealed a wide range of intrinsic neocortical network dysfunction involving abnormal spontaneous, rhythmic, and excitatory/inhibitory activity (Bashir et al., 2012; De Beaumont et al., 2012; Huang et al., 2016a; Luo et al., 2013; Mayer et al., 2011; Palacios et al., 2017; Sponheim et al., 2011; Tremblay et al., 2011). Additionally, recent DTI studies of neocortical GM have detected reactive changes suggesting that mTBI disrupts local structural connectivity (Bouix et al.,

2013; Ling et al., 2013; Newcombe et al., 2011). Collectively, these clinical findings strongly implicate that mTBI disrupts structural and functional connectivity in local neocortical networks formed by excitatory pyramidal neurons and inhibitory interneurons (Douglas and Martin, 2007; McCormick, 2003; Somogyi et al., 1998).

Although studying diffuse changes in the fine-scale structure of neocortex is difficult (Crick, 1979; Povlishock and Christman, 1995), emerging evidence supports that widespread terminal loss/deafferentation of neocortical networks contributes to mTBI morbidity and sets the stage for subsequent adaptive or maladaptive plasticity (Christman et al., 1997; Huang et al., 2009b; Marquez de la Plata et al., 2011; Patel et al., 2016; Phillips and Reeves, 2001; Povlishock et al., 1992; van der Horn et al., 2016). In addition to characterizing p-c-Jun as a somatic marker of DAI, in a previous report we also demonstrated an association with axon regeneration, showing DAI pyramidal neurons extend their processes over time. Interestingly, it appeared this regenerative attempted was halted at the subcortical white matter junction, suggesting re-connection with remote sites may be limited following mTBI. However, electrophysiological studies have suggested the potential for establishing recurrent excitatory projections after mTBI (Hånell et al., 2015a). Specifically, these new excitatory connections appeared to be maladaptive based on the observation of mTBI-induced overall network hyperexcitability. On the other hand, in an earlier report our lab showed neuroplasticity following moderate cFPI in the cat (Erb and Povlishock, 1991). Specifically, GABAergic terminal loss in the vestibular nucleus was followed by significant recovery of synapses over time. It is posited that this occurred via sprouting of contacts from adjacent intact/unaltered connections and not through re-connective mechanisms. Considering

adult homeostatic plasticity is mediated via GABAergic inhibition and PV+ interneurons axonal arbors are embedded within neocortical gray matter, raises many issues regarding the potential for reorganization following perisomatic DAI. For example, a crucial question is whether regenerative responses are mounted following PV+ PSAI. In contrast to long-distance projecting pyramidal neurons, PV+ interneurons may have increased potential for re-establishing (adaptive) connection since their axons project within neocortical gray matter, targeting postsynaptic sites typically within a few hundred microns distal from the soma of origin. Alternatively, similar to the observations made in cats, is the potential for deafferentated sites undergoing synaptogenesis via sprouting of adjacent intact fibers. Assuming the potential for both mechanisms, perhaps even more germane to this issue is if there is a differential outcome. Specifically, whether axonal regeneration after PV+ interneuron PSAI vs. reaming intact axon synaptogenesis mechanisms are adaptive or maladaptive plasticity, leading to recovery or progressive/chronic neurological impairment, respectively. Lastly, the question remains whether PV+ PSAI and/or downstream neuroplasticity are amenable to intervention.

Recommendations for Future Studies

While determining the actual functional consequences of [intact layer 5 pyramidal neuron perisomatic GAD67+ and PV+/GAD67+ puncta revealed a significant decrease] is beyond the scope of the current study, this parallel observation to our AIS findings provides additional evidence that local neocortical disruption is a consistent feature of mTBI. In future studies, it would be important to determine if such loss in presynaptic inhibitory input elicits postsynaptic AIS shortening to decrease pyramidal neuron

excitability to restore network homeostasis after mTBI. Such a finding would add further validity to the work of Kuba and others (2010) who have shown that decreasing presynaptic excitatory input may result in postsynaptic AIS elongation associated with increased excitability as a compensatory response to overall network hypoexcitability.

IPSCs play a major role in local (intrinsic) neocortical networks, which can operate independent of sensory (extrinsic) inputs via ongoing spontaneous activity (McCormick, 2003). In such a scenario local network dysfunction elicited by DAI within neocortical GM could provide a potential mechanism of clinically significant mTBI without WM tract involvement. While our electrophysiological assessments were not comprehensive, the paucity of information on the role of GABAergic interneurons in neocortical network dysfunction following mTBI adds importance to our findings and warrants future investigations. Specifically, future studies should record miniature and spontaneous IPSCs in pyramidal neuron to help gain insight into the physiologic association of loss of perisomatic GABAergic boutons with postsynaptic AIS plasticity. Moreover, since clinical studies implicate alterations in gamma oscillations, it would be imperative to assess neocortical networks by recording local field potentials. Specifically, it has been suggested that preclinical animal models should implement clinical endpoints when evaluating potential pharmacological interventions. Considering there have been over 200 failed clinical trials and to date there remains not treatment for mTBI, such approaches may be crucial for translational studies (Maas and Menon, 2012).

In this study we characterize GAD67 as a novel immunohistochemical DAI marker specific to GABAergic neurons. This finding has several implications for experimental mTBI studies outside of identifying GABAergic DAI. For example, real-

time tracking of DAI has never been preformed. However, our finding may make this possible. There are several genetically engineered mouse lines commercially available that expressed fluorescent protein-tagged GAD67. Since GABAergic DAI was observed in layer 2/3 neocortex, this means provides a means of following the evolution of DAI in real-time using shaved-skull mouse preparations using two-photon microscopy.

Concluding Remarks

Clinical and basic science research supports the premise that mTBI can induce network dysfunction. However, the cellular and neurophysiologic substrates remain unknown. Current thought suggests white matter DAI accounts for network dysfunction; however, this study provides compelling evidence that the scope of mTBI neuropathology may reside within the neocortical gray, where information processing occurs. Specifically, the cerebral cortex in all mammals has a conserved architecture, a cellular sheet composed of projection (pyramidal) and local circuit neurons (interneurons) deployed in horizontal layers, intersected by vertical (radial) columns that are considered the fundamental computational unit (DeFelipe et al., 2003; Mountcastle, 1979). Compared to cortical surface area across species, the thickness varies relatively little between brains of different size/species. In humans, the neocortex comprises approximately 80% of brain volume, containing functional homogeneous regions (nodes) that locally process information via complex microcircuits, which gets relayed via white matter tracts, together composing networks that support high-order processing (Mesulam, 1990). Neocortical columns microarchitecture is also stereotyped, similar across different brain regions, and demonstrate canonical microcircuitry. Specifically, PV interneurons are

highly intra-connected, and have been shown to non-selectively target almost every pyramidal neuron within their axonal arbor, forming reciprocal connections (Scholl et al., 2015). Even though PV interneurons comprise less than 10% of total cortical neurons, the impact of perisomatic axonal injury occurring in a single PV interneuron may potential disrupt the function of an entire column. PV interneurons represent a crucial component of excitatory-inhibitory systems, and can be used to assess the substrates of network disruption via investigation of neocortical microcircuitry in experimental models of mTBI helping reveal the full scope of mTBI induced changes. The perisomatic domain of pyramidal neurons represents an interface of excitation and inhibition. Specifically, perisomatic inhibition strong regulates excitatory pyramidal neuron AIS output. The AIS is a highly complex and dynamic domain (Grubb et al., 2011). Intrinsically linked structure-function relationships between scaffolding proteins and ion channels are a crucial for AIS activity. In this way, the neocortical pyramidal neuron AIS is a major determinant of network function and homeostatic plasticity. This premise has been evaluated in several studies showing AIS disruption associated with multiple disease states involving an imbalance of network function. Based on the current data, we posit that AIS plasticity may constitute a compensatory response to mTBI. However, future studies are needed to determine whether AIS structural-functional plasticity is adaptive or maladaptive, which has important implications for restoring excitatory-inhibitory balance in cortical networks disrupted by mTBI. Further, this study dismisses the notion that only axons within WM tracts are susceptible to mTBI forces. This study provides significant contributions to our understanding of mTBI, delivering a platform and novel molecular tools upon which to assess the anatomical sequelae of mTBI in local excitatory-inhibitory

circuits. Considering the neocortical column as the fundamental computational unit for higher-order information processing, understanding such inhibitory interneuron pathophysiology and its relation to changes in non-DAI/intact postsynaptic neuronal populations may be crucial for therapy development from a local network perspective. Ultimately, this study reshapes our knowledge of the cerebral landscape affected by mTBI in both animals and humans.

LIST OF REFERENCES

Abou-Hamden, A., Blumbergs, P. C., Scott, G., Manavis, J., Wainwright, H., Jones, N., et al. (1997). Axonal injury in falls. *J.Neurotrauma* 14, 699–713. doi:10.1089/neu.1997.14.699.

Adams, J. H. (1982). Diffuse axonal injury in non-missile head injury. *Injury* 13, 444–5.

Adams, J. H., Doyle, D., Ford, I., Gennarelli, T. A., Graham, D. I., and McLellan, D. R. (1989). Diffuse axonal injury in head injury: definition, diagnosis and grading. *Histopathology* 15, 49–59.

Adams, J. H., Gennarelli, T. A., and Graham, D. I. (1982a). Brain Damage in Non-Missile Head Injury. *Recent Adv. Neuropathol.*, 165–190.

Adams, J. H., Graham, D. I., Gennarelli, T. A., and Maxwell, W. L. (1991). Diffuse axonal injury in non-missile head injury. *J. Neurol. Neurosurg. Psychiatry* 54, 481–3.

Adams, J. H., Graham, D. I., Murray, L. S., and Scott, G. (1982b). Diffuse axonal injury due to nonmissile head injury in humans: an analysis of 45 cases. *Ann. Neurol.* 12, 557–63. doi:10.1002/ana.410120610.

Ainsworth, M., Lee, S., Cunningham, M. O., Traub, R. D., Kopell, N. J., and Whittington, M. A. (2012). Rates and Rhythms: A Synergistic View of Frequency and Temporal Coding in Neuronal Networks. *Neuron* 75, 572–583. doi:10.1016/j.neuron.2012.08.004.

Alexander, M. P. (1995). Mild traumatic brain injury: pathophysiology, natural history, and clinical management. *Neurology* 45, 1253–60.

Amyot, F., Arciniegas, D. B., Brazaitis, M. P., Curley, K. C., Diaz-Arrastia, R.,

Gandjbakhche, A., et al. (2015). A Review of the Effectiveness of Neuroimaging Modalities for the Detection of Traumatic Brain Injury. *J. Neurotrauma* 32, 1693–721. doi:10.1089/neu.2013.3306.

Andriessen, T. M. J. C., Jacobs, B., and Vos, P. E. (2010). Clinical characteristics and pathophysiological mechanisms of focal and diffuse traumatic brain injury. *J. Cell. Mol. Med.* 14, 2381–92. doi:10.1111/j.1582-4934.2010.01164.x.

Antonakakis, M., Dimitriadis, S. I., Zervakis, M., Micheloyannis, S., Rezaie, R., Babajani-Feremi, A., et al. (2016). Altered cross-frequency coupling in resting-state MEG after mild traumatic brain injury. *Int. J. Psychophysiol.* 102, 1–11. doi:10.1016/j.ijpsycho.2016.02.002.

Arenivas, A., Diaz-Arrastia, R., Spence, J., Cullum, C. M., Krishnan, K., Bosworth, C., et al. (2012). Three approaches to investigating functional compromise to the default mode network after traumatic axonal injury. *Brain Imaging Behav.* doi:10.1007/s11682-012-9191-2.

Aron, A. R. (2007). The neural basis of inhibition in cognitive control. *Neuroscientist* 13, 214–228. doi:10.1177/1073858407299288.

Atallah, B. V, and Scanziani, M. (2009). Instantaneous modulation of gamma oscillation frequency by balancing excitation with inhibition. *Neuron* 62, 566–77. doi:10.1016/j.neuron.2009.04.027.

Baalman, K. L., Cotton, R. J., Rasband, S. N., and Rasband, M. N. (2013). Blast Wave Exposure Impairs Memory and Decreases Axon Initial Segment Length. *J. Neurotrauma* 11, 1–11. doi:10.1089/neu.2012.2478.

Baker, a J., Phan, N., Moulton, R. J., Fehlings, M. G., Yucel, Y., Zhao, M., et al. (2002).

Attenuation of the electrophysiological function of the corpus callosum after fluid percussion injury in the rat. *J. Neurotrauma* 19, 587–99. doi:10.1089/089771502753754064.

Barkhoudarian, G., Hovda, D. a, and Giza, C. C. (2011). The molecular pathophysiology of concussive brain injury. *Clin. Sports Med.* 30, 33–48, vii–iii. doi:10.1016/j.csm.2010.09.001.

Bartos, M., Vida, I., and Jonas, P. (2007). Synaptic mechanisms of synchronized gamma oscillations in inhibitory interneuron networks. *Nat. Rev. Neurosci.* 8, 45–56. doi:10.1038/nrn2044.

Bashir, S., Vernet, M., Yoo, W.-K., Mizrahi, I., Theoret, H., and Pascual-Leone, A. (2012). Changes in cortical plasticity after mild traumatic brain injury. *Restor. Neurol. Neurosci.* 30, 277–82. doi:10.3233/RNN-2012-110207.

Bassett, D. S., and Bullmore, E. D. (2006). Small-World Brain Networks. *Neuroscientist* 12, 512–523. doi:10.1177/1073858406293182.

Bassett, D. S., and Sporns, O. (2017). Network neuroscience. *Nat. Neurosci.* 20, 353. doi:10.1038/nn.4502.

Bazarian, J. J., Blyth, B., and Cimpello, L. (2006). Bench to bedside: evidence for brain injury after concussion--looking beyond the computed tomography scan. *Acad. Emerg. Med.* 13, 199–214. doi:10.1197/j.aem.2005.07.031.

Benali, A., Weiler, E., Benali, Y., Dinse, H. R., and Eysel, U. T. (2008). Excitation and inhibition jointly regulate cortical reorganization in adult rats. *J. Neurosci.* 28, 12284–93. doi:10.1523/JNEUROSCI.1952-08.2008.

Bender, K. J., and Trussell, L. O. (2012). The physiology of the axon initial segment.

Annu. Rev. Neurosci. 35, 249–65. doi:10.1146/annurev-neuro-062111-150339.

Bigler, E. D. (2004). Neuropsychological results and neuropathological findings at autopsy in a case of mild traumatic brain injury. *J. Int. Neuropsychol. Soc.* 10, 794–806. doi:10.1017/S1355617704105146.

Bigler, E. D., and Bazarian, J. J. (2010). Diffusion tensor imaging: A biomarker for mild traumatic brain injury? *Neurology* 74, 626–627. doi:10.1212/WNL.0b013e3181d3e43a.

Bigler, E. D., and Maxwell, W. L. (2012). Neuropathology of mild traumatic brain injury: relationship to neuroimaging findings. *Brain Imaging Behav.* 6, 108–36. doi:10.1007/s11682-011-9145-0.

Bigler, E. D., and Snyder, J. L. (1995). Neuropsychological outcome and quantitative neuroimaging in mild head injury. *Arch. Clin. Neuropsychol.* 10, 159–74.

Blumbergs, P. C., Scott, G., Manavis, J., Wainwright, H., Simpson, D. A., and McLean, A. J. (1994). Staining of amyloid precursor protein to study axonal damage in mild head injury. *Lancet (London, England)* 344, 1055–6.

Blumbergs, P. C., Scott, G., Manavis, J., Wainwright, H., Simpson, D. a, and McLean, A. J. (1995). Topography of axonal injury as defined by amyloid precursor protein and the sector scoring method in mild and severe closed head injury. *J. Neurotrauma* 12, 565–572. doi:10.1089/neu.1995.12.565.

Blyth, B. J., and Bazarian, J. J. (2010). Traumatic alterations in consciousness: traumatic brain injury. *Emerg. Med. Clin. North Am.* 28, 571–94. doi:10.1016/j.emc.2010.03.003.

Bonifazi, P., Goldin, M., Picardo, M. a, Jorquera, I., Cattani, a, Bianconi, G., et al.

(2009). GABAergic hub neurons orchestrate synchrony in developing hippocampal networks. *Science* 326, 1419–24. doi:10.1126/science.1175509.

Borg, J., Holm, L., Cassidy, J. D., Peloso, P. M., Carroll, L. J., von Holst, H., et al. (2004). Diagnostic procedures in mild traumatic brain injury: results of the WHO Collaborating Centre Task Force on Mild Traumatic Brain Injury. *J. Rehabil. Med.*, 61–75.

Bouix, S., Pasternak, O., Rathi, Y., Pelavin, P. E., Zafonte, R., and Shenton, M. E. (2013). Increased Gray Matter Diffusion Anisotropy in Patients with Persistent Post-Concussive Symptoms following Mild Traumatic Brain Injury. *PLoS One* 8, e66205. doi:10.1371/journal.pone.0066205.

Bressler, S. L., and Menon, V. (2010). Large-scale brain networks in cognition: emerging methods and principles. *Trends Cogn. Sci.* 14, 277–90. doi:10.1016/j.tics.2010.04.004.

Buckner, R. L., Andrews-Hanna, J. R., and Schacter, D. L. (2008). The brain's default network: anatomy, function, and relevance to disease. *Ann. N. Y. Acad. Sci.* 1124, 1–38. doi:10.1196/annals.1440.011.

Buckner, R. L., Krienen, F. M., and Yeo, B. T. T. (2013). Opportunities and limitations of intrinsic functional connectivity MRI. *Nat. Neurosci.* 16, 832–7. doi:10.1038/nn.3423.

Buffington, S. a, and Rasband, M. N. (2011). The axon initial segment in nervous system disease and injury. *Eur. J. Neurosci.* 34, 1609–19. doi:10.1111/j.1460-9568.2011.07875.x.

Buhl, E. H., Tamás, G., Szilágyi, T., Stricker, C., Paulsen, O., and Somogyi, P. (1997).

Effect, number and location of synapses made by single pyramidal cells onto aspiny interneurones of cat visual cortex. *J. Physiol.* 500 (Pt 3, 689–713.

Büki, a, and Povlishock, J. T. (2006). All roads lead to disconnection?--Traumatic axonal injury revisited. *Acta Neurochir. (Wien).* 148, 181-93–4. doi:10.1007/s00701-005-0674-4.

Bullmore, E., and Sporns, O. (2009). Complex brain networks: graph theoretical analysis of structural and functional systems. *Nat. Rev. Neurosci.* 10, 186–98. doi:10.1038/nrn2575.

Buzsaki, G. (2004). Neuronal Oscillations in Cortical Networks. *Science (80-.).* 304, 1926–1929. doi:10.1126/science.1099745.

Buzsáki, G. (2006). *Rhythms of the Brain*. New York: Oxford University Press doi:10.1093/acprof:oso/9780195301069.001.0001.

Buzsáki, G., Anastassiou, C. a, and Koch, C. (2012). The origin of extracellular fields and currents--EEG, ECoG, LFP and spikes. *Nat. Rev. Neurosci.* 13, 407–20. doi:10.1038/nrn3241.

Buzsáki, G., and Draguhn, A. (2004). Neuronal oscillations in cortical networks. *Science* 304, 1926–9. doi:10.1126/science.1099745.

Buzsáki, G., Kaila, K., and Raichle, M. (2007). Inhibition and Brain Work. *Neuron* 56, 771–783. doi:10.1016/j.neuron.2007.11.008.

Buzsáki, G., and Wang, X.-J. (2012a). Mechanisms of Gamma Oscillations. *Annu. Rev. Neurosci.* 35, 203–225. doi:10.1146/annurev-neuro-062111-150444.

Buzsáki, G., and Wang, X.-J. (2012b). Mechanisms of Gamma Oscillations. *Annu. Rev. Neurosci.*, 203–225. doi:10.1146/annurev-neuro-062111-150444.

Caeyenberghs, K., Leemans, A., Heitger, M. H., Leunissen, I., Dhollander, T., Sunaert, S., et al. (2012). Graph analysis of functional brain networks for cognitive control of action in traumatic brain injury. *Brain* 135, 1293–1307. doi:10.1093/brain/aws048.

Cantu, D., Walker, K., Andresen, L., Taylor-Weiner, A., Hampton, D., Tesco, G., et al. (2015). Traumatic Brain Injury Increases Cortical Glutamate Network Activity by Compromising GABAergic Control. *Cereb. Cortex* 25, 2306–20. doi:10.1093/cercor/bhu041.

Cardin, J. a, Carlén, M., Meletis, K., Knoblich, U., Zhang, F., Deisseroth, K., et al. (2009). Driving fast-spiking cells induces gamma rhythm and controls sensory responses. *Nature* 459, 663–7. doi:10.1038/nature08002.

Carlo, C. N., and Stevens, C. F. (2013). Structural uniformity of neocortex, revisited. *Proc. Natl. Acad. Sci. U. S. A.* 110, 1488–93. doi:10.1073/pnas.1221398110.

Carron, S. F., Yan, E. B., Alwis, D. S., and Rajan, R. (2016). Differential susceptibility of cortical and subcortical inhibitory neurons and astrocytes in the long term following diffuse traumatic brain injury. *J. Comp. Neurol.* 524, 3530–3560. doi:10.1002/cne.24014.

Cassidy, J. D., Carroll, L. J., Peloso, P. M., Borg, J., von Holst, H., Holm, L., et al. (2004). Incidence, risk factors and prevention of mild traumatic brain injury: results of the WHO Collaborating Centre Task Force on Mild Traumatic Brain Injury. *J. Rehabil. Med.* 36, 28–60. doi:10.1080/16501960410023732.

CDC (2003). Report to Congress on Mild Traumatic Brain Injury in the United States: Steps to Prevent a Serious Public Health Problem. Atlanta, GA: Centers for Disease Control and Prevention.

CDC (2015). Report to Congress on Traumatic Brain Injury in the United States: Epidemiology and Rehabilitation. Atlanta.

Chagnac-Amitai, Y., and Connors, B. W. (1989). Horizontal spread of synchronized activity in neocortex and its control by GABA-mediated inhibition. *J. Neurophysiol.* 61, 747–58.

Chagnac-Amitai, Y., Luhmann, H. J., and Prince, D. a (1990). Burst generating and regular spiking layer 5 pyramidal neurons of rat neocortex have different morphological features. *J. Comp. Neurol.* 296, 598–613. doi:10.1002/cne.902960407.

Christman, C. W., Grady, M. S., Walker, S. A., Holloway, K. L., and Povlishock, J. T. (1994). Ultrastructural studies of diffuse axonal injury in humans. *J. Neurotrauma* 11, 173–86.

Christman, C. W., Salvant, J. B., Walker, S. A., and Povlishock, J. T. (1997). Characterization of a prolonged regenerative attempt by diffusely injured axons following traumatic brain injury in adult cat: a light and electron microscopic immunocytochemical study. *Acta Neuropathol.* 94, 329–37.

Cicerone, K. D. (1996). Attention deficits and dual task demands after mild traumatic brain injury. *Brain Inj.* 10, 79–89.

Cohen, A. S., Pfister, B. J., Schwarzbach, E., Grady, M. S., Goforth, P. B., and Satin, L. S. (2007). Injury-induced alterations in CNS electrophysiology. *Prog. Brain Res.* 161, 143–69. doi:10.1016/S0079-6123(06)61010-8.

Collette, F., and Van der Linden, M. (2002). Brain imaging of the central executive component of working memory. *Neurosci. Biobehav. Rev.* 26, 105–25.

Coronado, V. G., Haileyesus, T., Cheng, T. A., Bell, J. M., Haarbauer-Krupa, J., Lionbarger, M. R., et al. (2015). Trends in Sports- and Recreation-Related Traumatic Brain Injuries Treated in US Emergency Departments: The National Electronic Injury Surveillance System-All Injury Program (NEISS-AIP) 2001-2012. *J. Head Trauma Rehabil.* 30, 185–197. doi:10.1097/HTR.0000000000000156.

Coronado, V. G., Xu, L., Basavaraju, S. V, McGuire, L. C., Wald, M. M., Faul, M. D., et al. (2011). Surveillance for traumatic brain injury-related deaths--United States, 1997-2007. *MMWR. Surveill. Summ.* 60, 1–32. doi:2011-723-011/21044.

Corrigan, J. D., Selassie, A. W., and Orman, J. A. L. (2010). The epidemiology of traumatic brain injury. *J. Head Trauma Rehabil.* 25, 72–80. doi:10.1097/HTR.0b013e3181ccc8b4.

Crick, F. H. (1979). Thinking about the brain. *Sci. Am.* 241, 219–32.

De Beaumont, L., Tremblay, S., Poirier, J., Lassonde, M., and Théoret, H. (2012). Altered bidirectional plasticity and reduced implicit motor learning in concussed athletes. *Cereb. Cortex* 22, 112–21. doi:10.1093/cercor/bhr096.

Dean, P. J. A., Sato, J. R., Vieira, G., McNamara, A., and Sterr, A. (2015). Long-term structural changes after mTBI and their relation to post-concussion symptoms. *Brain Inj.* 29, 1–8. doi:10.3109/02699052.2015.1035334.

DeFelipe, J., Alonso-Nanclares, L., and Arellano, J. I. (2003). Microstructure of the neocortex: comparative aspects. *J. Neurocytol.* 31, 299–316.

Dimitriadis, S. I., Zouridakis, G., Rezaie, R., Babajani-Feremi, A., and Papanicolaou, A. C. (2015). Functional connectivity changes detected with magnetoencephalography after mild traumatic brain injury. *NeuroImage Clin.* 9, 519–531.

doi:10.1016/j.nicl.2015.09.011.

Dixon, C. E., Lyeth, B. G., Povlishock, J. T., Findling, R. L., Hamm, R. J., Marmarou, a, et al. (1987). A fluid percussion model of experimental brain injury in the rat. *J. Neurosurg.* 67, 110–119. doi:10.3171/jns.1987.67.1.0110.

Dodd, A. B., Epstein, K., Ling, J. M., and Mayer, A. R. (2014). Diffusion Tensor Imaging Findings in Semi-Acute Mild Traumatic Brain Injury. *J. Neurotrauma* 31, 1235–1248. doi:10.1089/neu.2014.3337.

Donner, T. H., and Siegel, M. (2011). A framework for local cortical oscillation patterns. *Trends Cogn. Sci.* 15, 191–199. doi:10.1016/j.tics.2011.03.007.

Douglas, R. J., Koch, C., Mahowald, M., Martin, K. a, and Suarez, H. H. (1995). Recurrent excitation in neocortical circuits. *Science* 269, 981–5.

Douglas, R. J., and Martin, K. a C. (2004). Neuronal circuits of the neocortex. *Annu. Rev. Neurosci.* 27, 419–51. doi:10.1146/annurev.neuro.27.070203.144152.

Douglas, R. J., and Martin, K. a C. (2007). Recurrent neuronal circuits in the neocortex. *Curr. Biol.* 17, R496-500. doi:10.1016/j.cub.2007.04.024.

Engel, A. K., Fries, P., and Singer, W. (2001). Dynamic predictions: oscillations and synchrony in top-down processing. *Nat. Rev. Neurosci.* 2, 704–16. doi:10.1038/35094565.

Erb, D. E., and Povlishock, J. T. (1991). Neuroplasticity following traumatic brain injury: a study of GABAergic terminal loss and recovery in the cat dorsal lateral vestibular nucleus. *Exp. Brain Res.* 83, 253–67.

Fagerholm, E. D., Hellyer, P. J., Scott, G., Leech, R., and Sharp, D. J. (2015). Disconnection of network hubs and cognitive impairment after traumatic brain

injury. *Brain*, 1696–1709. doi:10.1093/brain/awv075.

Farkas, O., Lifshitz, J., and Povlishock, J. T. (2006). Mechanoporation induced by diffuse traumatic brain injury: an irreversible or reversible response to injury? *J. Neurosci.* 26, 3130–40. doi:10.1523/JNEUROSCI.5119-05.2006.

Farkas, O., and Povlishock, J. T. (2007). Cellular and subcellular change evoked by diffuse traumatic brain injury: a complex web of change extending far beyond focal damage. *Prog. Brain Res.* 161, 43–59. doi:10.1016/S0079-6123(06)61004-2.

Faul, M., Xu, L., Wald, M. M., and Coronado, V. G. (2010). Traumatic Brain Injury in the United States: Emergency Department Visits, Hospitalizations and Deaths 2002–2006.

Fox, M. D., Snyder, A. Z., Vincent, J. L., Corbetta, M., Van Essen, D. C., and Raichle, M. E. (2005). The human brain is intrinsically organized into dynamic, anticorrelated functional networks. *Proc. Natl. Acad. Sci. U. S. A.* 102, 9673–8. doi:10.1073/pnas.0504136102.

Freund, T. F., and Katona, I. (2007). Perisomatic inhibition. *Neuron* 56, 33–42. doi:10.1016/j.neuron.2007.09.012.

Fries, P. (2009). Neuronal Gamma-Band Synchronization as a Fundamental Process in Cortical Computation. *Annu. Rev. Neurosci.* 32, 209–224. doi:10.1146/annurev.neuro.051508.135603.

Fries, P. (2015). Rhythms for Cognition: Communication through Coherence. *Neuron* 88, 220–235. doi:10.1016/j.neuron.2015.09.034.

Friston, K. J., Buechel, C., Fink, G. R., Morris, J., Rolls, E., and Dolan, R. J. (1997). Psychophysiological and modulatory interactions in neuroimaging. *Neuroimage* 6,

218–29. doi:10.1006/nimg.1997.0291.

Galarreta, M., and Hestrin, S. (2001). Spike transmission and synchrony detection in networks of GABAergic interneurons. *Science* 292, 2295–9. doi:10.1126/science.1061395.

Gardner, A., Kay-Lambkin, F., Stanwell, P., Donnelly, J., Williams, W. H., Hiles, A., et al. (2012). A systematic review of diffusion tensor imaging findings in sports-related concussion. *J. Neurotrauma* 29, 2521–38. doi:10.1089/neu.2012.2628.

Gentleman, S. M., Nash, M. J., Sweeting, C. J., Graham, D. I., and Roberts, G. W. (1993). Beta-amyloid precursor protein (beta APP) as a marker for axonal injury after head injury. *Neurosci. Lett.* 160, 139–44.

Gentry, L. R., Godersky, J. C., Thompson, B., and Dunn, V. D. (1988). Prospective comparative study of intermediate-field MR and CT in the evaluation of closed head trauma. *AJR. Am. J. Roentgenol.* 150, 673–82. doi:10.2214/ajr.150.3.673.

Gerstner, W., Kreiter, a K., Markram, H., and Herz, a V (1997). Neural codes: firing rates and beyond. *Proc. Natl. Acad. Sci. U. S. A.* 94, 12740–1. doi:10.1073/pnas.94.24.12740.

Giza, C. C., and Hovda, D. A. (2014). The new neurometabolic cascade of concussion. *Neurosurgery* 75 Suppl 4, S24-33. doi:10.1227/NEU.0000000000000505.

Gogolla, N., Leblanc, J. J., Quast, K. B., Südhof, T. C., Fagiolini, M., and Hensch, T. K. (2009). Common circuit defect of excitatory-inhibitory balance in mouse models of autism. *J. Neurodev. Disord.* 1, 172–81. doi:10.1007/s11689-009-9023-x.

Graham, D. I., Adams, J. H., Nicoll, J. A., Maxwell, W. L., and Gennarelli, T. A. (1995). The nature, distribution and causes of traumatic brain injury. *Brain Pathol.* 5, 397–

406.

Graham, D. I., McLellan, D., Adams, J. H., Doyle, D., Kerr, A., and Murray, L. S. (1983). The neuropathology of the vegetative state and severe disability after non-missile head injury. *Acta Neurochir. Suppl. (Wien).* 32, 65–7.

Greer, J. E., Hånell, A., McGinn, M. J., and Povlishock, J. T. (2013). Mild traumatic brain injury in the mouse induces axotomy primarily within the axon initial segment. *Acta Neuropathol.* 126, 59–74. doi:10.1007/s00401-013-1119-4.

Greer, J. E., McGinn, M. J., and Povlishock, J. T. (2011). Diffuse Traumatic Axonal Injury in the Mouse Induces Atrophy, c-Jun Activation, and Axonal Outgrowth in the Axotomized Neuronal Population. *J. Neurosci.* 31, 5089–5105. doi:10.1523/JNEUROSCI.5103-10.2011.

Greer, J. E., Povlishock, J. T., and Jacobs, K. M. (2012). Electrophysiological Abnormalities in Both Axotomized and Nonaxotomized Pyramidal Neurons following Mild Traumatic Brain Injury. *J. Neurosci.* 32, 6682–6687. doi:10.1523/JNEUROSCI.0881-12.2012.

Grimm, K., Lamont, L., Tranquilli, W., Greene, S., and Roberston, S. (2015). *Veterinary Anesthesia and Analgesia*. The Fifth. John Wiley and Sons.

Grubb, M. S., and Burrone, J. (2010a). Activity-dependent relocation of the axon initial segment fine-tunes neuronal excitability. *Nature* 465, 1070–4. doi:10.1038/nature09160.

Grubb, M. S., and Burrone, J. (2010b). Building and maintaining the axon initial segment. *Curr. Opin. Neurobiol.* 20, 481–8. doi:10.1016/j.conb.2010.04.012.

Grubb, M. S., Shu, Y., Kuba, H., Rasband, M. N., Wimmer, V. C., and Bender, K. J.

(2011). Short- and long-term plasticity at the axon initial segment. *J. Neurosci.* 31, 16049–55. doi:10.1523/JNEUROSCI.4064-11.2011.

Guerrero, J. L., Thurman, D. J., and Sniezek, J. E. (2000). Emergency department visits associated with traumatic brain injury: United States, 1995-1996. *Brain Inj.* 14, 181–6.

Guerriero, R. M., Giza, C. C., and Rotenberg, A. (2015). Glutamate and GABA imbalance following traumatic brain injury. *Curr. Neurol. Neurosci. Rep.* 15, 27. doi:10.1007/s11910-015-0545-1.

Gütig, R., and Sompolinsky, H. (2009). The tempotron: a neuron that learns spike timing–based decisions. *Nat. Neurosci.* 9, 420–428. doi:10.1038/nn1643.

Gutzmann, A., Ergül, N., Grossmann, R., Schultz, C., Wahle, P., and Engelhardt, M. (2014). A period of structural plasticity at the axon initial segment in developing visual cortex. *Front. Neuroanat.* 8, 11. doi:10.3389/fnana.2014.00011.

Hagmann, P., Cammoun, L., Gigandet, X., Meuli, R., Honey, C. J., Wedeen, V. J., et al. (2008). Mapping the structural core of human cerebral cortex. *PLoS Biol.* 6, e159. doi:10.1371/journal.pbio.0060159.

Hagmann, P., Jonasson, L., Maeder, P., Thiran, J., Wedeen, V. J., and Meuli, R. (2006). Understanding diffusion MR imaging techniques: from scalar diffusion-weighted imaging to diffusion tensor imaging and beyond. *Radiographics* 26 Suppl 1, S205-23. doi:10.1148/rg.26si065510.

Haider, B., Duque, A., Hasenstaub, A. R., and McCormick, D. a (2006). Neocortical network activity in vivo is generated through a dynamic balance of excitation and inhibition. *J. Neurosci.* 26, 4535–45. doi:10.1523/JNEUROSCI.5297-05.2006.

Haider, B., and McCormick, D. a (2009). Rapid neocortical dynamics: cellular and network mechanisms. *Neuron* 62, 171–89. doi:10.1016/j.neuron.2009.04.008.

Hallermann, S., de Kock, C. P. J., Stuart, G. J., and Kole, M. H. P. (2012). State and location dependence of action potential metabolic cost in cortical pyramidal neurons. *Nat. Neurosci.* 15, 1007–14. doi:10.1038/nn.3132.

Hammond-Tooke, G. D., Goei, J., du Plessis, L. J., and Franz, E. a (2010). Concussion causes transient dysfunction in cortical inhibitory networks but not the corpus callosum. *J. Clin. Neurosci.* 17, 315–9. doi:10.1016/j.jocn.2009.06.026.

Han, K., Mac Donald, C. L., Johnson, A. M., Barnes, Y., Wierzechowski, L., Zonies, D., et al. (2014). Disrupted modular organization of resting-state cortical functional connectivity in U.S. military personnel following concussive "mild" blast-related traumatic brain injury. *Neuroimage* 84, 76–96. doi:10.1016/j.neuroimage.2013.08.017.

Hanakawa, T., Immisch, I., Toma, K., Dimyan, M. a, Van Gelderen, P., and Hallett, M. (2003). Functional properties of brain areas associated with motor execution and imagery. *J. Neurophysiol.* 89, 989–1002. doi:10.1152/jn.00132.2002.

Hånell, A., Greer, J. E., and Jacobs, K. M. (2015a). Increased Network Excitability Due to Altered Synaptic Inputs to Neocortical Layer V Intact and Axotomized Pyramidal Neurons after Mild Traumatic Brain Injury. *J. Neurotrauma* 32, 1590–8. doi:10.1089/neu.2014.3592.

Hånell, A., Greer, J. E., McGinn, M. J., and Povlishock, J. T. (2015b). Traumatic brain injury-induced axonal phenotypes react differently to treatment. *Acta Neuropathol.* 129, 317–32. doi:10.1007/s00401-014-1376-x.

Hasenstaub, A., Shu, Y., Haider, B., Kraushaar, U., Duque, A., and McCormick, D. a (2005). Inhibitory postsynaptic potentials carry synchronized frequency information in active cortical networks. *Neuron* 47, 423–35. doi:10.1016/j.neuron.2005.06.016.

Hattox, A. M., and Nelson, S. B. (2007). Layer V neurons in mouse cortex projecting to different targets have distinct physiological properties. *J. Neurophysiol.* 98, 3330–3340. doi:10.1152/jn.00397.2007.

He, H.-Y., Hodos, W., and Quinlan, E. M. (2006). Visual deprivation reactivates rapid ocular dominance plasticity in adult visual cortex. *J. Neurosci.* 26, 2951–5. doi:10.1523/JNEUROSCI.5554-05.2006.

Hedstrom, K. L., Ogawa, Y., and Rasband, M. N. (2008). AnkyrinG is required for maintenance of the axon initial segment and neuronal polarity. *J. Cell Biol.* 183, 635–40. doi:10.1083/jcb.200806112.

Hedstrom, K. L., Xu, X., Ogawa, Y., Frischknecht, R., Seidenbecher, C. I., Shrager, P., et al. (2007). Neurofascin assembles a specialized extracellular matrix at the axon initial segment. *J. Cell Biol.* 178, 875–86. doi:10.1083/jcb.200705119.

Heffernan, M. E., Huang, W., Sicard, K. M., Bratane, B. T., Sikoglu, E. M., Zhang, N., et al. (2013). Multi-Modal Approach for Investigating Brain and Behavior Changes in an Animal Model of Traumatic Brain Injury. *J. Neurotrauma* 6, 1–6. doi:10.1089/neu.2012.2366.

Heiss, J. E., Katz, Y., Ganmor, E., and Lampl, I. (2008). Shift in the balance between excitation and inhibition during sensory adaptation of S1 neurons. *J. Neurosci.* 28, 13320–30. doi:10.1523/JNEUROSCI.2646-08.2008.

Hellyer, P. J., Leech, R., Ham, T. E., Bonnelle, V., and Sharp, D. J. (2012). Individual

prediction of white matter injury following traumatic brain injury. *Ann. Neurol.*, 489–499. doi:10.1002/ana.23824.

Hemphill, M. A., Dauth, S., Yu, C. J., Dabiri, B. E., and Parker, K. K. (2015). Traumatic Brain Injury and the Neuronal Microenvironment: A Potential Role for Neuropathological Mechanotransduction. *Neuron* 85, 1177–1192. doi:10.1016/j.neuron.2015.02.041.

Hinman, J. D., Rasband, M. N., and Carmichael, S. T. (2013). Remodeling of the axon initial segment after focal cortical and white matter stroke. *Stroke.* 44, online supplement. doi:10.1161/STROKEAHA.112.668749.

Hipp, J. F., Hawellek, D. J., Corbetta, M., Siegel, M., and Engel, A. K. (2012). Large-scale cortical correlation structure of spontaneous oscillatory activity. *Nat. Neurosci.* 15, 884–890. doi:10.1038/nn.3101.

Hoge, C. W., Castro, C. A., Messer, S. C., McGurk, D., Cotting, D. I., and Koffman, R. L. (2004). Combat duty in Iraq and Afghanistan, mental health problems, and barriers to care. *N. Engl. J. Med.* 351, 13–22. doi:10.1056/NEJMoa040603.

Hoge, C. W., McGurk, D., Thomas, J. L., Cox, A. L., Engel, C. C., and Castro, C. A. (2008). Mild traumatic brain injury in U.S. Soldiers returning from Iraq. *N. Engl. J. Med.* 358, 453–63. doi:10.1056/NEJMoa072972.

Hollrigel, G. S., Toth, K., and Soltesz, I. (1996). Neuroprotection by propofol in acute mechanical injury: role of GABAergic inhibition. *J. Neurophysiol.* 76, 2412–22.

Holm, L., David Cassidy, J., Carroll, L., and Borg, J. (2005). Summary of the WHO collaborating centre for neurotrauma task force on mild traumatic brain injury. *J. Rehabil. Med.* 37, 137–141. doi:10.1080/16501970510027321.

Horton, J. C., and Adams, D. L. (2005). The cortical column: a structure without a function. *Philos. Trans. R. Soc. B Biol. Sci.* 360, 837–862. doi:10.1098/rstb.2005.1623.

Howard, A., Tamas, G., and Soltesz, I. (2005). Lighting the chandelier: new vistas for axo-axonic cells. *Trends Neurosci.* 28, 310–6. doi:10.1016/j.tins.2005.04.004.

Howard, M. W. (2003). Gamma Oscillations Correlate with Working Memory Load in Humans. *Cereb. Cortex* 13, 1369–1374. doi:10.1093/cercor/bhg084.

Hsieh, T.-H., Lee, H. H. C., Hameed, M. Q., Pascual-Leone, A., Hensch, T. K., and Rotenberg, A. (2016). Trajectory of Parvalbumin Cell Impairment and Loss of Cortical Inhibition in Traumatic Brain Injury. *Cereb. Cortex*. doi:10.1093/cercor/bhw318.

Hu, H., Gan, J., and Jonas, P. (2014). Interneurons. Fast-spiking, parvalbumin^{+} GABAergic interneurons: from cellular design to microcircuit function. *Science* 345, 1255263. doi:10.1126/science.1255263.

Huang, M.-X., Harrington, D. L., Robb Swan, A., Angeles Quinto, A., Nichols, S., Drake, A., et al. (2016a). Resting-State Magnetoencephalography Reveals Different Patterns of Aberrant Functional Connectivity in Combat-Related Mild Traumatic Brain Injury. *J. Neurotrauma*. doi:10.1089/neu.2016.4581.

Huang, M.-X., Theilmann, R. J., Robb, A., Angeles, A., Nichols, S., Drake, A., et al. (2009a). Integrated Imaging Approach with MEG and DTI to Detect Mild Traumatic Brain Injury in Military and Civilian Patients. *J. Neurotrauma* 26, 1213–1226. doi:10.1089/neu.2008.0672.

Huang, M.-X., Theilmann, R. J., Robb, A., Angeles, A., Nichols, S., Drake, A., et al.

(2009b). Integrated imaging approach with MEG and DTI to detect mild traumatic brain injury in military and civilian patients. *J. Neurotrauma* 26, 1213–26. doi:10.1089/neu.2008.0672.

Huang, M., Harrington, D. L., Robb, A., Angeles, A., Nichols, S., Drake, A. I., et al. (2016b). Resting-state MEG Reveals Different Patterns of Aberrant Functional Connectivity in Combat-related Mild Traumatic Brain Injury. *J. Neurotrauma* 15, neu.2016.4581. doi:10.1089/neu.2016.4581.

Huisman, T. a G. M., Schwamm, L. H., Schaefer, P. W., Koroshetz, W. J., Shetty-Alva, N., Ozsunar, Y., et al. (2004). Diffusion tensor imaging as potential biomarker of white matter injury in diffuse axonal injury. *AJNR. Am. J. Neuroradiol.* 25, 370–6.

Hunt, R. F., Boychuk, J. a, and Smith, B. N. (2013). Neural circuit mechanisms of post-traumatic epilepsy. *Front. Cell. Neurosci.* 7, 89. doi:10.3389/fncel.2013.00089.

Hunt, R. F., Scheff, S. W., and Smith, B. N. (2011). Synaptic reorganization of inhibitory hilar interneuron circuitry after traumatic brain injury in mice. *J. Neurosci.* 31, 6880–90. doi:10.1523/JNEUROSCI.0032-11.2011.

Hyder, A. a, Wunderlich, C. a, Puvanachandra, P., Gururaj, G., and Kobusingye, O. C. (2007). The impact of traumatic brain injuries: a global perspective. *NeuroRehabilitation* 22, 341–353. doi:http://iospress.metapress.com/content/103177/?sortorder=asc.

Hylin, M. J., Orsi, S. a, Zhao, J., Bockhorst, K., Perez, A., Moore, A. N., et al. (2013). Behavioral and Histopathological Alterations Resulting from Mild Fluid Percussion Injury. *J. Neurotrauma* 715, 702–715. doi:10.1089/neu.2012.2630.

Ilvesmäki, T., Luoto, T. M., Hakulinen, U., Brander, A., Ryymin, P., Eskola, H., et al.

(2014). Acute mild traumatic brain injury is not associated with white matter change on diffusion tensor imaging. *Brain* 137, 1876–82. doi:10.1093/brain/awu095.

Imbrosci, B., and Mittmann, T. (2011). Functional consequences of the disturbances in the GABA-mediated inhibition induced by injuries in the cerebral cortex. *Neural Plast.* 2011, 614329. doi:10.1155/2011/614329.

Isaacson, J. S., and Scanziani, M. (2011). How inhibition shapes cortical activity. *Neuron* 72, 231–43. doi:10.1016/j.neuron.2011.09.027.

Iverson, G. L. (2005). Outcome from mild traumatic brain injury. *Curr. Opin. Psychiatry* 18, 301–17. doi:10.1097/01.yco.0000165601.29047.ae.

Iverson, G. L., Lovell, M. R., Smith, S., and Franzen, M. D. (2000). Prevalence of abnormal CT-scans following mild head injury. *Brain Inj.* 14, 1057–61.

Johnson, V. E., Stewart, W., and Smith, D. H. (2013). Axonal pathology in traumatic brain injury. *Exp. Neurol.* 246, 35–43. doi:10.1016/j.expneurol.2012.01.013.

Jones, D. K. (2008). Studying connections in the living human brain with diffusion MRI. *Cortex.* 44, 936–52. doi:10.1016/j.cortex.2008.05.002.

Kandel, ER; Schwartz, JH; Jessell, T. (2000). Principles of Neural Science.

Kann, O. (2016). The interneuron energy hypothesis: Implications for brain disease. *Neurobiol. Dis.* 90, 75–85. doi:10.1016/j.nbd.2015.08.005.

Kann, O., Papageorgiou, I. E., and Draguhn, A. (2014). Highly energized inhibitory interneurons are a central element for information processing in cortical networks. *J. Cereb. Blood Flow Metab.* 34, 1270–82. doi:10.1038/jcbfm.2014.104.

Kaphzan, H., Buffington, S. a, Jung, J. I., Rasband, M. N., and Klann, E. (2011). Alterations in intrinsic membrane properties and the axon initial segment in a mouse

model of Angelman syndrome. *J. Neurosci.* 31, 17637–48. doi:10.1523/JNEUROSCI.4162-11.2011.

Kasahara, M., Menon, D. K., Salmond, C. H., Outtrim, J. G., Taylor Tavares, J. V, Carpenter, T. a, et al. (2010). Altered functional connectivity in the motor network after traumatic brain injury. *Neurology* 75, 168–76. doi:10.1212/WNL.0b013e3181e7ca58.

Kay, T., Douglas, D., Adams, R., Anderson, T., Berrol, S., Cicerone, K., et al. (1993). Definition of mild traumatic brain injury. *J. Head Trauma Rehabil.* 8, 86–87. doi:10.1097/00001199-199309000-00010.

Kelley, B. J., Farkas, O., Lifshitz, J., and Povlishock, J. T. (2006). Traumatic axonal injury in the perisomatic domain triggers ultrarapid secondary axotomy and Wallerian degeneration. *Exp. Neurol.* 198, 350–60. doi:10.1016/j.expneurol.2005.12.017.

Kelley, B. J., Lifshitz, J., and Povlishock, J. T. (2007). Neuroinflammatory responses after experimental diffuse traumatic brain injury. *J. Neuropathol. Exp. Neurol.* 66, 989–1001. doi:10.1097/NEN.0b013e3181588245.

Kepecs, A., and Fishell, G. (2014). Interneuron cell types are fit to function. *Nature* 505, 318–326. doi:10.1038/nature12983.

Kim, H., Ährlund-Richter, S., Wang, X., Deisseroth, K., and Carlén, M. (2016). Prefrontal Parvalbumin Neurons in Control of Attention. *Cell* 164, 208–218. doi:10.1016/j.cell.2015.11.038.

King, N. S., Crawford, S., Wenden, F. J., Moss, N. E., and Wade, D. T. (1995). The Rivermead Post Concussion Symptoms Questionnaire: a measure of symptoms

commonly experienced after head injury and its reliability. *J. Neurol.* 242, 587–92.

Kinnunen, K. M., Greenwood, R., Powell, J. H., Leech, R., Hawkins, P. C., Bonnelle, V., et al. (2011). White matter damage and cognitive impairment after traumatic brain injury. *Brain* 134, 449–63. doi:10.1093/brain/awq347.

Klein, F. (1981). Silent Epidemic: Head Injuries, Often Difficult to Diagnose, Get Rising Attention. *Wall Str. J.*, 1. doi:10.1016/j.pcad.2015.11.006.

Kobori, N., and Dash, P. K. (2006). Reversal of brain injury-induced prefrontal glutamic acid decarboxylase expression and working memory deficits by D1 receptor antagonism. *J. Neurosci.* 26, 4236–46. doi:10.1523/JNEUROSCI.4687-05.2006.

Kole, M. H. P. (2011). First node of Ranvier facilitates high-frequency burst encoding. *Neuron* 71, 671–82. doi:10.1016/j.neuron.2011.06.024.

Kole, M. H. P., Ilschner, S. U., Kampa, B. M., Williams, S. R., Ruben, P. C., and Stuart, G. J. (2008). Action potential generation requires a high sodium channel density in the axon initial segment. *Nat. Neurosci.* 11, 178–86. doi:10.1038/nn2040.

Kole, M. H. P., and Stuart, G. J. (2012). Signal processing in the axon initial segment. *Neuron* 73, 235–47. doi:10.1016/j.neuron.2012.01.007.

Kraus, M. F., Susmaras, T., Caughlin, B. P., Walker, C. J., Sweeney, J. a, and Little, D. M. (2007). White matter integrity and cognition in chronic traumatic brain injury: a diffusion tensor imaging study. *Brain* 130, 2508–19. doi:10.1093/brain/awm216.

Kuba, H. (2012). Structural tuning and plasticity of the axon initial segment in auditory neurons. *J. Physiol.* 590, 5571–9. doi:10.1113/jphysiol.2012.237305.

Kuba, H., Oichi, Y., and Ohmori, H. (2010). Presynaptic activity regulates Na(+) channel distribution at the axon initial segment. *Nature* 465, 1075–8.

doi:10.1038/nature09087.

Kuhlman, S. J., Olivas, N. D., Tring, E., Ikrar, T., Xu, X., and Trachtenberg, J. T. (2013). A disinhibitory microcircuit initiates critical-period plasticity in the visual cortex. *Nature* 501, 543–6. doi:10.1038/nature12485.

Lafrenaye, A. D., Krahe, T. E., and Povlishock, J. T. (2014). Moderately elevated intracranial pressure after diffuse traumatic brain injury is associated with exacerbated neuronal pathology and behavioral morbidity in the rat. *J. Cereb. Blood Flow Metab.*, 1–9. doi:10.1038/jcbfm.2014.122.

Lafrenaye, A. D., McGinn, M. J., and Povlishock, J. T. (2012). Increased intracranial pressure after diffuse traumatic brain injury exacerbates neuronal somatic membrane poration but not axonal injury: evidence for primary intracranial pressure-induced neuronal perturbation. *J. Cereb. Blood Flow Metab.* 32, 1919–32. doi:10.1038/jcbfm.2012.95.

Lange, R. T., Iverson, G. L., and Franzen, M. D. (2009). Neuropsychological functioning following complicated vs. uncomplicated mild traumatic brain injury. *Brain Inj.* 23, 83–91. doi:10.1080/02699050802635281.

Langlois, J. A., Rutland-Brown, W., and Wald, M. M. (2006). The epidemiology and impact of traumatic brain injury: a brief overview. *J. Head Trauma Rehabil.* 21, 375–8.

Lauritzen, M. (2001). Relationship of spikes, synaptic activity, and local changes of cerebral blood flow. *J. Cereb. Blood Flow Metab.* 21, 1367–83. doi:10.1097/00004647-200112000-00001.

Lauritzen, M., and Gold, L. (2003). Brain function and neurophysiological correlates of

signals used in functional neuroimaging. *J. Neurosci.* 23, 3972–80.

Lazarus, M. S., Krishnan, K., and Huang, Z. J. (2015). GAD67 deficiency in parvalbumin interneurons produces deficits in inhibitory transmission and network disinhibition in mouse prefrontal cortex. *Cereb. Cortex* 25, 1290–6. doi:10.1093/cercor/bht322.

Le Bé, J.-V., Silberberg, G., Wang, Y., and Markram, H. (2007). Morphological, electrophysiological, and synaptic properties of corticocallosal pyramidal cells in the neonatal rat neocortex. *Cereb. Cortex* 17, 2204–13. doi:10.1093/cercor/bhl127.

Le Bihan, D., and Johansen-Berg, H. (2012). Diffusion MRI at 25: exploring brain tissue structure and function. *Neuroimage* 61, 324–41. doi:10.1016/j.neuroimage.2011.11.006.

Lewis, D. a (2013). Inhibitory neurons in human cortical circuits: substrate for cognitive dysfunction in schizophrenia. *Curr. Opin. Neurobiol.* 26C, 22–26. doi:10.1016/j.conb.2013.11.003.

Lifshitz, J., Rowe, R. K., Griffiths, D. R., Evilsizor, M. N., Thomas, T. C., Adelson, P. D., et al. (2016). Clinical relevance of midline fluid percussion brain injury: Acute deficits, chronic morbidities and the utility of biomarkers. *Brain Inj.* 30, 1–9. doi:10.1080/02699052.2016.1193628.

Ling, J. M., Klimaj, S., Toulouse, T., and Mayer, A. R. (2013). A prospective study of gray matter abnormalities in mild traumatic brain injury. *Neurology* 81, 2121–2127. doi:10.1212/01.wnl.0000437302.36064.b1.

Lipton, M. L., Gellella, E., Lo, C., Gold, T., Ardekani, B. a, Shifteh, K., et al. (2008). Multifocal white matter ultrastructural abnormalities in mild traumatic brain injury with cognitive disability: a voxel-wise analysis of diffusion tensor imaging. *J.*

Neurotrauma 25, 1335–42. doi:10.1089/neu.2008.0547.

Lipton, M. L., Gulko, E., Zimmerman, M. E., Friedman, B. W., Kim, M., Gellella, E., et al. (2009). Diffusion-tensor imaging implicates prefrontal axonal injury in executive function impairment following very mild traumatic brain injury. *Radiology* 252, 816–24. doi:10.1148/radiol.2523081584.

Lisman, J. E., and Jensen, O. (2013). The Theta-Gamma Neural Code. *Neuron* 77, 1002–1016. doi:10.1016/j.neuron.2013.03.007.

Logothetis, N. K. (2008). What we can do and what we cannot do with fMRI. *Nature* 453, 869–78. doi:10.1038/nature06976.

Logothetis, N. K., Pauls, J., Augath, M., Trinath, T., and Oeltermann, A. (2001). Neurophysiological investigation of the basis of the fMRI signal. *Nature* 412, 150–157. doi:10.1038/35084005.

Lorincz, A., and Nusser, Z. (2008). Cell-type-dependent molecular composition of the axon initial segment. *J. Neurosci.* 28, 14329–40. doi:10.1523/JNEUROSCI.4833-08.2008.

Lotze, M., Montoya, P., Erb, M., Hülsmann, E., Flor, H., Klose, U., et al. (1999). Activation of cortical and cerebellar motor areas during executed and imagined hand movements: an fMRI study. *J. Cogn. Neurosci.* 11, 491–501.

Lowenstein, D. H., Thomas, M. J., Smith, D. H., and McIntosh, T. K. (1992). Selective vulnerability of dentate hilar neurons following traumatic brain injury: a potential mechanistic link between head trauma and disorders of the hippocampus. *J. Neurosci.* 12, 4846–53.

Luo, Q., Xu, D., Roskos, T., Stout, J., Kull, L., Cheng, X., et al. (2013). Complexity

analysis of resting state magnetoencephalography activity in traumatic brain injury patients. *J. Neurotrauma* 30, 1702–9. doi:10.1089/neu.2012.2679.

Maas, A. I. R., and Menon, D. K. (2012). Traumatic brain injury: rethinking ideas and approaches. *Lancet Neurol.* 11, 12–3. doi:10.1016/S1474-4422(11)70267-8.

Mac Donald, C. L., Dikranian, K., Bayly, P., Holtzman, D., and Brody, D. (2007). Diffusion tensor imaging reliably detects experimental traumatic axonal injury and indicates approximate time of injury. *J. Neurosci.* 27, 11869–76. doi:10.1523/JNEUROSCI.3647-07.2007.

Mac Donald, C. L., Johnson, A. M., Cooper, D., Nelson, E. C., Werner, N. J., Shimony, J. S., et al. (2011). Detection of blast-related traumatic brain injury in U.S. military personnel. *N. Engl. J. Med.* 364, 2091–100. doi:10.1056/NEJMoa1008069.

Madisen, L., Zwingman, T. a, Sunkin, S. M., Oh, S. W., Zariwala, H. a, Gu, H., et al. (2010). A robust and high-throughput Cre reporting and characterization system for the whole mouse brain. *Nat. Neurosci.* 13, 133–40. doi:10.1038/nn.2467.

Mannix, R., Meehan III, W. P., and Pascual-Leone, A. (2016). Sports-related concussions - media, science and policy. *Nat. Rev. Neurol.* 12, 486–490. doi:10.1038/nrneurol.2016.99.

Markram, H., Toledo-Rodriguez, M., Wang, Y., Gupta, A., Silberberg, G., and Wu, C. (2004). Interneurons of the neocortical inhibitory system. *Nat. Rev. Neurosci.* 5, 793–807. doi:10.1038/nrn1519.

Marquez de la Plata, C. D., Garces, J., Shokri Kojori, E., Grinnan, J., Krishnan, K., Pidikiti, R., et al. (2011). Deficits in functional connectivity of hippocampal and frontal lobe circuits after traumatic axonal injury. *Arch. Neurol.* 68, 74–84.

doi:10.1001/archneurol.2010.342.

Masel, B. E., and DeWitt, D. S. (2010). Traumatic brain injury: a disease process, not an event. *J. Neurotrauma* 27, 1529–40. doi:10.1089/neu.2010.1358.

Maxwell, W. L., Povlishock, J. T., and Graham, D. L. (1997). A mechanistic analysis of nondisruptive axonal injury: a review. *J. Neurotrauma* 14, 419–40.

Mayer, A. R., Mannell, M. V, Ling, J., Gasparovic, C., and Yeo, R. a (2011). Functional connectivity in mild traumatic brain injury. *Hum. Brain Mapp.* 32, 1825–35. doi:10.1002/hbm.21151.

Mayer, a. R., Ling, J., Mannell, M. V., Gasparovic, C., Phillips, J. P., Doezema, D., et al. (2010). A prospective diffusion tensor imaging study in mild traumatic brain injury. *Neurology* 74, 643–650. doi:10.1212/WNL.0b013e3181d0ccdd.

Mazzoni, A., Whittingstall, K., Brunel, N., Logothetis, N. K., and Panzeri, S. (2010). Understanding the relationships between spike rate and delta/gamma frequency bands of LFPs and EEGs using a local cortical network model. *Neuroimage* 52, 956–972. doi:10.1016/j.neuroimage.2009.12.040.

McAllister, T. W. (1992). Neuropsychiatric sequelae of head injuries. *Psychiatr. Clin. North Am.* 15, 395–413.

McBain, C. J., and Fisahn, a (2001). Interneurons unbound. *Nat. Rev. Neurosci.* 2, 11–23. doi:10.1038/35049047.

McCormick, D. a. (2003). Persistent Cortical Activity: Mechanisms of Generation and Effects on Neuronal Excitability. *Cereb. Cortex* 13, 1219–1231. doi:10.1093/cercor/bhg104.

McGinn, M. J., Kelley, B. J., Akinyi, L., Oli, M. W., Liu, M. C., Hayes, R. L., et al.

(2009). Biochemical, Structural, and Biomarker Evidence for Calpain-Mediated Cytoskeletal Change After Diffuse Brain Injury Uncomplicated by Contusion. *J. Neuropathol. Exp. Neurol.* 68, 241–249. doi:10.1097/NEN.0b013e3181996bfe.

McGinn, M. J., and Povlishock, J. T. (2016). Pathophysiology of Traumatic Brain Injury. *Neurosurg. Clin. N. Am.* 27, 397–407. doi:10.1016/j.nec.2016.06.002.

Messé, A., Caplain, S., Pélégrini-Issac, M., Blancho, S., Lévy, R., Aghakhani, N., et al. (2013). Specific and evolving resting-state network alterations in post-concussion syndrome following mild traumatic brain injury. *PLoS One* 8, e65470. doi:10.1371/journal.pone.0065470.

Mesulam, M. M. (1990). Large-scale neurocognitive networks and distributed processing for attention, language, and memory. *Ann. Neurol.* 28, 597–613. doi:10.1002/ana.410280502.

Miller, R. (1996). Neural assemblies and laminar interactions in the cerebral cortex. *Biol. Cybern.* 75, 253–261. doi:10.1007/s004220050292.

Mittl, R. L., Grossman, R. I., Hiehle, J. F., Hurst, R. W., Kauder, D. R., Gennarelli, T. A., et al. (1994). Prevalence of MR evidence of diffuse axonal injury in patients with mild head injury and normal head CT findings. *AJNR. Am. J. Neuroradiol.* 15, 1583–9.

Mountcastle, V. (1979). "An organizing principle for cerebral function: the unit module and the distributed system," in *The Neurosciences, `Fourth Study Program*, eds. F. Schmidt and F. Worden (MIT Press), 21–42.

Murphy, K. M., Beston, B. R., Boley, P. M., and Jones, D. G. (2005). Development of human visual cortex: a balance between excitatory and inhibitory plasticity

mechanisms. *Dev. Psychobiol.* 46, 209–21. doi:10.1002/dev.20053.

Newcombe, V. F. J., Outtrim, J. G., Chatfield, D. a, Manktelow, A., Hutchinson, P. J., Coles, J. P., et al. (2011). Parcellating the neuroanatomical basis of impaired decision-making in traumatic brain injury. *Brain* 134, 759–68. doi:10.1093/brain/awq388.

Nortje, J., and Menon, D. K. (2004). Traumatic brain injury : physiology , mechanisms , and outcome. *Curr. Opin. Neurobiol.* 17, 711–718. doi:http://dx.doi.org/10.1097/00019052-200412000-00011.

Ogawa, Y., and Rasband, M. N. (2008). The functional organization and assembly of the axon initial segment. *Curr. Opin. Neurobiol.* 18, 307–13. doi:10.1016/j.conb.2008.08.008.

Packer, A. M., and Yuste, R. (2011). Dense, unspecific connectivity of neocortical parvalbumin-positive interneurons: a canonical microcircuit for inhibition? *J. Neurosci.* 31, 13260–71. doi:10.1523/JNEUROSCI.3131-11.2011.

Palacios, E. M., Yuh, E. L., Chang, Y.-S., Yue, J. K., Schnyer, D. M., Okonkwo, D. O., et al. (2017). Resting-State Functional Connectivity Alterations Associated with Six-Month Outcomes in Mild Traumatic Brain Injury. *J. Neurotrauma*. doi:10.1089/neu.2016.4752.

Parikh, S., Koch, M., and Narayan, R. K. (2007). Traumatic brain injury. *Int. Anesthesiol. Clin.* 45, 119–35. doi:10.1097/AIA.0b013e318078cfe7.

Patel, V. C., Jurgens, C. W. D., Krahe, T. E., and Povlishock, J. T. (2016). Adaptive reorganization of retinogeniculate axon terminals in dorsal lateral geniculate nucleus following experimental mild traumatic brain injury. *Exp. Neurol.* 289, 85–95.

doi:10.1016/j.expneurol.2016.12.012.

Paterno, R., Metheny, H., Xiong, G., Elkind, J., and Cohen, A. S. (2016). Mild Traumatic Brain Injury Decreases Broadband Power in Area CA1. *J. Neurotrauma* 33, 1645–9. doi:10.1089/neu.2015.4107.

Perrais, D., and Ropert, N. (2000). Altering the concentration of GABA in the synaptic cleft potentiates miniature IPSCs in rat occipital cortex. *Eur. J. Neurosci.* 12, 400–4.

Petersen, S. E., and Sporns, O. (2015). Brain Networks and Cognitive Architectures. *Neuron* 88, 207–219. doi:10.1016/j.neuron.2015.09.027.

Pevzner, A., Izadi, A., Lee, D. J., Shahlaie, K., and Gurkoff, G. G. (2016). Making Waves in the Brain: What Are Oscillations, and Why Modulating Them Makes Sense for Brain Injury. *Front. Syst. Neurosci.* 10, 30. doi:10.3389/fnsys.2016.00030.

Pfeffer, C. K., Xue, M., He, M., Huang, Z. J., and Scanziani, M. (2013). Inhibition of inhibition in visual cortex: the logic of connections between molecularly distinct interneurons. *Nat. Neurosci.* 16, 1068–76. doi:10.1038/nn.3446.

Phillips, L. L., Lyeth, B. G., Hamm, R. J., and Povlishock, J. T. (1994). Combined fluid percussion brain injury and entorhinal cortical lesion: a model for assessing the interaction between neuroexcitation and deafferentation. *J. Neurotrauma* 11, 641–56.

Phillips, L. L., and Reeves, T. M. (2001). Interactive pathology following traumatic brain injury modifies hippocampal plasticity. *Restor. Neurol. Neurosci.* 19, 213–35.

Pilz, P. (1983). Axonal injury in head injury. *Acta Neurochir. Suppl. (Wien).* 32, 119–23.

Pitkänen, A., and McIntosh, T. K. (2006). Animal models of post-traumatic epilepsy. *J. Neurotrauma* 23, 241–61. doi:10.1089/neu.2006.23.241.

Popovic, M. a, Foust, A. J., McCormick, D. a, and Zecevic, D. (2011). The spatio-temporal characteristics of action potential initiation in layer 5 pyramidal neurons: a voltage imaging study. *J. Physiol.* 589, 4167–87. doi:10.1113/jphysiol.2011.209015.

Povlishock, J., and Stone, J. (2001). "Traumatic Axonal Injury," in *Head Trauma: Basic, Preclinical, and Clinical Directions*, eds. L. Miller, R. Hayes, and J. Newcomb (New York: John Wiley & Sons, Inc), 281–301.

Povlishock, J. T. (1992). Traumatically induced axonal injury: pathogenesis and pathobiological implications. *Brain Pathol.* 2, 1–12.

Povlishock, J. T. (1993). Pathobiology of traumatically induced axonal injury in animals and man. *Ann. Emerg. Med.* 22, 980–6.

Povlishock, J. T., and Christman, C. W. (1995). The pathobiology of traumatically induced axonal injury in animals and humans: a review of current thoughts. *J. Neurotrauma* 12, 555–64.

Povlishock, J. T., Erb, D. E., and Astruc, J. (1992). Axonal response to traumatic brain injury: reactive axonal change, deafferentation, and neuroplasticity. *J. Neurotrauma* 9 Suppl 1, S189-200.

Povlishock, J. T., and Katz, D. I. (2005). Update of neuropathology and neurological recovery after traumatic brain injury. *J. Head Trauma Rehabil.* 20, 76–94.

Raichle, M. E. (2010). Two views of brain function. *Trends Cogn. Sci.* 14, 180–90. doi:10.1016/j.tics.2010.01.008.

Raichle, M. E., MacLeod, a M., Snyder, a Z., Powers, W. J., Gusnard, D. a, and Shulman, G. L. (2001). A default mode of brain function. *Proc. Natl. Acad. Sci. U. S. A.* 98, 676–82. doi:10.1073/pnas.98.2.676.

Raivich, G., Bohatschek, M., Da Costa, C., Iwata, O., Galiano, M., Hristova, M., et al. (2004). The AP-1 transcription factor c-Jun is required for efficient axonal regeneration. *Neuron* 43, 57–67. doi:10.1016/j.neuron.2004.06.005.

Rasband, M. N. (2011). Composition, assembly, and maintenance of excitable membrane domains in myelinated axons. *Semin. Cell Dev. Biol.* 22, 178–84. doi:10.1016/j.semcdb.2010.09.010.

Reeves, T. M., Lyeth, B. G., Phillips, L. L., Hamm, R. J., and Povlishock, J. T. (1997). The effects of traumatic brain injury on inhibition in the hippocampus and dentate gyrus. *Brain Res.* 757, 119–32.

Reeves, T. M., Lyeth, B. G., and Povlishock, J. T. (1995). Long-term potentiation deficits and excitability changes following traumatic brain injury. *Exp. Brain Res.* 106, 248–56.

Reynolds, J. R., West, R., and Braver, T. (2009). Distinct neural circuits support transient and sustained processes in prospective memory and working memory. *Cereb. Cortex* 19, 1208–21. doi:10.1093/cercor/bhn164.

Ross, D. T., Meaney, D. F., Sabol, M. K., Smith, D. H., and Gennarelli, T. A. (1994). Distribution of forebrain diffuse axonal injury following inertial closed head injury in miniature swine. *Exp. Neurol.* 126, 291–9. doi:10.1006/exnr.1994.1067.

Rudy, B., Fishell, G., Lee, S., and Hjerling-Leffler, J. (2011). Three groups of interneurons account for nearly 100% of neocortical GABAergic neurons. *Dev. Neurobiol.* 71, 45–61. doi:10.1002/dneu.20853.

Ryan, G. A., McLean, A. J., Vilenius, A. T. S., Kloeden, C. N., Simpson, D. A., Blumbergs, P. C., et al. (1994). Brain injury patterns in fatally injured pedestrians. *J.*

Trauma - Inj. Infect. Crit. Care 36, 469–476.

Salkoff, D. B., Zagha, E., Yuzgec, O., and McCormick, D. A. (2015). Synaptic Mechanisms of Tight Spike Synchrony at Gamma Frequency in Cerebral Cortex. *J Neurosci* 35, 10236–10251. doi:10.1523/JNEUROSCI.0828-15.2015.

Scheeringa, R., Fries, P., Petersson, K. M., Oostenveld, R., Grothe, I., Norris, D. G., et al. (2011). Neuronal Dynamics Underlying High- and Low-Frequency EEG Oscillations Contribute Independently to the Human BOLD Signal. *Neuron* 69, 572–583. doi:10.1016/j.neuron.2010.11.044.

Scheid, R., Walther, K., Guthke, T., Preul, C., and von Cramon, D. Y. (2006). Cognitive sequelae of diffuse axonal injury. *Arch. Neurol.* 63, 418–24. doi:10.1001/archneur.63.3.418.

Scholl, B., Pattadkal, J. J., Dilly, G. A., Priebe, N. J., and Zemelman, B. V. (2015). Local Integration Accounts for Weak Selectivity of Mouse Neocortical Parvalbumin Interneurons. *Neuron* 87, 424–436. doi:10.1016/j.neuron.2015.06.030.

Schölvinck, M. L., Maier, A., Ye, F. Q., Duyn, J. H., and Leopold, D. A. (2010). Neural basis of global resting-state fMRI activity. *Proc. Natl. Acad. Sci. U. S. A.* 107, 10238–43. doi:10.1073/pnas.0913110107.

Schubert, D., Kötter, R., Luhmann, H. J., and Staiger, J. F. (2006). Morphology, electrophysiology and functional input connectivity of pyramidal neurons characterizes a genuine layer va in the primary somatosensory cortex. *Cereb. Cortex* 16, 223–36. doi:10.1093/cercor/bhi100.

Schubert, D., Staiger, J. F., Cho, N., Ko, R., Zilles, K., and Luhmann, H. J. (2001). Layer-Specific Intracolumnar and Transcolumnar Functional Connectivity of Layer

V Pyramidal Cells in Rat Barrel Cortex. 21, 3580–3592.

Shadlen, M. N., and Newsome, W. T. (1994). Noise, neural codes and cortical organization. *Curr. Opin. Neurobiol.* 4, 569–79.

Sharp, D. J., and Ham, T. E. (2011). Investigating white matter injury after mild traumatic brain injury. *Curr. Opin. Neurol.* 24, 558–63. doi:10.1097/WCO.0b013e32834cd523.

Sharp, D. J., and Jenkins, P. O. (2015). Concussion is confusing us all. *Pract. Neurol.* 15, 172–186. doi:10.1136/practneurol-2015-001087.

Sharp, D. J., Scott, G., and Leech, R. (2014). Network dysfunction after traumatic brain injury. *Nat. Rev. Neurol.* 10, 156–66. doi:10.1038/nrneurol.2014.15.

Shenton, M. E., Hamoda, H. M., Schneiderman, J. S., Bouix, S., Pasternak, O., Rathi, Y., et al. (2012). A review of magnetic resonance imaging and diffusion tensor imaging findings in mild traumatic brain injury. *Brain Imaging Behav.* 6, 137–92. doi:10.1007/s11682-012-9156-5.

Sherriff, F., Bridges, L., and Sivaloganathan, S. (1994a). Early detection of axonal injury after human head trauma using immunocytochemistry for beta-amyloid precursor protein. *Acta Neuropathol.* 87, 55–62.

Sherriff, F. E., Bridges, L. R., Gentleman, S. M., Sivaloganathan, S., and Wilson, S. (1994b). Markers of axonal injury in post mortem human brain. *Acta Neuropathol.* 88, 433–9.

Shu, Y., Hasenstaub, A., and McCormick, D. A. (2003). Turning on and off recurrent balanced cortical activity. *Nature* 423, 288–93. doi:10.1038/nature01616.

Shultz, S. R., McDonald, S. J., Vonder Haar, C., Meconi, A., Vink, R., van Donkelaar, P.,

et al. (2016). The potential for animal models to provide insight into mild traumatic brain injury: Translational challenges and strategies. *Neurosci. Biobehav. Rev.* doi:10.1016/j.neubiorev.2016.09.014.

Siegel, M., Donner, T. H., and Engel, A. K. (2012). Spectral fingerprints of large-scale neuronal interactions. *Nat. Rev. Neurosci.* 13, 20–25. doi:10.1038/nrn3137.

Singleton, R. H., Zhu, J., Stone, J. R., and Povlishock, J. T. (2002). Traumatically induced axotomy adjacent to the soma does not result in acute neuronal death. *J. Neurosci.* 22, 791–802.

Smith, D. H., Hicks, R., and Povlishock, J. T. (2013). Therapy Development for Diffuse Axonal Injury. *J. Neurotrauma* 323, 307–323. doi:10.1089/neu.2012.2825.

Sohal, V. S., Zhang, F., Yizhar, O., and Deisseroth, K. (2009). Parvalbumin neurons and gamma rhythms enhance cortical circuit performance. *Nature* 459, 698–702. doi:10.1038/nature07991.

Somogyi, P., Tamás, G., Lujan, R., and Buhl, E. H. (1998). Salient features of synaptic organisation in the cerebral cortex. *Brain Res. Brain Res. Rev.* 26, 113–35.

Spain, A., Daumas, S., Lifshitz, J., Rhodes, J., Andrews, P. J. D., Horsburgh, K., et al. (2010). Mild fluid percussion injury in mice produces evolving selective axonal pathology and cognitive deficits relevant to human brain injury. *J. Neurotrauma* 27, 1429–38. doi:10.1089/neu.2010.1288.

Spolidoro, M., Sale, A., Berardi, N., and Maffei, L. (2009). Plasticity in the adult brain: lessons from the visual system. *Exp. Brain Res.* 192, 335–41. doi:10.1007/s00221-008-1509-3.

Sponheim, S. R., McGuire, K. a, Kang, S. S., Davenport, N. D., Aviyente, S., Bernat, E.

M., et al. (2011). Evidence of disrupted functional connectivity in the brain after combat-related blast injury. *Neuroimage* 54 Suppl 1, S21-9. doi:10.1016/j.neuroimage.2010.09.007.

Sporns, O. (2014). Contributions and challenges for network models in cognitive neuroscience. *Nat. Neurosci.* doi:10.1038/nn.3690.

Stam, C. J. (2014). Modern network science of neurological disorders. *Nat. Rev. Neurosci.* 15, 683–695. doi:10.1038/nrn3801.

Sterr, A., Herron, K. a, Hayward, C., and Montaldi, D. (2006). Are mild head injuries as mild as we think? Neurobehavioral concomitants of chronic post-concussion syndrome. *BMC Neurol.* 6, 7. doi:10.1186/1471-2377-6-7.

Stiell, I. G., Wells, G. A., Vandemheen, K., Clement, C., Lesiuk, H., Laupacis, A., et al. (2001). The Canadian CT Head Rule for patients with minor head injury. *Lancet* 357, 1391–1396. doi:10.1016/S0140-6736(00)04561-X.

Stone, J. R., Singleton, R. H., and Povlishock, J. T. (2000). Antibodies to the C-terminus of the beta-amyloid precursor protein (APP): a site specific marker for the detection of traumatic axonal injury. *Brain Res.* 871, 288–302.

STRICH, S. (1961). SHEARING OF NERVE FIBRES AS A CAUSE OF BRAIN DAMAGE DUE TO HEAD INJURY A Pathological Study of Twenty Cases. *Lancet* 278, 443–448. doi:10.1016/S0140-6736(61)92426-6.

Strich, S. J. (1956). Diffuse Degeneration Of The Cerebral White Matter In Severe Dementia Following Head Injury. *J. Neurol. Neurosurg. Psychiatry* 19, 163–185. doi:10.1136/jnnp.19.3.163.

Sugiyama, K., Kondo, T., Oouchida, Y., Suzukamo, Y., Higano, S., Endo, M., et al.

(2009). Clinical utility of diffusion tensor imaging for evaluating patients with diffuse axonal injury and cognitive disorders in the chronic stage. *J. Neurotrauma* 26, 1879–90. doi:10.1089/neu.2008-0839.

Sun, J., and Jacobs, K. M. (2016). Knockout of Cyclophilin-D Provides Partial Amelioration of Intrinsic and Synaptic Properties Altered by Mild Traumatic Brain Injury. *Front. Syst. Neurosci.* 10, 63. doi:10.3389/fnsys.2016.00063.

Tagamets, M. a, and Horwitz, B. (2001). Interpreting PET and fMRI measures of functional neural activity: the effects of synaptic inhibition on cortical activation in human imaging studies. *Brain Res. Bull.* 54, 267–73.

Tamás, G., Buhl, E. H., Lörincz, A., and Somogyi, P. (2000). Proximally targeted GABAergic synapses and gap junctions synchronize cortical interneurons. *Nat. Neurosci.* 3, 366–371. doi:10.1038/73936.

Taniguchi, H., He, M., Wu, P., Kim, S., Paik, R., Sugino, K., et al. (2011). A resource of Cre driver lines for genetic targeting of GABAergic neurons in cerebral cortex. *Neuron* 71, 995–1013. doi:10.1016/j.neuron.2011.07.026.

Thatcher, R. W. (2006). "ELECTROENCEPHALGRAPHY AND MILD TRAUMATIC BRAIN INJURY," in *Foundations of Sport-Related Brain Injuries*.

Thatcher, R. W., Camacho, M., Salazar, A., Linden, C., Biver, C., and Clarke, L. (1997). Quantitative MRI of the gray-white matter distribution in traumatic brain injury. *J. Neurotrauma* 14, 1–14.

Thurman, D. J., Alverson, C., Dunn, K. A., Guerrero, J., and Sniezek, J. E. (1999). Traumatic brain injury in the United States: A public health perspective. *J. Head Trauma Rehabil.* 14, 602–15.

Tononi, G., Boly, M., Massimini, M., and Koch, C. (2016). Integrated Information Theory: from consciousness to its physical substrates. *Nat. Rev. Neurosci.* in press, 450–461. doi:10.1038/nrn.2016.44.

Tononi, G., and Koch, C. (2008). The neural correlates of consciousness: An update. *Ann. N. Y. Acad. Sci.* 1124, 239–261. doi:10.1196/annals.1440.004.

Toth, Z., Hollrigel, G. S., Gorcs, T., and Soltesz, I. (1997). Instantaneous perturbation of dentate interneuronal networks by a pressure wave-transient delivered to the neocortex. *J. Neurosci.* 17, 8106–17.

Trachtenberg, J. T. (2015). Parvalbumin Interneurons: All Forest, No Trees. *Neuron* 87, 247–248. doi:10.1016/j.neuron.2015.06.041.

Traub, R. D., Whittington, M. a, Colling, S. B., Buzsáki, G., and Jefferys, J. G. (1996). Analysis of gamma rhythms in the rat hippocampus in vitro and in vivo. *J. Physiol.* 493 (Pt 2, 471–84. doi:10.1113/jphysiol.1996.sp021397.

Tremblay, S., Beaulé, V., Proulx, S., Tremblay, S., Marjańska, M., Doyon, J., et al. (2014). Multimodal assessment of primary motor cortex integrity following sport concussion in asymptomatic athletes. *Clin. Neurophysiol.* 125, 1371–1379. doi:10.1016/j.clinph.2013.11.040.

Tremblay, S., de Beaumont, L., Lassonde, M., and Théoret, H. (2011). Evidence for the specificity of intracortical inhibitory dysfunction in asymptomatic concussed athletes. *J. Neurotrauma* 28, 493–502. doi:10.1089/neu.2010.1615.

Tremblay, S., Vernet, M., Bashir, S., Pascual-Leone, A., and Théoret, H. (2015). Theta burst stimulation to characterize changes in brain plasticity following mild traumatic brain injury: A proof-of-principle study. *Restor. Neurol. Neurosci.* 33, 611–20.

doi:10.3233/RNN-140459.

van den Heuvel, M. P., and Sporns, O. (2011). Rich-club organization of the human connectome. *J. Neurosci.* 31, 15775–86. doi:10.1523/JNEUROSCI.3539-11.2011.

van den Heuvel, M. P., and Sporns, O. (2013). Network hubs in the human brain. *Trends Cogn. Sci.* 17, 683–96. doi:10.1016/j.tics.2013.09.012.

van der Horn, H. J., Kok, J. G., de Koning, M. E., Scheenen, M. E., Leemans, A., Spikman, J. M., et al. (2016). Altered Wiring of the Human Structural Connectome in Adults with Mild Traumatic Brain Injury. *J. Neurotrauma*. doi:10.1089/neu.2016.4659.

Van Essen, D. C. (1997). A tension-based theory of morphogenesis and compact wiring in the central nervous system. *Nature* 385, 313–318. doi:10.1038/385313a0.

Van Wart, A., Trimmer, J. S., and Matthews, G. (2007). Polarized distribution of ion channels within microdomains of the axon initial segment. *J. Comp. Neurol.* 500, 339–52. doi:10.1002/cne.21173.

Vanderploeg, R. D., Curtiss, G., Belanger, H. G., Curtiss, G., Demery, J. A., Lebowitz, B. K., et al. (2005). Long-term neuropsychological outcomes following mild traumatic brain injury. *J. Int. Neuropsychol. Soc.* 11, 228–236. doi:10.1017/S1355617705050277.

Varela, F., Lachaux, J. P., Rodriguez, E., and Martinerie, J. (2001). The brainweb: phase synchronization and large-scale integration. *Nat. Rev. Neurosci.* 2, 229–239. doi:10.1038/35067550.

Walhovd, K. B., Johansen-Berg, H., and Káradóttir, R. T. (2014). Unraveling the secrets of white matter--bridging the gap between cellular, animal and human imaging

studies. *Neuroscience* 276, 2–13. doi:10.1016/j.neuroscience.2014.06.058.

Wäljas, M., Lange, R. T., Hakulinen, U., Huhtala, H., Dastidar, P., Hartikainen, K., et al. (2014). Biopsychosocial outcome after uncomplicated mild traumatic brain injury. *J. Neurotrauma* 31, 108–24. doi:10.1089/neu.2013.2941.

Wang, J., Fox, M. A., and Povlishock, J. T. (2013). Diffuse traumatic axonal injury in the optic nerve does not elicit retinal ganglion cell loss. *J. Neuropathol. Exp. Neurol.* 72, 768–81. doi:10.1097/NEN.0b013e31829d8d9d.

Warner, M. a, Marquez de la Plata, C., Spence, J., Wang, J. Y., Harper, C., Moore, C., et al. (2010). Assessing spatial relationships between axonal integrity, regional brain volumes, and neuropsychological outcomes after traumatic axonal injury. *J. Neurotrauma* 27, 2121–2130. doi:10.1089/neu.2010.1429.

Watts, D. J., and Strogatz, S. H. (1998). Collective dynamics of "small-world" networks. *Nature* 393, 440–2. doi:10.1038/30918.

Weissman, D. H., Roberts, K. C., Visscher, K. M., and Woldorff, M. G. (2006). The neural bases of momentary lapses in attention. *Nat. Neurosci.* 9, 971–8. doi:10.1038/nn1727.

Whittington, M. A., Traub, R. D., Kopell, N., Ermentrout, B., and Buhl, E. H. (2000). Inhibition-based rhythms: Experimental and mathematical observations on network dynamics. *Int. J. Psychophysiol.* 38, 315–336. doi:10.1016/S0167-8760(00)00173-2.

Witgen, B. M., Lifshitz, J., Smith, M. L., Schwarzbach, E., Liang, S.-L., Grady, M. S., et al. (2005). Regional hippocampal alteration associated with cognitive deficit following experimental brain injury: a systems, network and cellular evaluation. *Neuroscience* 133, 1–15. doi:10.1016/j.neuroscience.2005.01.052.

Wolf, J. A., and Koch, P. F. (2016). Disruption of Network Synchrony and Cognitive Dysfunction After Traumatic Brain Injury. *Front. Syst. Neurosci.* 10, 43. doi:10.3389/fnsys.2016.00043.

Yizhar, O., Fenno, L. E., Prigge, M., Schneider, F., Davidson, T. J., O'Shea, D. J., et al. (2011). Neocortical excitation/inhibition balance in information processing and social dysfunction. *Nature* 477, 171–8. doi:10.1038/nature10360.

Yuen, T. J., Browne, K. D., Iwata, A., and Smith, D. H. (2009). Sodium channelopathy induced by mild axonal trauma worsens outcome after a repeat injury. *J. Neurosci. Res.* 87, 3620–5. doi:10.1002/jnr.22161.

Yuh, E. L., Mukherjee, P., Lingsma, H. F., Yue, J. K., Ferguson, A. R., Gordon, W. A., et al. (2013). Magnetic resonance imaging improves 3-month outcome prediction in mild traumatic brain injury. *Ann. Neurol.* 73, 224–235. doi:10.1002/ana.23783.

Zhang, D., and Raichle, M. E. (2010). Disease and the brain's dark energy. *Nat. Rev. Neurol.* 6, 15–28. doi:10.1038/nrneurol.2009.198.

Zhang, K., Johnson, B., Gay, M., Horovitz, S. G., Hallett, M., Sebastianelli, W., et al. (2012). Default mode network in concussed individuals in response to the YMCA physical stress test. *J. Neurotrauma* 29, 756–65. doi:10.1089/neu.2011.2125.

Zhang, K., Johnson, B., Pennell, D., Ray, W., Sebastianelli, W., and Slobounov, S. (2010). Are functional deficits in concussed individuals consistent with white matter structural alterations: combined FMRI & DTI study. *Exp. Brain Res.* 204, 57–70. doi:10.1007/s00221-010-2294-3.

Zhang, K., and Sejnowski, T. J. (2000). A universal scaling law between gray matter and white matter of cerebral cortex. *Proc. Natl. Acad. Sci. U. S. A.* 97, 5621–6.

doi:10.1073/pnas.090504197.

Zhang, L., Yang, K. H., and King, A. I. (2004). A proposed injury threshold for mild traumatic brain injury. *J. Biomech. Eng.* 126, 226–36. doi:10.1115/1.1691446.

Zhou, F., Chen, H., and Roper, S. N. (2009). Balance of inhibitory and excitatory synaptic activity is altered in fast-spiking interneurons in experimental cortical dysplasia. *J. Neurophysiol.* 102, 2514–25. doi:10.1152/jn.00557.2009.

Ziebell, J. M., Taylor, S. E., Cao, T., Harrison, J. L., and Lifshitz, J. (2012). Rod microglia: elongation, alignment, and coupling to form trains across the somatosensory cortex after experimental diffuse brain injury. *J. Neuroinflammation* 9, 247. doi:10.1186/1742-2094-9-247.

ZOURIDAKIS, G., PATIDAR, U., SITU, N., REZAIE, R., CASTILLO, E. M., LEVIN, H. S., et al. (2012). Functional Connectivity Changes in Mild Traumatic Brain Injury Assessed Using Magnetoencephalography. *J. Mech. Med. Biol.* 12, 1240006. doi:10.1142/S0219519412400064.

VITA

MICHAL VASCAK was born in Košice, Slovak Republic (former Czechoslovakia) in 1984. He was raised in New York and received a Bachelor's in Science degree with a concentration in biochemistry from Ramapo College of New Jersey in 2008. After college, Michal received a Cancer Research Training Award from the National Cancer Institute, and did a two-year post-baccalaureate fellowship at the National Institutes of Health in Bethesda, Maryland. In 2010, Michal was accepted into the MD/PhD program at the Virginia Commonwealth University School of Medicine, where he completed his neuroscience graduate training under the mentorship of John T. Povlishock, PhD. This thesis was defended April 11th, 2017 against the opponent PhD committee.